

Alma Mater Studiorum – Università di Bologna

DOTTORATO DI RICERCA IN

CHIMICA

Ciclo XXVI

Settore Concorsuale di afferenza: 03/C1

Settore Scientifico disciplinare: CHIM/06

**LIPOPHILIC NUCLEOSIDES: STUDIES TOWARD
SELF-ASSEMBLED FUNCTIONAL MATERIALS**

Presentata da: Lucia Gramigna

Coordinatore Dottorato

Prof. Aldo Roda

Relatore

Prof. Stefano Masiero

Esame finale anno 2014

Dottorando: Lucia Gramigna

Tutor: Prof. Stefano Masiero

Curriculum, indirizzo: Curriculum Chimica Farmaceutica, Indirizzo Chimica Organica

Titolo tesi: Lipophilic nucleosides: studies toward self-assembled functional materials

Il lavoro della Dott.ssa Lucia Gramigna nel triennio di frequenza del Dottorato in Chimica è stato volto alla sintesi e caratterizzazione di nucleosidi funzionalizzati per applicazioni nell'ambito dei nanomateriali.

Nel corso dei primi due anni l'attenzione è stata volta alla sintesi di queste molecole; in particolar modo sono stati seguiti due progetti principali:

- sintesi di guanosine aventi sostituenti tiofenici per lo studio di nuovi materiali semiconduttori organici per transistor a effetto di campo (OFET);
- sintesi dei vari nucleosidi diversi, funzionalizzati con due o tre code alchiliche, per la preparazione di films di Langmuir-Blodgett.

Lo studio delle guanosine lipofile è correlato alla capacità di tali molecole di autoassemblarsi a seconda delle condizioni (solventi, presenza di ioni) in strutture altamente ordinate sia in soluzione che su superficie. Questa caratteristica ha riscosso molto interesse negli ultimi anni soprattutto nel campo dell'elettronica organica, in cui la possibilità di ottenere ma soprattutto di controllare l'organizzazione delle molecole in layer ordinati risulta uno dei goal fondamentali. Nell'ambito degli OFET, gli oligotiofeni risultano tra i migliori prototipi di semiconduttori organici e sfruttare l'autoassemblaggio della guanosina per controllarne l'organizzazione è stato il primo obiettivo perseguito durante il dottorato di ricerca. Stati preparati vari derivati della guanosine aventi sostituenti sia tiofenici che tertiofenici. Questi composti, una volta studiata la loro aggregazione supramolecolare in soluzione, sono stati caratterizzati su superficie: tramite immagini AFM ed STM è stato possibile determinare la formazione di aggregati nastriformi una volta depositato il materiale su diversi substrati (mica, grafite, ossido di silicio). Sono state anche effettuate alcune misure elettriche depositando il materiale tra elettrodi di oro in un dispositivo a tre terminali, ma per il momento non si è stati ancora in grado di ottimizzare il processo di preparazione del film conduttivo.

Per quanto riguarda il secondo obiettivo, sono stati sintetizzati nucleosidi quali adenosina, citosina, timidina e uracile aventi lo zucchero funzionalizzato con due o tre code alchiliche a lunga catena: lo scopo era quello di confrontare l'abilità di questi nucleosidi nel formare films di Langmuir-Blodgett con quella già riscontrata negli analoghi derivati della guanosina. I films di Langmuir-Blodgett sono costituiti da uno o più layers di una molecola organica generalmente anfifilica e si formano sulla superficie di un liquido (acqua) per essere poi trasferiti su un substrato solido: la struttura di questi films è simile a quella di un monostrato fosfolipidico e i nucleosidi, costituita da una "testa" (base azotata) idrofila e da code alchiliche (10 atomi di carbonio) sembrano ottimi candidati allo scopo. L'analisi di questi films ha portato a concludere che la guanosina, in particolare il derivato della desossiguanosina con due code deciliche, risulta l'unica molecola in grado di dare films omogenei e idonei all'applicazione in nanotecnologia.

Gli studi superficie sono stati svolti durante un periodo di tre mesi nel corso del terzo anno di dottorato presso il laboratorio di nano chimica dell'Institut de Science et d'Ingénierie Supramoléculaire a Strasburgo, sotto la supervisione del Prof. Paolo Samorì. L'apprendimento di tecniche quali AFM, STM e l'uso di strumenti per misure elettriche hanno permesso la completa caratterizzazione dei composti preparati.

I risultati dello studio sui films di Lagmuir-Blodgett sono stati pubblicati, mentre ulteriori studi sono in corso per ultimare il progetto sui derivati tiofenici, i cui risultati parziali sono stati presentati in quattro congressi sia nazionali che internazionali.

Nel corso del triennio di dottorato, la dott.ssa Gramigna ha acquisito una solida competenza nello studio dei fenomeni di autoassemblaggio mediati da legami a idrogeno ed una notevole padronanza delle tecniche sintetiche ed analitiche finalizzate a tali studi. In particolare, soprattutto per quanto riguarda il lavoro sintetico, ha dimostrato grandi capacità di organizzazione ed intraprendenza, riuscendo a gestire in autonomia il proprio lavoro ed al tempo stesso supportando i colleghi più giovani.

Abstract

Molecular self-assembly takes advantage of supramolecular non-covalent interactions (ionic, hydrophobic, van der Waals, hydrogen and coordination bonds) for the construction of organized and tunable systems. In this field, lipophilic guanosines can represent powerful building blocks thanks to their aggregation properties in organic solvents, which can be controlled by addition or removal of cations. For example, potassium ion can template the formation of piled G-quartets structures, while in its absence ribbon-like G aggregates are generated in solution.

In this thesis we explored the possibility of using guanosines as scaffolds to direct the construction of ordered and self-assembled architectures, one of the main goals of bottom-up approach in nanotechnology. In Chapter III we will describe Langmuir-Blodgett films obtained from guanosines and other lipophilic nucleosides, revealing the “special” behavior of guanine in comparison with the other nucleobases. In Chapter IV we will report the synthesis of several thiophene-functionalized guanosines and the studies towards their possible use in organic electronics: the pre-programmed organization of terthiophene residues in ribbon aggregates could allow charge conduction through π - π stacked oligothiophene functionalities. The construction and the behavior of some simple electronic nanodevices based on these organized thiophene-guanosine hybrids has been explored.

Table of contents

Chapter I: Introduction *Page 1*

1. Supramolecular chemistry **Page 2**

1.1 Concept and evolution of supramolecular chemistry Page 2

1.2 Self-assembly through hydrogen-bonding Page 5

2. Guanine, a special nucleobase **Page 8**

2.1 G-quadruplex Page 9

2.1.1 G-quadruplex: structure details *Page 9*

2.1.2 G-quadruplex role during DNA replication *Page 10*

2.1.3 Telemores: target for G-quadruplex ligands *Page 11*

2.1.4 G-4 in genetic regulation *Page 13*

2.1.5 Methods for studying G-quadruplexes *Page 14*

3. Conclusions **Page 19**

Bibliography Page 20

Chapter II: Structure and behaviour of lipophilic guanosines *Page 23*

1. Introduction: how the story began **Page 24**

2. Self-assembly of lipophilic guanosines **Page 26**

2.1 Self-assembly in presence of metal ions Page 26

2.2 Self-assembly in the absence of metal ions Page 33

3. Guanosine lipophilic assemblies for smart functional materials **Page 37**

3.1 From guanosines gels to liquid crystalline mesophases Page 37

3.2 Supramolecular dynamer: switching between assemblies Page 39

3.3 Molecular electronic devices Page 41

4. Conclusions Page 45

Bibliography Page 46

Chapter III: Liponucleoside thin films: the special behaviour of guanosine *Page 49*

1. Introduction **Page 50**

1.1 Langmuir-Blodgett films: preparation and characterization Page 50

2 Surface structure of Langmuir-Blodgett films of lipophilic guanosine derivatives **Page 54**

3. Liponucleoside thin films **Page 59**

3.1 Synthesis of liponucleosides Page 59

3.2 Results Page 60

3.2.1 Langmuir films isotherm *Page 60*

3.2.2 Real time Brewster angle microscopy *Page 64*

3.2.3 Atomic force microscopy of films transferred to mica surface *Page 66*

3.3 Discussion Page 67

4. Conclusions **Page 70**

Bibliography **Page 71**

Chapter IV: Functionalized guanosines for organic electronic devices *Page 73*

1. Organic semiconductor for Field-Effect Transistor (FET) **Page 74**

1.1 OFET working principles Page 74

1.2 Organic semiconductors Page 76

2. Guanosine derivatives as semiconductors in field effect transistors **Page 79**

2.1 Guanosine-based OFET Page 79

2.2 Functionalized guanosines: a new challenge Page 81

2.2.1 Supramolecular switching triggered by external stimuli *Page 84*

2.2.2 Supramolecular studies on surface *Page 88*

3. Thiophene functionalized guanosines: a structural investigation **Page 91**

3.1 Thiophene disubstituted guanosine Page 92

3.1.1 Synthetic procedure *Page 92*

3.1.2 <i>Supramolecular studies in solution</i>	Page 93
3.1.3 <i>Aggregation on surface</i>	Page 95
3.2 <u>Terthiophene guanosine derivatives</u>	Page 99
3.2.1 <i>Synthetic procedure</i>	Page 99
3.2.2 <i>Supramolecular studies in solution</i>	Page 103
3.2.3 <i>Aggregation on surface</i>	Page 105
3.2.4 <i>Electrical measurments</i>	Page 109
4. Conclusions	Page 112
Bibliography	Page 113
<i>Chapter V: Experimental section</i>	<i>Page 115</i>
1. General	Page 116
2. Synthesis of lipophilic nucleosides	Page 117
3. Synthesis of thiophene functionalized guanosines	Page 123
3.1 <u>Synthesis of 3',5'-Di-O-[7-(thiophen-2-yl)-heptan-1-oyl]-2'-deoxyguanosine</u>	Page 123
3.2 <u>Synthesis of 2',3'-O-Isopropylidene-5'-O-[6-(5"-hexyl-[2,2';5',2"]-terthiophen-5-yl)-hexanoyl]-guanosine</u>	Page 126
3.3 <u>Synthesis of 2',3'-O-Isopropylidene-5'-O-[7-([2,2';5',2"]-terthiophen-5-yl)-heptanoyl]-guanosine</u>	Page 134
Bibliography	Page 138

Chapter I: Introduction

1. Supramolecular Chemistry

1.1 Concept and evolution of supramolecular chemistry^{1, 2}

“Übermolekül”, German word for “Supermolecule”, appeared in the literature in 1937, describing the intermolecular interaction of coordinatively saturated species as dimers of carboxylic acids³, but it took more than 40 years to Lehn’s definition of Supramolecular Chemistry as “chemistry beyond the molecule”⁴ that gave birth to this new research area.⁵

It started and developed as the chemistry of the entities generated via intermolecular non-covalent interactions, such as electrostatic interactions, hydrogen bonding, π - π stacking, Van der Waals forces and hydrophobic effect. By the appropriate manipulation of these interactions, it became progressively the chemistry of molecular information, involving the storage of information at the molecular level, in the structural features, and its retrieval, transfer, processing at the supramolecular level, through molecular recognition processes operating via specific spatial relationships and interaction patterns.

An optimal molecular recognition is achieved with a good shape and interaction complementary of the molecules involved, according to Ficher’s “lock and key model”: the host-guest chemistry is the first type of supramolecular chemistry (**Figure 1.1.1**), where large ‘host’ molecule are capable of enclosing smaller ‘guest’ molecules. Examples of host molecules are crown ethers, cryptands, calixarenes and cyclodextrins, (**Figure 1.1.1, a.**); selectivity for specific guests and co-operativity when more than one binding site are present, play crucial roles in complex formation.

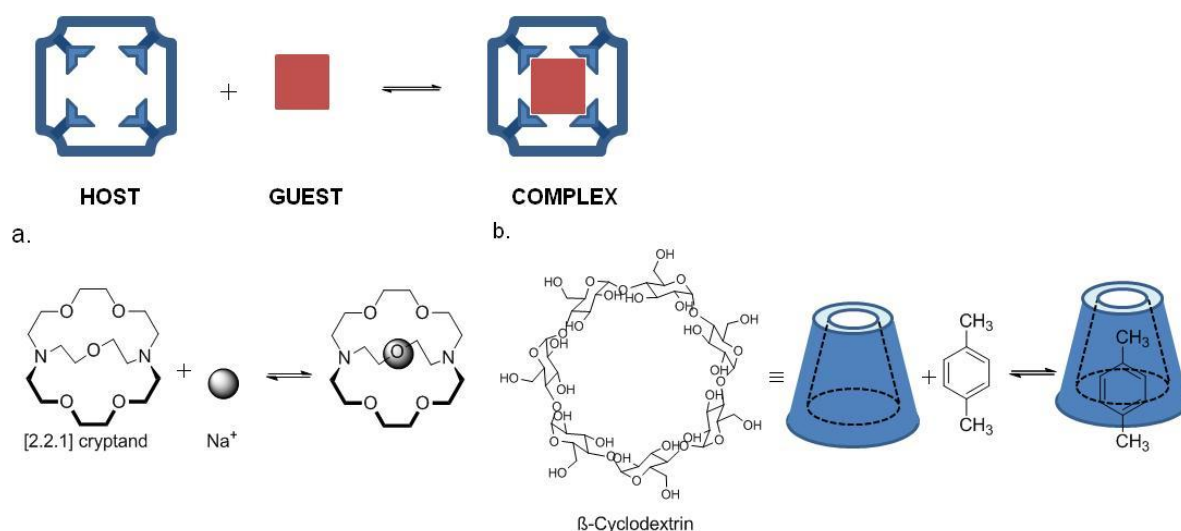


Figure 1.1.1: Host-guest chemistry. a. [2.2.1] cryptand, selective for Na⁺; b. β-cyclodextrin complex with *p*-xylene.

One step forward is the design of self-organized system, in which molecular species form spontaneously and reversibly more complex supramolecular entities according to the intrinsic information in the components: self-assembly is the second type of supramolecular chemistry, a process that is ubiquitous in nature. DNA, virus and proteins are few examples of biological self-assembled aggregates. Artificial synthetic systems can be generated in two different ways:

- by discrete assembly (**Figure 1.1.2**) through non-covalent bond (H-bonding, π - π stacking...) in more or less well-defined microscopic organization and macroscopic features depending on their nature (layers, film...); the assembly can be templated by metal ions, such as grids, polygone and helicates (**Figure 1.1.2**, a.);

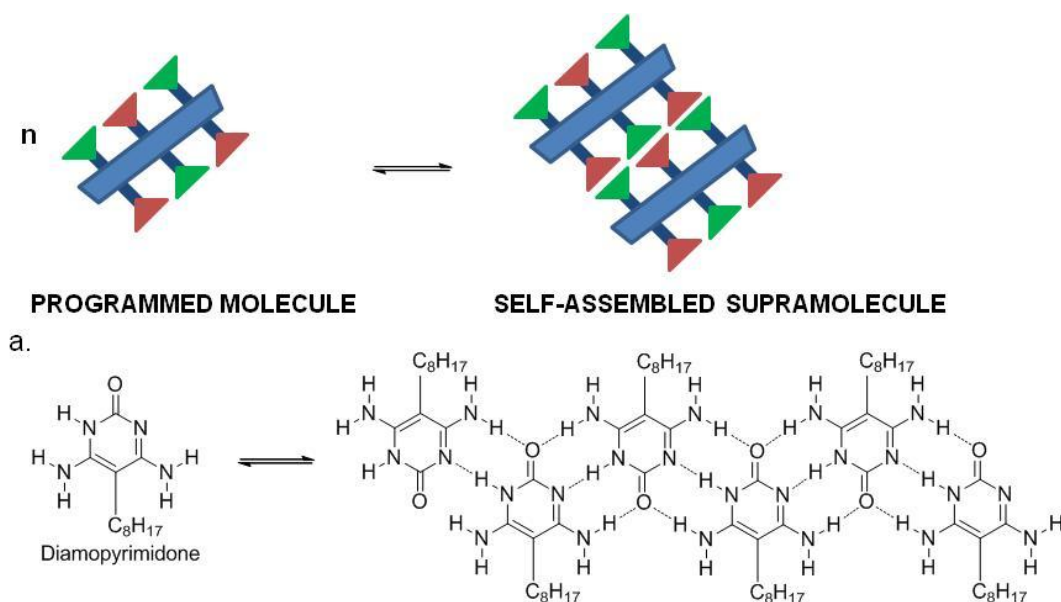


Figure 1.1.2.: Discrete assembly of supramolecules; a. DAP 1D supramolecular motif through hydrogen bonding⁷.

- by mechanical interlocking of molecules (**Figure 1.1.3**), held together by supramolecular interactions; these species are said to be topologically connected and some examples are catenanes and rotaxanes (**Figure 1.1.3**, a.). Such system are topical models for future nanoscale molecular machines.

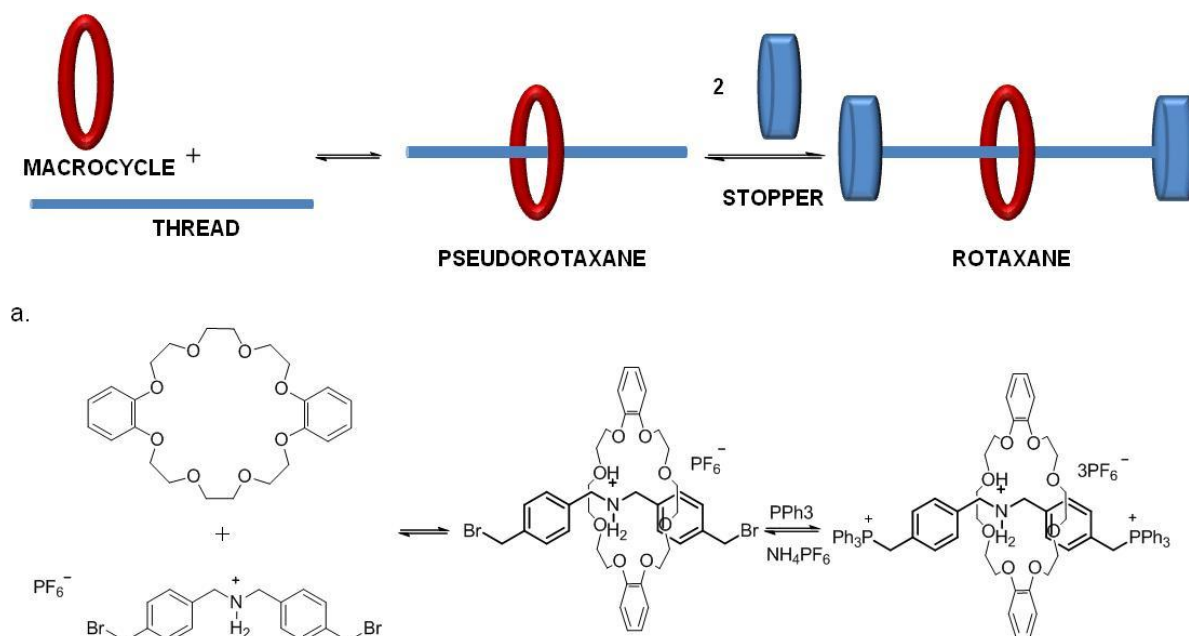


Figure 1.1.3: Synthesis of a [2]-rotaxane via threading⁸: the macrocycle first encircles the thread, origins the “pseudorotaxane”, held together by non covalent interactions, which is then converted in “rotaxane” by reacting the ends of the threaded guest with large stopper groups, preventing disassociation. a. Synthesis of a rotaxane.

Chapter I: Introduction

Self organization processes are of major interest for supramolecular science and engineering: they give access to advanced functional materials, such as supramolecular polymers, liquid crystals and lipid vesicles as well as solid-state assemblies. The aim is the self-fabrication of “smart materials” from suitable and programmed building block, a powerful alternative to nanofabrication and nanomanipulation. For these purposes a fundamental role is played by the ability of a system to select the correct molecular components for the generation of a given supramolecular entity from a collection of building blocks. This selectivity, together with the reversibility of the non-covalent interactions formed, make supramolecular chemistry a dynamic chemistry, in particular a Constitutional Dynamic Chemistry (CDC), whereby a chemical entity, be it molecular as well as supramolecular, undergoes continuous change in its constitution through dissociation into various components and reconstitution into the same entity or into different ones. The generation of diversity and the operation of selection by CDC systems have been implemented in a great number of cases involving the search for receptors, substrates, and biologically active substances, the self-assembly of dynamic nanostructures, as well as the development of constitutional dynamic aggregates and materials. In the last case, constitutional response to different stimuli or effectors opens the way towards adaptive materials, which are able to change the response of the system to physical or chemical agents, such as environmental/medium influences, phase exchange, physical stimuli (temperature, light, pressure), chemical effectors (protons, ions), morphological switching. This leads to Adaptive Chemistry and further to Evolutive Chemistry when the acquired features are conserved. The goal is to progressively discover, understand, and implement the processes that govern the evolution from inanimate to animate matter and beyond, to ultimately acquire the ability to create new forms of complex matter.⁹

1.2 Self-assembly through hydrogen-bonding

As mentioned before, self-assembly is a powerful tool to obtain complex supramolecular architectures and it is an important aspect of bottom-up approach in nanotechnology. Among the weak interactions, hydrogen bond (ca. 20kJ/mol) is widely used due to its directionality and versatility: it is the interaction between a positive dipole or charge on a hydrogen atom in the donor site (D) and an electronegative group in the acceptor site (A)¹⁰. The strength of the bonds depends on different type of D (N-H, O-H) and A (C=O, :N, C=N), on the

environmental conditions¹¹ and on the numbers of hydrogen bonds formed. In particular, to enhance binding strength in hydrogen bonding systems the usual approach is the use of multiple hydrogen bonds in an array^{12, 13}: the inspiration comes again from nature, for example from DNA (**Figure 1.2.1**), where double and triple hydrogen bonds (Watson-Crick interactions) allow the formation of the famous double helix and provide the means to read out and to replicate the information stored in it¹³.

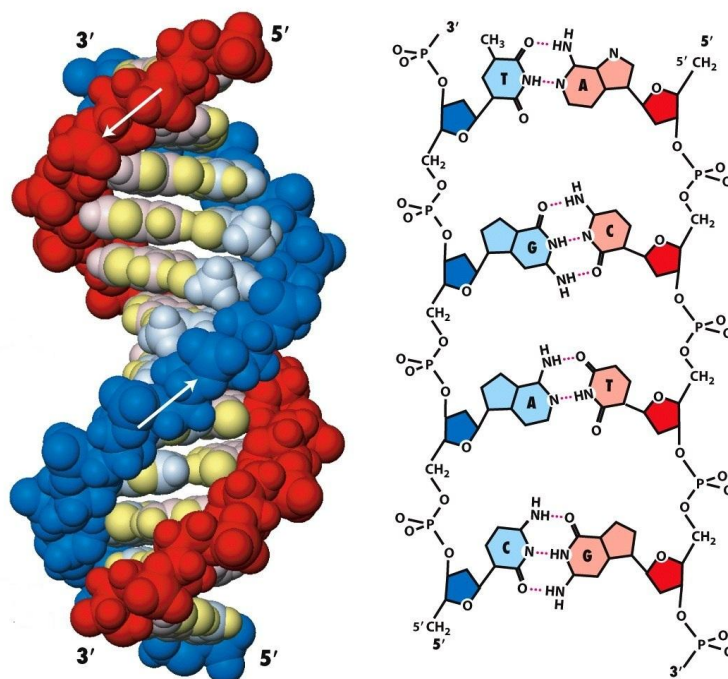


Figure 1.2.1: DNA double helix and nucleobases coupling through hydrogen bonding interactions.

Interactions between nucleic acids are provided by purine e pyrimidine bases: they are heteroaromatic modules, which are geometrically well defined and can lead to the formation of linear array of hydrogen bond donor and acceptor groups. Due to these advantages, also synthetic self-assembling systems use heteroaromatic compounds, with different arrays of donor and acceptor groups¹⁴, to obtain flexible and complex supramolecular architectures for application in nanotechnology. Recently Qin et al.¹⁵ reported a new material for solar cells which consists in a new self-assembled polythiophene copolymer (BCP) with isoorotic acids moieties and a diaminopyridine tethered fullerene (PCBP) strongly complexed through “three-point” complementary hydrogen bonding interactions (**Figure 1.2.2, a.**); cooperative effects from orthogonal noncovalent interactions, i.e. complementary hydrogen bonding and BCP self-assembly, led to not only much improved device stability, but also tunable and long-

Chapter I: Introduction

range ordered morphologies (**Figure 1.2.2**, b.) by simply adjusting the amount and nature of fullerene derivatives.

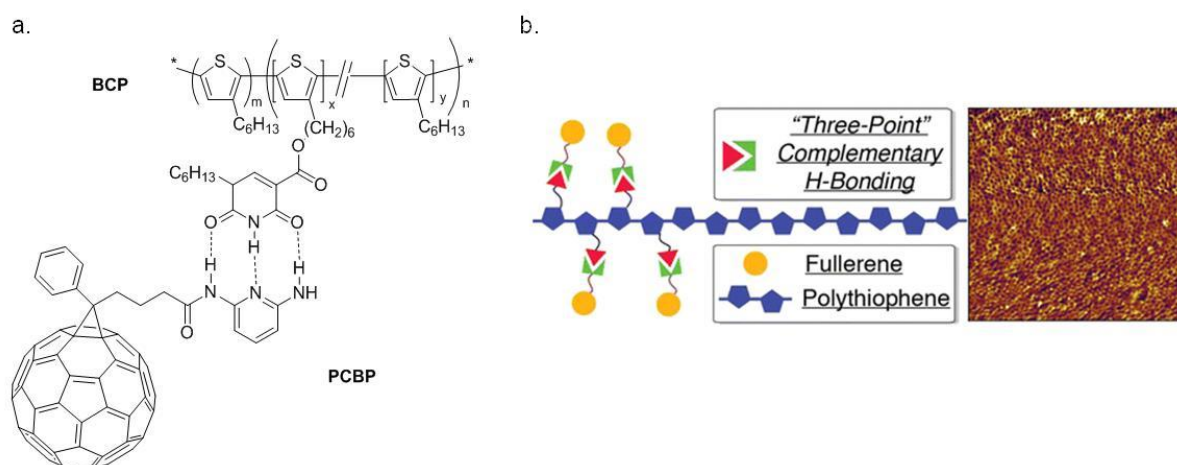


Figure 1.2.2: a. “Three point” hydrogen bond interactions between PCBP and BCP; b. Schematic representation of copolymer and AFM image of its supramolecular assemblies (figure from “Complementary Hydrogen Bonding and Block Copolymer Self-Assembly in Cooperation toward Stable Solar Cells with Tunable Morphologies”¹⁵)

2. Guanine, a special nucleobase

As mentioned before, nucleobases are excellent building blocks for construction of supramolecular aggregates. Among nucleobases, guanine is a versatile scaffold due to the array and relative orientation of H-bond donors and acceptors, which allow the formation of both linear and cyclic arrangements,¹⁶ depending on environmental conditions. Therefore in addition to linear supramolecular polymers (ribbons, **Figure 2.1**), guanine can self-assemble in discrete tetrads, known as G-quartets (**Figure 2.1**), formed through hydrogen bonding interactions which involve different site on guanine base:

- Watson-Crick site, used also in the formation of the double helix arrangement; in this case two hydrogen bond donor groups (N^1H and N^2H) are involved
- Hoogsten site, used in non-canonical base coupling, with two hydrogen bonding acceptor groups (O^6 and N^7);

Electronegative carbonylic moieties point to the center of these quartets, creating a negative charge which is stabilized through coordination of O^6 with a monovalent cation of suitable size (Na^+ , K^+).

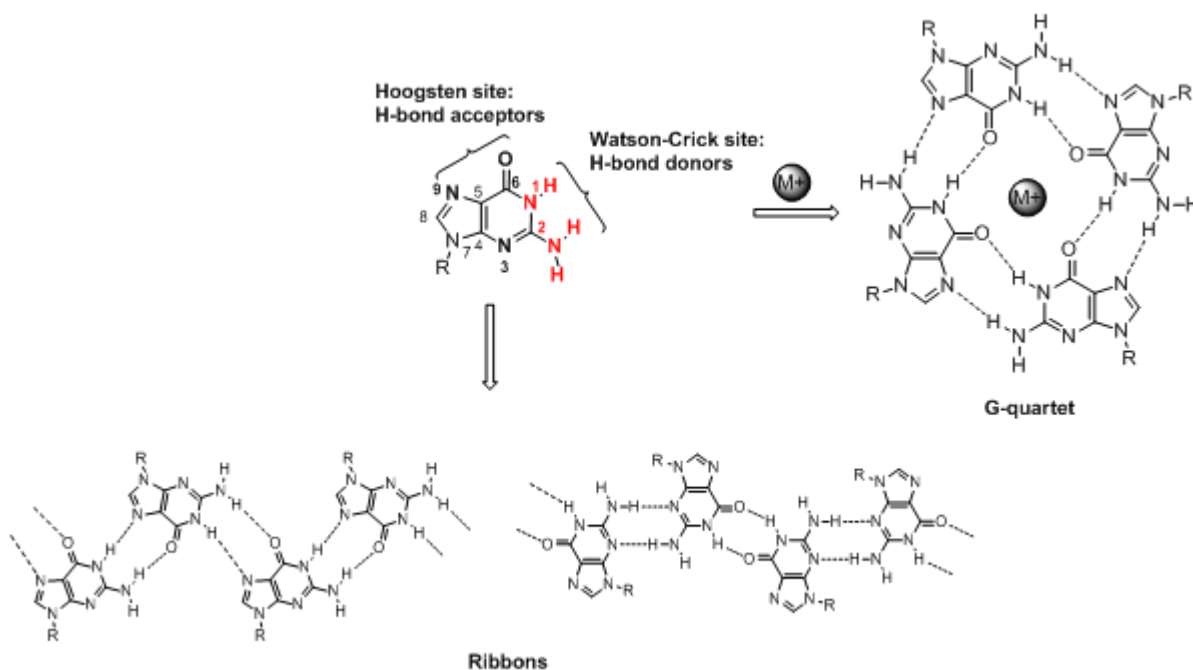


Figure 2.1: Guanine structure with hydrogen bonding acceptor (black) and donor (red) groups and possible linear and cyclic self-assembled structures.

Chapter I: Introduction

These supramolecular structures can be found both in biological context (G-quadruplex in DNA and RNA) and in organic media, with specifically modified lipophilic guanosines. In this section only G-quadruplex will be discussed: for a detailed description of lipophilic guanosines behavior see next chapter “Lipophilic guanosines”.

2.1 G-quadruplex

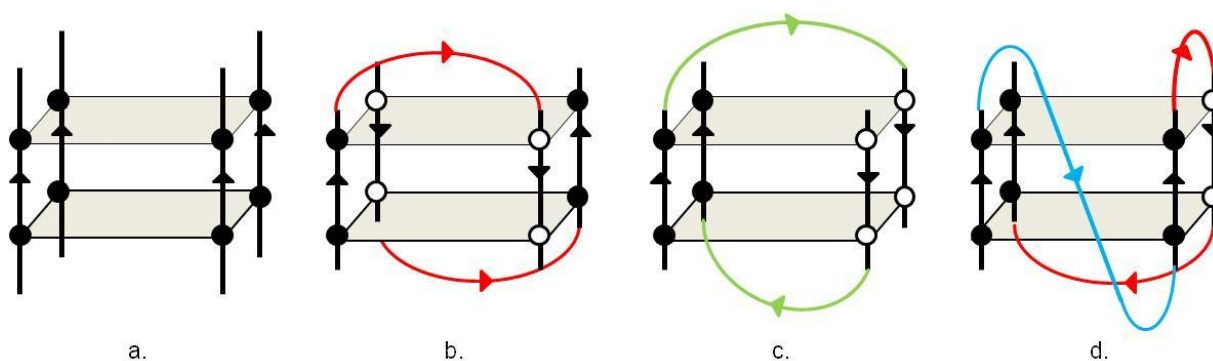
2.1.1 G-quadruplex: structure details

The right-hand double helical structure is only one of the possible conformation that DNA can adopt; among the various secondary structures, G-quadruplex is one of the most interesting due to its high stability and its potential role in DNA transcription processes.

G-quadruplex structures can form in particularly guanine-rich DNA or RNA sequences and consist in guanine tetrads (G-quartets) stacked together and stabilized by central monovalent cations; in mammalian cells this role is mainly played by K^+ , which has a higher intracellular concentration (140 mM) than Na^+ (10 mM).

The ability of guanine derivatives to form aggregates is known since 1910, when Bang¹⁷ reported gel formation of a highly concentrated solutions of guanylic acid (Guanosine monophosphate, 5'-GMP); fifty years later Gellert¹⁸ identified the G-quartet structure through X-ray diffraction of these concentrated solutions.

There are a different types of G-quadruplex structures, depending on the involvement of one or more strands, on the length and composition of G-rich sequences. They can form within a single strand of DNA or RNA (intramolecular G-quadruplex) or from the interaction of two or more strands (intermolecular G-quadruplex). The mutual orientation between these strands can be parallel or antiparallel, giving rise to four different relative strands orientations¹⁹ (**Figure 2.1.1.1**): four parallel strands (parallel stranded core), three parallel and one in the opposite direction ([3+1] core), two adjacent strands parallel and the remaining two oriented in opposite direction (up–up–down–down core), two strands across one diagonal parallel and the remaining oriented in opposite direction (up-down-up-down core). Also the glycosidic conformation of guanosines depends on strands orientation: guanines from parallel G-tracts have the same conformation, whereas those from antiparallel G-tracts have a different conformations. Usually there are little loop sequences (1-7 nucleotides) that connect G-quartets and that can be divided in four categories: edgewise, which connect two adjacent antiparallel strads; diagonal which connect two opposite antiparallel strands; double chain reversal which connect two adjacent parallel strads; V-shaped which connect two stacked tetrads.



2.1.1.1: Different type of G-quadruplex structures: tetramolecular parallel stranded core G-4 (a); bimolecular up-down-up-down core G-4 (b) with two edgewise loops (red); bimolecular up-up-down-down core G-4 (c) with two diagonal loops (green); intramolecular [3+1] core G-4 (d) with a V-shaped loop (blue) and two edgewise loops (red).

Computational studies demonstrate that G-rich regions are not randomly located *in vivo*: in human, yeast and bacterial genomes G4 motifs are over-represented in certain functional regions, such as promoters and telomeres²⁰. This specific distribution and the evolutionary conservation of these sequences suggests that G4-motifs have important functions in cells. The role of G-quadruplexes has been elucidated in some instances.

2.1.2 G-quadruplex role during DNA replication

DNA replication starts with the separation of double helix by helicase, a specific enzyme, into two strands, which template the synthesis of two new DNA molecules: the leading strand, which is continuously synthesized in the 5' to 3' direction by polymerase; the lagging strand, synthesized in the opposite direction in short separated fragments (Okazaki fragments), joined together by DNA ligase. This discontinuous replication makes the lagging strand transiently one-stranded, providing the opportunity for G4-structures formation. These structures must be resolved to continue the duplication process because the sequence that include a G-4 structure cannot serve as template until it is unfolded.²¹

G-4 unwinding is a non-specific activity of many DNA-helicases and some of these enzymes are more efficient than others: *Saccharomyces cerevisiae* Pif1 helicase is the prototypical member of the Pif1 DNA helicase family and it is an exceptionally potent G-quadruplex unwinding enzyme that prevents replication pausing at G-4 motifs²² (**Figure 2.1.2.1**). Several genetic assays reveal that in the absence of PiF1 double strand breaks occur at many of the G4 motifs that are normally bound by Pif1, causing genome instability²¹; furthermore mutations

Chapter I: Introduction

of a conserved PIF1 residue in the Pif1 family signature motif is associated with increased cancer risk²³.

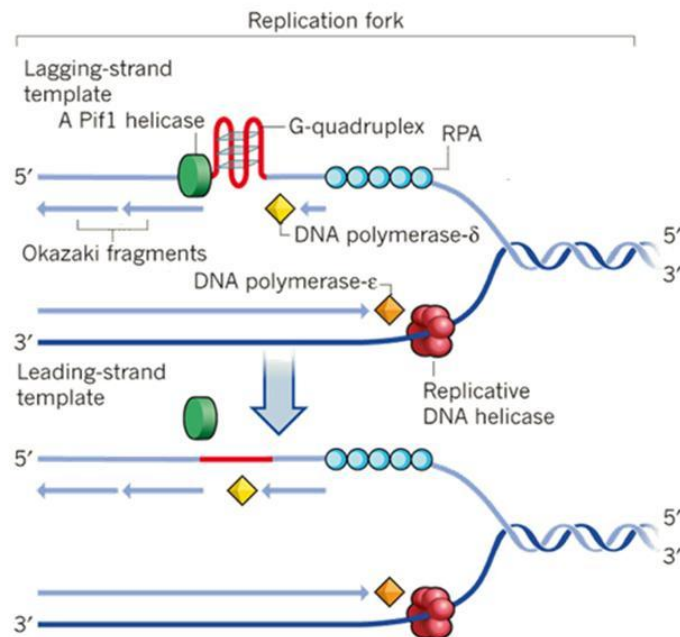


Figure 2.1.2.1: G-4 unwinding role of Pif1 helicase during DNA duplication which allows replication progress past this obstacle (figure from “DNA replication: Driving past four-stranded snags”, Sergei M. Mirkin²⁴).

2.1.3 Telomeres: target for G-quadruplex ligands

The first evidence of G-quadruplex existence *in vivo* was reported in 1987²⁵ in chromosomal telomeric DNA. Telomeres consist in repeated sequences of nucleotides at the termini of linear chromosomes, typically $d(\text{GGGTTT})_n$ in vertebrates, composed by a double-stranded region (1000 repeats of this sequence in humans) and a G-rich 3' single-stranded overhang (1-200 bases). Their function is to protect chromosomes from degradation: polymerase cannot replicate the extreme 5' end of DNA, which is then degraded and without telomeres the genome would progressively lose information. For this reason, telomere double stranded fragment becomes shorter with every cell division, leading to cell senescence. In most organisms telomerase, a telomere-dedicated reverse transcriptase which uses its RNA subunit as a template to lengthen the G-strand of the telomere, is active only in stem cells, which need to be immortal. Human telomerase is instead upregulated in most cancers (~85%) to overcome the “end replication problem” and promote lifespan of malignant cells²⁶: telomerase is therefore recognized as potential cancer-specific target for antitumoral drug discovery²⁷. It

is known that human telomeric sequence $d(\text{GGGTTA})_n$ folds spontaneously in intramolecular G-quadruplexes, stable at physiological conditions²⁸, and this structure blocks telomerase activity²⁹: in this context a variety of small molecules that can bind and stabilize G-4 structures were tested as telomerase inhibitors (**Figure 2.1.3.1**).

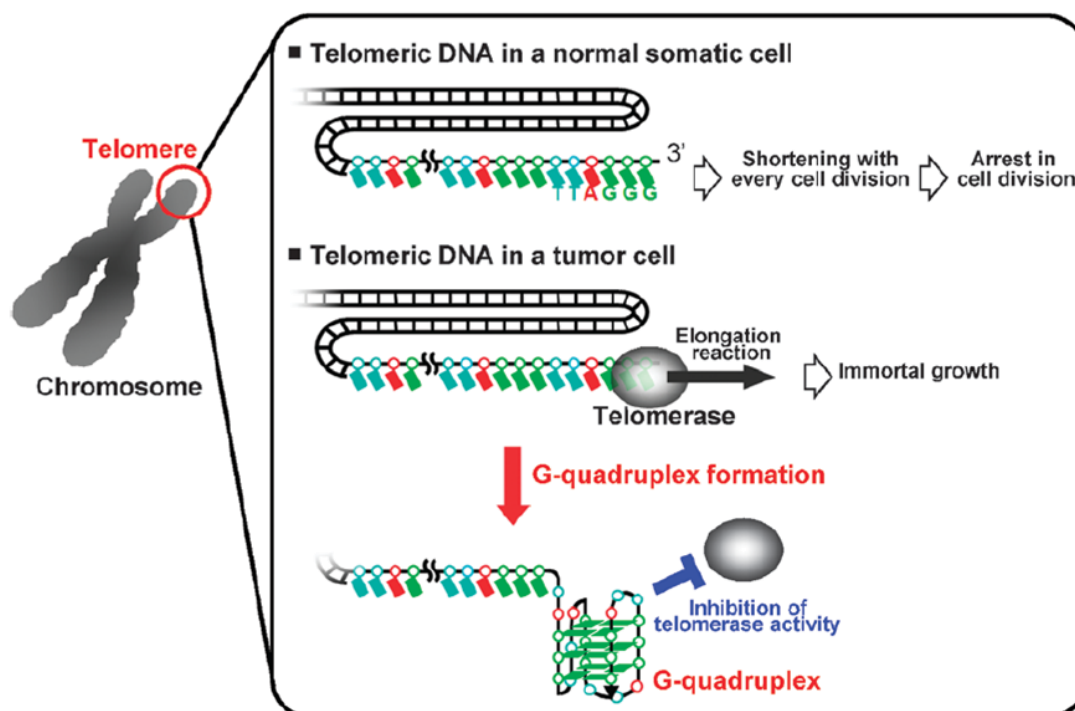


Figure 2.1.3.1: Telomeres in somatic and tumor cells: G-quadruplex as inhibitor of telomerase activity (figure from “Phtalocyanine: a new class of G-quadruplex ligands with many potential applications”³⁰).

Recognition modes between these ligands and G-quadruplex are different¹⁹:

- stacking on the ends of G-tetrads core or intercalation between G-tetrads;
- interacting with external atoms in the backbone (edge interaction);
- interacting with single stranded loops;
- groove binding;
- taking place of one or more strands in the core.

The first molecule which exhibited anti-telomerase activity was an anthraquinone³¹, but the selectivity of this ligand for G-quadruplex vs DNA helix was insufficient for biological applications; subsequent modifications in core and sidearm structure led to a new class of 3,6-disubstituted acridines³² (**Figure 2.1.3.2, a.**): these derivatives showed π - π interactions between the flat aromatic core of the ligand and the accessible G-tetrad and additional electrostatic interactions between the two protonable sidechains of the ligand and the

Chapter I: Introduction

quadruplex-grooves³³ (**Figure 2.1.3.2**, b.). At this class belongs BRACO-19, which demonstrated high efficiency as inhibitor of cancer cells proliferation³⁴.

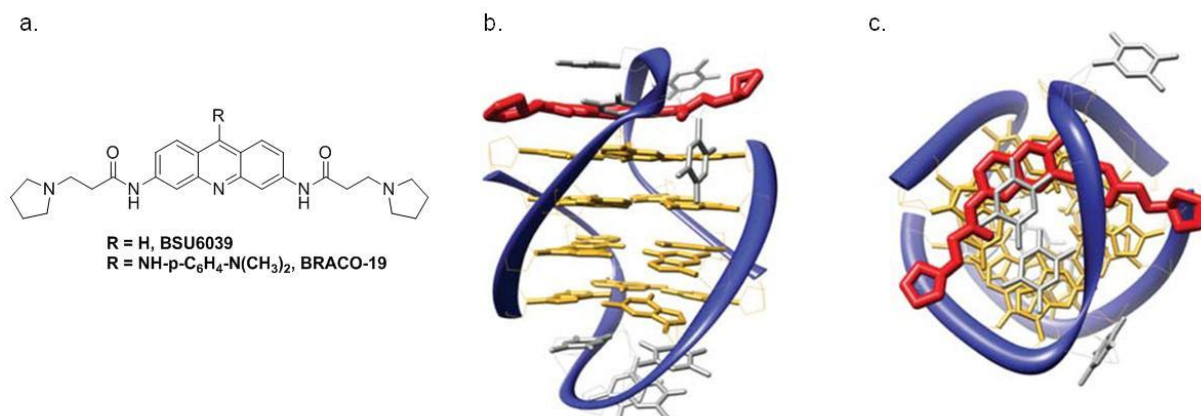


Figure 2.1.3.2: G-quadruplex acridine ligands (BSU6039 and BRACO-19, a.) and X-ray structure of BSU6039 complex with bimolecular quadruplex-DNA (d[G₄T₄G₄]₂) (figure from “A hitchhiker’s guide to G-quadruplex ligands”³³).

2.1.4 G-4 in genetic regulation

High concentrations of G-rich sequences are present in promoter regions of 50% of human genes. These regions are located near the transcriptional start site (TSS)³⁵ of genes: this finding suggests that G-4 structures in or near promoter regions may influence transcription in both negative and positive ways. One of the first examples of this system was reported by Hurley and co-workers³⁶ for oncogene *c-myc*, an important transcription factor involved in cell proliferation; *c-myc* is overexpressed in 80% of human cancer cells and this increases tumorigenesis. Transcription of this gene is mainly controlled by Nuclease Hypersensitive Element III₁, located upstream on promoter region, which contains G4 motif that can fold in G-quadruplex structures *in vitro*³⁷. Treatment of lymphoma cells with TMPyT4 (**Figure 2.1.4.1**, a.), a cationic porphyrin studied as G-quadruplex ligand, reduces *c-myc* transcription³⁸, but the same molecule has no effects in transcription in a cell line with NHEIII₁ deleted from the promoter³⁶: this reduction seems to be related to TMPyT4 interaction with G-quadruplex in NHEIII₁ region (**Figure 2.14.1**, b.).

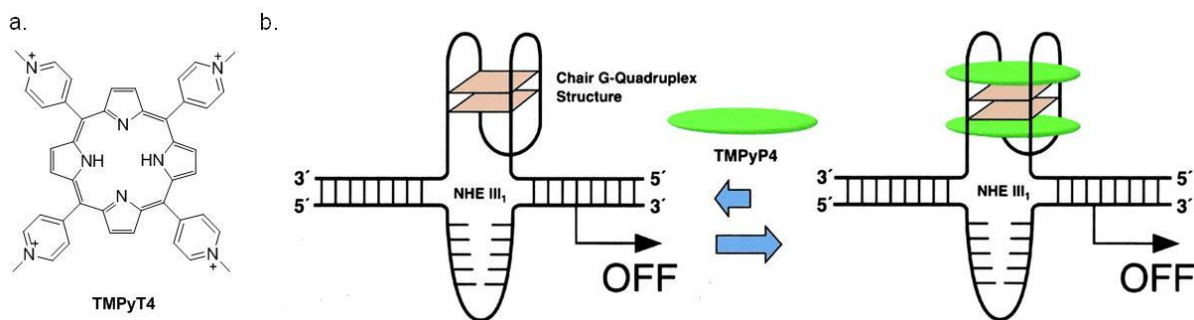


Figure 2.1.4.1: Stabilization of G-quadruplex by TMPyT4 (a) and inhibition of transcription of *c-myc* (b. from “Direct evidence for a G-quadruplex in a promoter region and its targeting with a small molecule to repress c-MYC transcription”³⁶)

2.1.5 Methods for studying G-quadruplexes

Different techniques can be used for the characterization of G-quadruplexes. The first method used was X-ray crystallography³⁹: obtain a single crystal is still a slow and uncertain procedure, but with this technique is achieved a high resolution (sometimes below 1 Å) that allow the determination of more than 50 crystal structures of G-quadruplex (available in Nucleic acid Data Bank, NDB) (**Figure 2.1.5.1, a.**). The disadvantage of X-ray method is that only the structure adopted in solid state is reported: G-quadruplex structures are frequently highly polymorphic and the crystal structure obtained represent the form that crystallizes more easy, not the favored one in solution. For collecting information on G-quadruplex structures in solution, NMR is a very useful technique:⁴⁰ useful information can be gathered simply by 1-D ¹H NMR spectroscopy, where characteristic guanine N¹H imino proton shift indicates its involvement in hydrogen bonds; multidimensional spectra, and sometimes partial labeling (¹⁵N, ¹³C, ³¹P), are needed for resonance assignment and backbone conformation determination (**Figure 2.1.5.1, b.**).

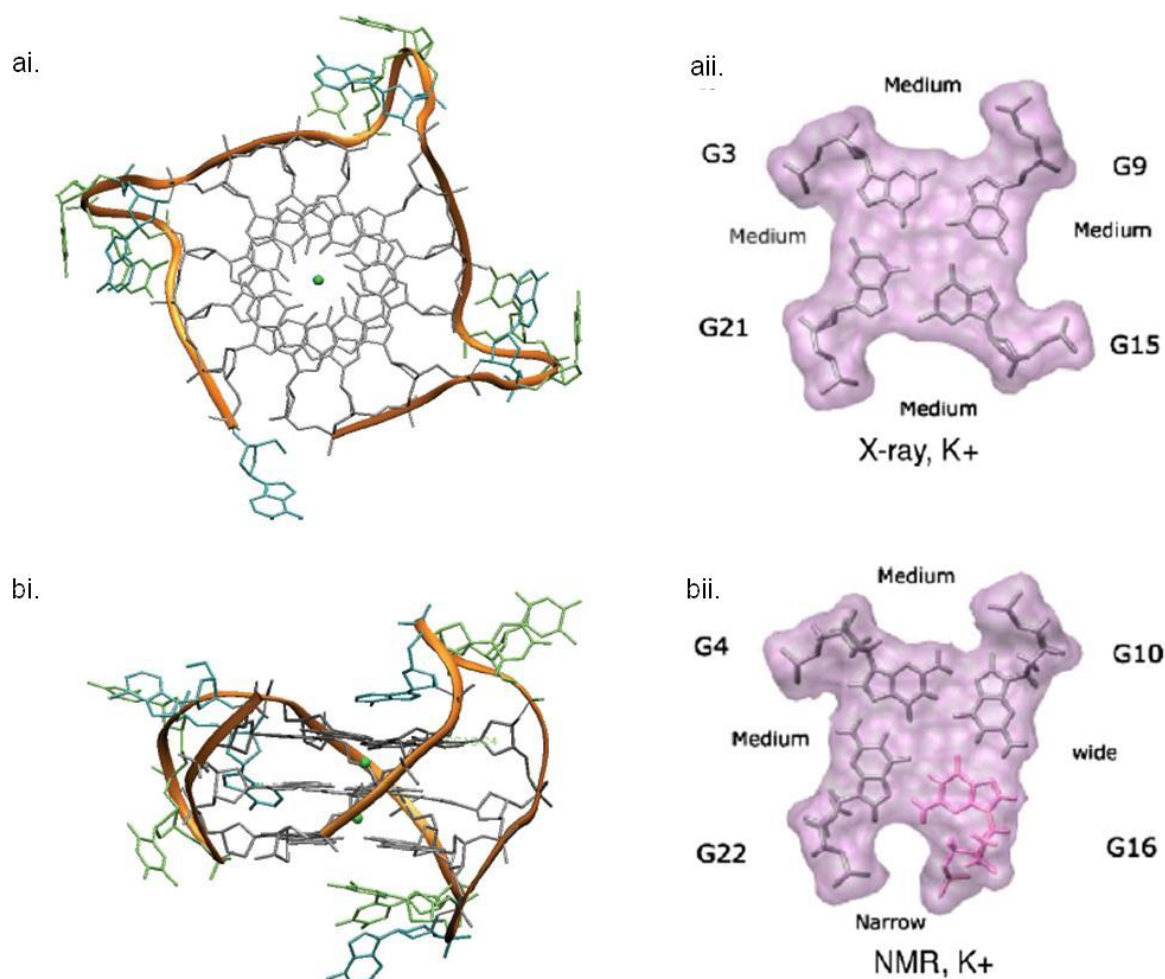


Figure 2.1.5.1: Structure of human unimolecular telomeric quadruplex formed from the sequence d[AGGG(TTAGGG)3]: K⁺ form A determined by crystallography (ai⁴¹, aii³⁹) and K⁺ form B determined by NMR (bi⁴¹, bii³⁹).

Circular Dichroism spectroscopy is a widely used technique to study several chiral 3D structures in solution and can be employed to identify different G-quadruplex structures^{42,43}. In CD spectroscopy, circularly polarized light is shone through a solution, and if there is a chiral species in the solution, it will generally interact asymmetrically with the enantiomeric forms of light, and the asymmetry varies with wavelength; the main aim of this method is to assign the absolute configuration of a chiral molecule, but it can be used in studying subtle conformation changes and supramolecular interactions.

A CD signal is observed in solution when two or more strongly absorbing chromophores are chirally oriented with respect to each other: the exciton spectrum is characterized by the presence of two bands with opposite signs, where λ max in absorption corresponds, or nearly corresponds, to zero CD intensity⁴⁴. In the case of G-quadruplex, the chromophore is the guanine moiety, which has two absorption bands (240-290 nm) corresponding to π - π^*

transitions at ca. 279 nm (short axis polarized) and 248 nm (long axis polarized) (**Figure 2.1.5.2, a.**). G-quadruplex CD spectra arise from mutual rotation of piled G-tetrads, that cause a chiral exciton coupling between transition dipole moments located in near-neighbour guanines. G-quartet has two heterotopic faces, head (black quartet, **Figure 2.1.5.2, b.**) and tail (red quartet, **Figure 2.1.5.2, b.**), leading to two different stacking modes:

- homopolar stacking, head-to-tail configuration;
- heteropolar stacking, where a tetrads stack onto the adjacent one through the opposite face (head-to-head or tail-to-tail).

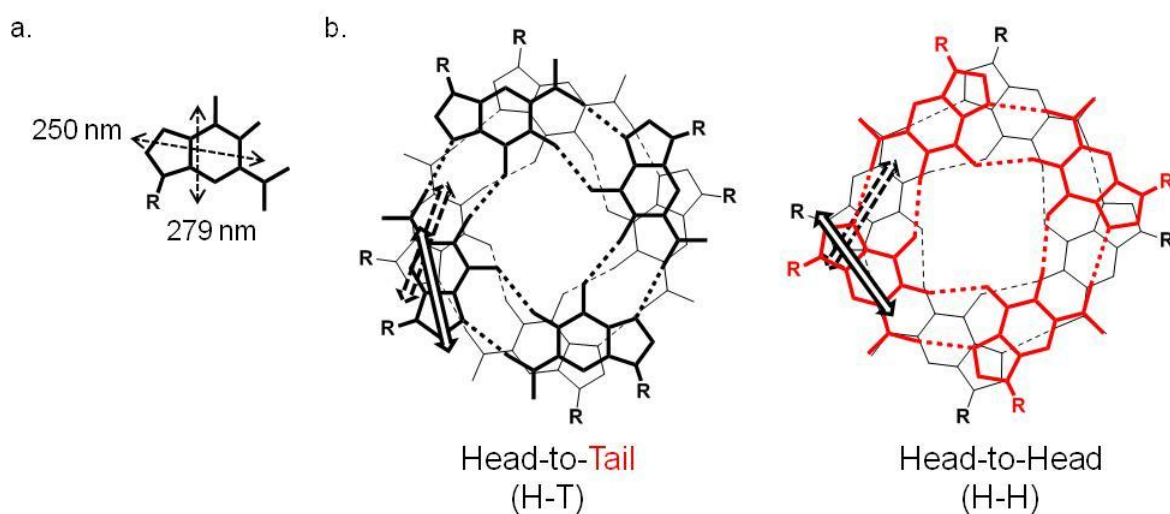


Figure 2.1.5.2: a. Representation of $\pi\text{-}\pi^*$ axis polarized transitions in guanine structure; b. Two possible stacking modes of guanine octamers.

This two stacking modes origin different excitons in CD spectra (at the 248 nm transition), which arise from the relative orientation of the transition moments located in the closest guanines in stacked tetrads. Rotational Strength R_{0a} , which is related to CD band area (and consequently to CD signal intensity), of an electronic transition from ground state 0 to excited state a is the product of electric and magnetic transition moment associated to this specific transition; therefore to be CD active a transition must have both electric and magnetic moment. In the case of two stacked G-tetrads, the magnetic moment is due to the coupling of two non-coplanar electric moments of guanine in adjacent quartets (**Figure 2.1.5.3, a.**); in this case there are two possible non-degenerative coupling modes which lead to parallel or antiparallel magnetic moment with respect to the electric one. Therefore the product of electric and magnetic moments gives rise to one positive (parallel mutual orientation) and one negative (antiparallel orientation) rotational strength (**Figure 2.1.5.3, b.**), with the lower

energy coupling at higher wavelength. For heteropolar stacking a positive exciton couplets is expected, while a negative exciton couplets is predicted for homopolar stacking (**Figure 2.1.5.3, c.**).

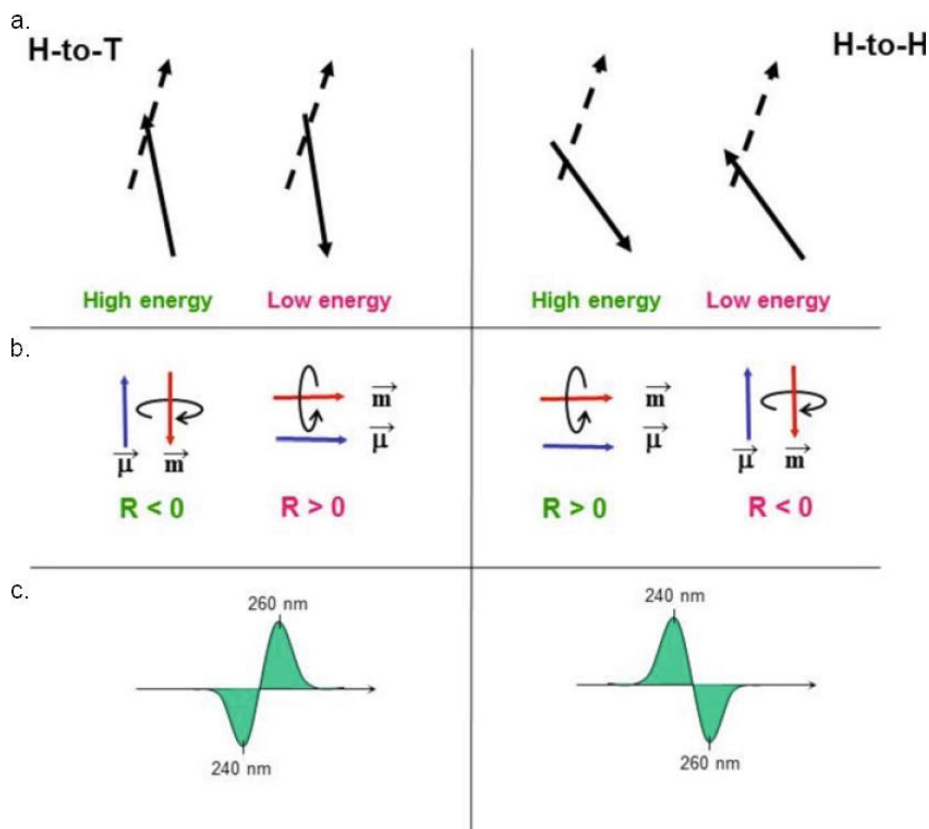


Figure 2.1.5.3: Origin of excitons in stacked guanine quartets CD spectra (from “A non-empirical chromophoric interpretation of CD spectra of DNA G-quadruplex structures”⁴²)

Considering now the case of parallel G4-DNAs, in which four strands with all glycosidic bonds in *anti* conformation run parallel to each other, with an H-to-T orientation of adjacent quartets: there are a negative peak at ~ 240 nm and a positive band at ~ 260 nm, which are in agreement with the positive exciton couplets expected for this stacking way.

More complicated is the case of an antiparallel G4-DNA, where the G-quartet polarity alternate due to alternation of guanosine glycosidic bond conformations (*syn/anti*) along each strand, leading to heteropolar stacking of adjacent guanines. In addition to a negative exciton couplet, as expected for H-to-H or T-to-T arrangement, centered at ~ 250 nm, a positive peak at around 290 nm is observed: in 2002 Wen and Gray⁴⁵ specifically proposed that a positive band in CD spectrum appears at 260 nm in case of homopolar stacking and at longer wavelength in case of heteropolar stacking (**Figure 2.1.5.4, a.**).

Chapter I: Introduction

Few years later⁴⁶ Gray et al. performed CD spectral calculations with the dipole–dipole approximation of two G-quartets stacked with the same or opposite polarity, confirming both the computations of Gottarelli et al.⁴⁷ on homopolar stacking system and the positive band at 290 nm related to heteropolar G-quartet stacking. These studies suggest a direct relationship between CD bands of G4-DNAs and adjacent G-quartets stacking mode (homo- or heteropolar), but the CD spectra cannot be directly related to relative strands orientation (Figure 2.1.5.4, b.).

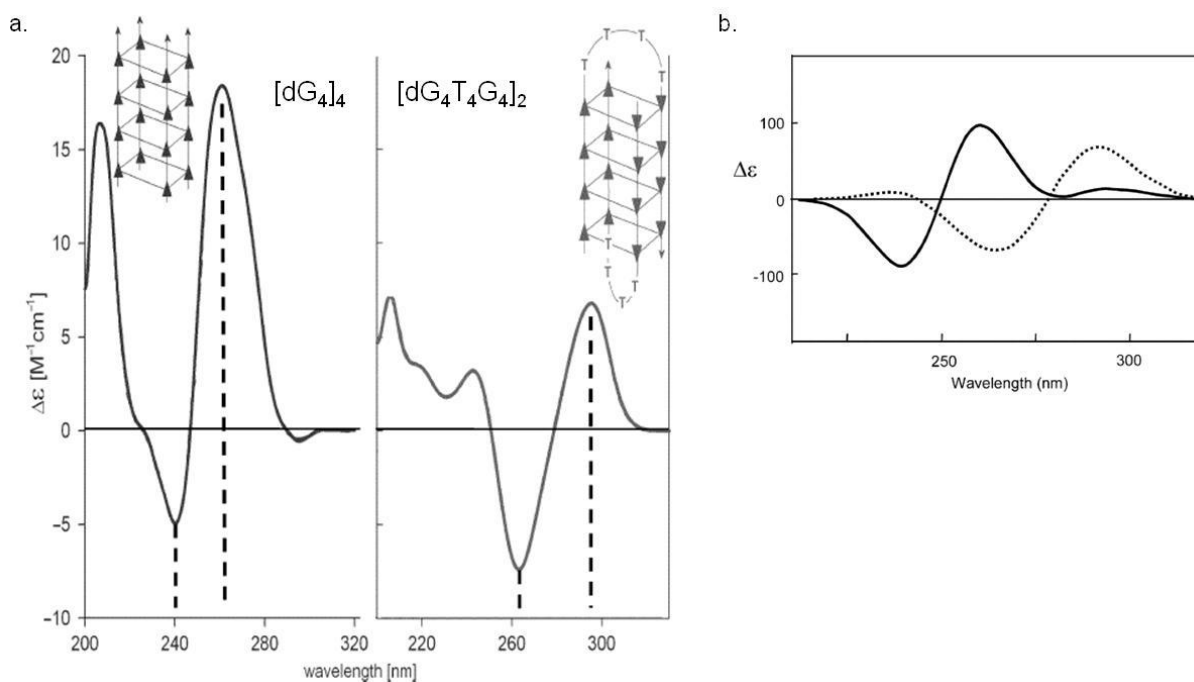


Figure 2.1.5.4: a. Experimental CD spectra of G-DNAs: on the left the parallelstranded quadruplex $[d(G_4)]_4$ stabilized by 16 mM K⁺, on the right Na⁺-induced antiparallel bimolecular quadruplex of $[d(G_4T_4G_4)]_2$ ⁴⁸; b. calculated CD spectra of two G-quartets stacked in the H-to-T (solid line) or H-to-H (dashed line) orientation⁴⁶.

3. Conclusions

Supramolecular chemistry represents a step forward with the respect to molecular chemistry, giving us the possibility of programming complex and organized systems from simple and smart molecules. In this context, guanine moiety is very useful, due to its particular chemical structure and proprieties: the countless biological roles played by G-quadruplex structures and the possibility of controlling their formation is of crucial interest in the development of novel therapies and drugs. Next chapter will be focused on nanotechnological applications of a different class of guanine derivatives: lipophilic guanosines.

Bibliography

1. Steed, J. W.; Turner, D. R.; Wallace, K., *Core Concepts In Supramolecular Chemistry And Nanochemistry*. Wiley: 2007.
2. Lehn, J. M., *Chemical Society Reviews* **2007**, 36 (2), 151-160.
3. Wolf, K. L.; Frahm, H.; Harms, H., *Z. Phys. Chem. (B)* **1937**, 36, 137.
4. Lehn, J. M., *Pure And Applied Chemistry* **1978**, 50 (9-10), 871-892.
5. Schalley, C. A., *Analytical Methods In Supramolecular Chemistry*. Wiley Online Library: 2007; Vol. 2.
6. Lehn, J. M., *Angewandte Chemie-International Edition In English* **1988**, 27 (1), 89-112.
7. Lehn, J. M.; Mascal, M.; Decian, A.; Fischer, J., *Journal Of The Chemical Society-Perkin Transactions 2* **1992**, (4), 461-467.
8. Chiu, S. H.; Rowan, S. J.; Cantrill, S. J.; Stoddart, J. F.; White, A. J. P.; Williams, D. L., *Chemistry-A European Journal* **2002**, 8 (22), 5170-5183.
9. Lehn, J. M., *Angewandte Chemie-International Edition* **2013**, 52 (10), 2836-2850.
10. Emsley, J., *Chemical Society Reviews* **1980**, 9 (1), 91-124.
11. Hunter, C. A., *Angewandte Chemie-International Edition* **2004**, 43 (40), 5310-5324.
12. Sherrington, D. C.; Taskinen, K. A., *Chemical Society Reviews* **2001**, 30 (2), 83-93.
13. Sijbesma, R.; Meijer, E., *Chemical Communications* **2003**, (1), 5-16.
14. Zimmerman, S. C.; Corbin, P. S., Heteroaromatic Modules For Self-Assembly Using Multiple Hydrogen Bonds. In *Molecular Self-Assembly Organic Versus Inorganic Approaches*, Springer: 2000; Pp 63-94.
15. Li, F.; Yager, K. G.; Dawson, N. M.; Yang, J.; Malloy, K. J.; Qin, Y., *Macromolecules* **2013**, 46 (22).
16. Rivera, J. M., Functional Assemblies Made From Supramolecular G-Quadruplex. In *Guanine Quartet. Structure And Application*, 2013, Ed. Rcs Publishing: P 15.
17. Bang, I., *Biochem. Z.* **1910**, 26, 293.
18. Gellert, M.; Lipsett, M. N.; Davies, D. R., *Proc. Natl Acad. Sci. Usa* **1962**, 48, 2013.
19. Phan, A., *Febs Journal* **2010**, 277 (5), 1107-1117.
20. Huppert, J.; Balasubramanian, S., *Nucleic Acids Research* **2005**, 33 (9), 2908-2916.
21. Bochman, M.; Paeschke, K.; Zakian, V., *Nature Reviews Genetics* **2012**, 13 (11), 770-780.

Chapter I: Introduction

22. Paeschke, K.; Bochman, M.; Garcia, P.; Cejka, P.; Friedman, K.; Kowalczykowski, S.; Zakian, V., *Nature* **2013**, 497 (7450), 458-+.
23. Chisholm, K.; Aubert, S.; Freese, K.; Zakian, V.; King, M.; Welcsh, P., *Plos One* **2012**, 7 (2).
24. Mirkin, S., *Nature* **2013**, 497 (7450), 449-450.
25. Henderson, E.; Hardin, C.; Walk, S.; Tinoco, I.; Blackburn, E., *Cell* **1987**, 51 (6), 899-908.
26. Kim, N.; Piatyszek, M.; Prowse, K.; Harley, C.; West, M.; Ho, P.; Coviello, G.; Wright, W.; Weinrich, S.; Shay, J., *Science* **1994**, 266 (5193), 2011-2015.
27. Neidle, S.; Parkinson, G., *Nature Reviews Drug Discovery* **2002**, 1 (5), 383-393.
28. Neidle, S.; Parkinson, G., *Current Opinion In Structural Biology* **2003**, 13 (3), 275-283.
29. Zahler, A.; Williamson, J.; Cech, T.; Prescott, D., *Nature* **1991**, 350 (6320), 718-720.
30. Yaku, H.; Fujimoto, T.; Murashima, T.; Miyoshi, D.; Sugimoto, N., *Chemical Communications* **2012**, 48 (50), 6203-6216.
31. Sun, D.; Thompson, B.; Cathers, B.; Salazar, M.; Kerwin, S.; Trent, J.; Jenkins, T.; Neidle, S.; Hurley, L., *Journal Of Medicinal Chemistry* **1997**, 40 (14), 2113-2116.
32. Haider, S.; Parkinson, G.; Neidle, S., *Journal Of Molecular Biology* **2003**, 326 (1), 117-125.
33. Monchaud, D.; Teulade-Fichou, M., *Organic & Biomolecular Chemistry* **2008**, 6 (4), 627-636.
34. Gunaratnam, M.; Greciano, O.; Martins, C.; Reszka, A.; Schultes, C.; Morjani, H.; Riou, J.; Neidle, S., *Biochemical Pharmacology* **2007**, 74 (5), 679-689.
35. Huppert, J.; Balasubramanian, S., *Nucleic Acids Research* **2007**, 35 (2), 406-413.
36. Siddiqui-Jain, A.; Grand, C.; Bearss, D.; Hurley, L., *Proceedings Of The National Academy Of Sciences Of The United States Of America* **2002**, 99 (18), 11593-11598.
37. Simonsson, T.; Pecinka, P.; Kubista, M., *Nucleic Acids Research* **1998**, 26 (5), 1167-1172.
38. Han, H.; Langley, D.; Rangan, A.; Hurley, L., *Journal Of The American Chemical Society* **2001**, 123 (37), 8902-8913.
39. Campbell, N.; Parkinson, G., *Methods* **2007**, 43 (4), 252-263.
40. Da Silva, M., *Methods* **2007**, 43 (4), 264-277.
41. Burge, S.; Parkinson, G.; Hazel, P.; Todd, A.; Neidle, S., *Nucleic Acids Research* **2006**, 34 (19), 5402-5415.

Chapter I: Introduction

42. Masiero, S.; Trotta, R.; Pieraccini, S.; De Tito, S.; Perone, R.; Randazzo, A.; Spada, G., *Organic & Biomolecular Chemistry* **2010**, 8 (12), 2683-2692.
43. Randazzo, A.; Spada, G.; Da Silva, M.; Chaires, J.; Graves, D., *Quadruplex Nucleic Acids* **2013**, 330, 67-86.
44. Superchi, S.; Giorgio, E.; Rosini, C., *Chirality* **2004**, 16 (7), 422-451.
45. Wen, J.; Gray, D., *Biochemistry* **2002**, 41 (38), 11438-11448.
46. Gray, D.; Wen, J.; Gray, C.; Repges, R.; Repges, C.; Raabe, G.; Fleischhauer, J., *Chirality* **2008**, 20 (3-4), 431-440.
47. Gottarelli, G.; Masiero, S.; Spada, G., *Enantiomer* **1998**, 3 (6), 429-+.
48. Kypr, J.; Kejnovska, I.; Renciuik, D.; Vorlickova, M., *Nucleic Acids Research* **2009**, 37 (6), 1713-1725.

*Chapter II: Structure and behaviour
of lipophilic guanosines*

1. Introduction: how the story began¹

“Water appears to be an indispensable solvent for the autoassociation of guanosine [...] organic solvents give rise to poorly organised aggregates”: with this sentence Guschlbauer² explained the shared idea that guanosines can assemble only in aqueous media, as reported in many examples in literature since the discovery of gelation ability of guanylic acid (5'-GMP)³.

Our group started the research on the supramolecular behavior of guanine-related compounds in late 80's with the observation of the lyotropic properties exhibited by 2'-deoxyguanylyl-(3'-5')-2'-deoxyguanosine (d(GpG)) sodium salt in water⁴ (see **Figure 1.1**). After this an extensive investigation on several hydrophilic guanosine and guanine-related derivatives allowed us to demonstrate that these lyomesophases were originated through a stepwise supramolecular organization of the guanine bases where the G-quartet array played the role of intermediate building block: it is the piling up of G-quartets that produces the anisotropic rods responsible for the existence of the mesophases⁵. These columnar structures are glued together by sodium ions, that coordinate stacked G-quartets.

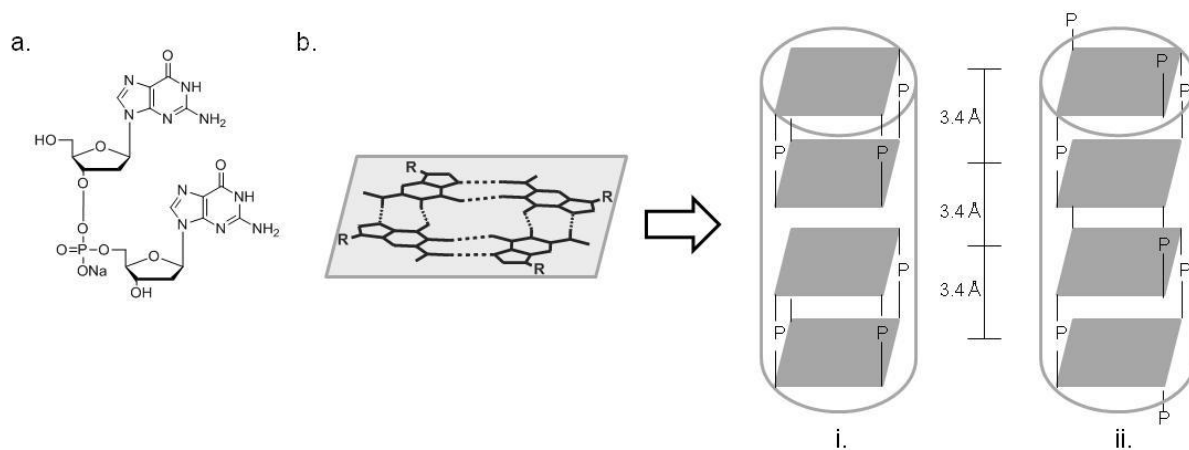


Figure 1.1: (a.) 2'-deoxyguanylyl-(3'-5')-2'-deoxyguanosine (d(GpG)) sodium salt and a sketch of two possible models for the rod structure formed by guanosine tetramers (grey rhombus): (a) piling of discrete pseudooctamers and (b) continuous array of cross-linked tetramers (P indicates the sugar-phosphodiesteric bridge). The distance between layers inside and among the pseudooctamers in the first case and between tetrads in the second case is the same, around 3.4 Å (X-ray experimental data)⁴.

In order to study guanosine behavior in absence of H-bonding competitors like water molecules, our group decided to synthesize lipophilic derivatives (LGs) which maintain the donor and acceptor groups in the nucleobase, but with long aliphatic chain in the sugar moiety

Chapter II: Structure and behaviour of lipophilic guanosines

(G, dG, and GAce, **Figure 1.2**); furthermore also guanine was modified with alkyl groups in N⁷ position to obtain lipophilic compounds (guanine, **Figure 1.2**).

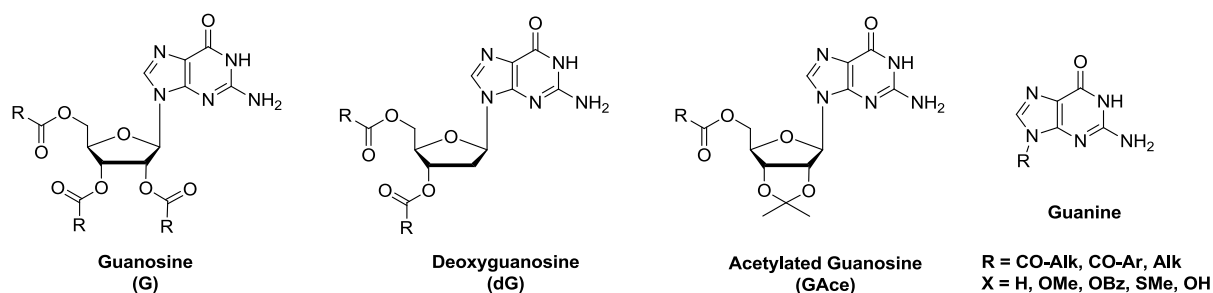


Figure 1.2: Structures of lipophilic guanosines and guanines.

From the very beginning, it was evident that these compounds can indeed easily self-assemble in organic solvents: in the next section the different ways of guanosines self-organization will be discussed in detail.

2. Self-assembly of lipophilic guanosines

2.1 Self-assembly in presence of metal ions

The previous experience with guanosine phosphates in water, where G-quartet structures sandwiching alkali metal ions are formed, inspired the following idea: maybe the lipophilic guanosines (LGs) could capture ions from water and transfer them into the organic phase, just as crown ethers do. To prove this, a simple experiment was performed⁶: in a test tube a yellow water solution of potassium picrate (KPic) and a colorless chloroform solution of a lipophilic guanosine, 3',5'-didecanoyl-2'-deoxyguanosine (dG(C10)₂, **I**) are shaken for a few minutes and “the yellow color” migrates from water to chloroform (**Figure 2.1.1**, a.). As potassium picrate is completely insoluble in chloroform, the appearance of the color in the organic solution is an evidence of the ionophoric behavior of the LG aggregate. The NMR spectrum of the LG/K⁺ complex was clearly different from that of the LG molecule before extraction, and the determination of the complex stoichiometry was straightforward: we had an 8:1 LG/K⁺ ratio (the octamer) when a little potassium picrate was present; with more potassium picrate, a 4:1 LG/K⁺ structure (the *pseudo*-polymer) was formed. NMR and circular dichroism (CD) evidences indicated that both the octamer and the *pseudo*-polymer structures result from G-quartets stacking (**Figure 2.1.1**, b.).⁷

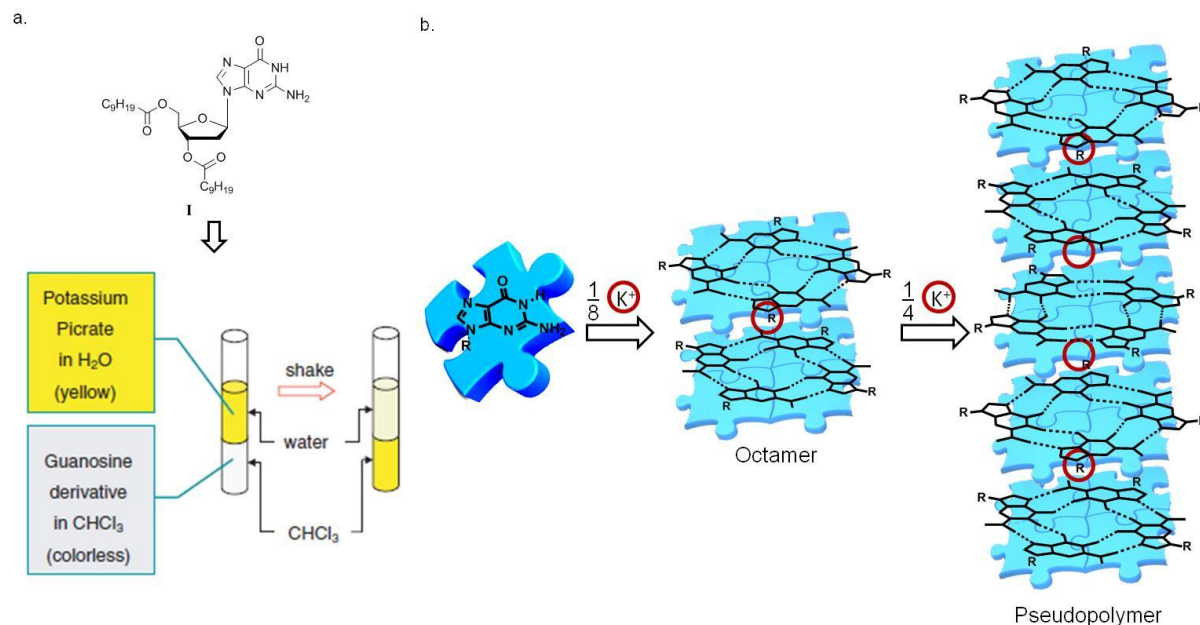


Figure 2.1.1: a. The set-up of the extraction experiment (from “The Stepwise Supramolecular Organisation of Guanosine Derivatives”⁷); b. The cation directed self-assembly of a lipophilic guanosine.

While our group were publishing our first results on LGs, Jeff Davis (University of Maryland) published similar experiments with lipophilic isoguanosines⁸. A fruitful cooperation soon started, which led first to the determination of the solution structure of the octamer, the first detectable intermediate in the cation-directed self-assembly of our LGs, by NMR spectroscopy⁹. This octameric assembly is very robust and its stability is impressive for a noncovalent assembly. The ¹H-NMR spectra of **I**, essentially temperature independent over more than 100°C, show two sets of signals in a 1:1 ratio corresponding each to nucleosides with different glycosydic conformation, *syn* and *anti* (**Figure 2.1.2**, a.).

Another stereochemical consequence to the cation-templated self-assembly of guanosine derivatives is the mutual orientation between the two stacked quartets, which have diastereotopic faces, known as head (H) and tail (T) (**Figure 2.1.2**, b.). In principle, the two quartets in the octamer can be arranged in three different ways: H-to-T (*C*₄ symmetry, homopolar stacking), H-to-H and T-to-T (*D*₄ symmetry, heteropolar stacking) (**Figure 2.1.2**, c.).

Therefore, considering these two stereochemical aspects (*syn/anti* glycosydic conformation and relative G-quartets orientation) several diastereoisomers are possible for the octamer LG₈K⁺. Remarkably, NMR data indicated that the octameric structure of dG(C10)₂ was a single diastereomer of *C*₄ symmetry and that in one G-quartet, all monomers had a *syn* conformation, while the other tetramer had an “all-*anti*” conformation. Furthermore nuclear-

Chapter II: Structure and behaviour of lipophilic guanosines

Overhauser-effect (NOE) interactions indicated a relative orientation with the head side of the “all-*anti*” G-quartet facing the tail side of the “all-*syn*” G-quartet (**Figure 2.1.2, c.**). This stereoselectivity and stereoregularity for the octameric noncovalent assembly is striking: the X-ray structure of 5-t-butyldimethylsilyl-2,3-isopropylidene-guanosine (**II**) obtained by Davis group¹⁰ confirm for this derivative a head-to-tail arrangement (**Figure 2.1.2, d.**), where guanosine conformation is “all-*syn*” in a quartet and “all-*anti*” in the other. Furthermore, the picrate anion is not passive, as it contributes to keep together the complex structure by means of hydrogen bonds with the exocyclic NHs of two different quartets: this binding contribution of the picrate anion was also evident from an ESI-MS study¹¹.

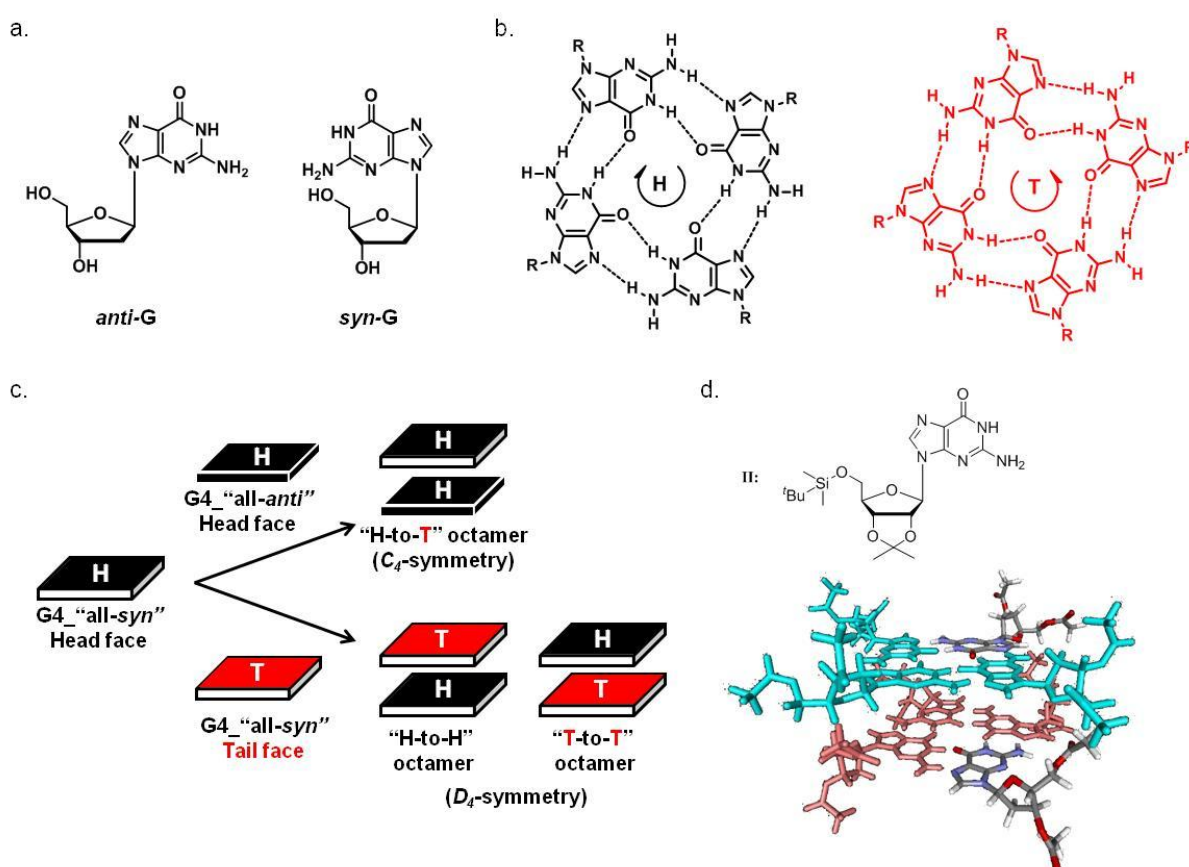


Figure 2.1.2: a. Glycosidic *syn* and *anti* conformations of guanosine; b. Two diastereotopic faces of guanosine; head (H) with a clockwise direction of hydrogen bondings and tail (T, anti-clockwise arrow); c. Schematic drawing of C_4 -symmetric octamer, with an all-*syn* G-quartet (white) with its tail-side (T, red) stacks on the head-side (H, black) of an all-*anti* (black) G-quartet, and a D_4 -symmetric octamer with two all-*syn* G-quartet stack facing their tail sides; d. The structure of the LG_8K^+ octameric complex (the metal ion at the center is not shown for clarity): an all-*anti* G-quartet (three molecules are colored in light blue) with its head side stacks on the tail side of an all-*syn* G-quartet (three molecules are colored in red).

Chapter II: Structure and behaviour of lipophilic guanosines

Subsequently, our group solved the solution structure of the $(\text{LG}_4 \cdot \text{K}^+)_n$ pseudo-polymer formed by **I** by NMR and small-angle neutron scattering (SANS) spectroscopy¹²: this assembly is stable over a temperature range of approximately 100 °C and ¹H-NMR spectra of the polymeric aggregate are relatively simple, showing three sets of signals (not interconverting on the NMR chemical shift time scale) in a 1:1:1 ratio. Each set corresponds to guanosine monomers with a different conformation and, like the C_4 -symmetric $\text{LG}_8 \cdot \text{K}^+$ octamer, each G-quartet within the polymer is homogeneous in terms of its rotamer composition: NMR data are consistent with a structure composed of three distinct G-quartets displaying an all-*anti* (A), an all-*syn1* (S1), and an all-*syn2* (S2) arrangement. The polymer is then a repetition of a dodecamer building block composed from these three different types of stacked G-quartets and, among the three possible combinations (AS1S2, AS2S1, and S1AS2) only the first is observed; in addition, considering the diastereotopicity of the quartet faces, eight (2^3) different relative orientations of the A, S1, and S2 quartets are possible, in principle, for the AS1S2 arrangement. NOESY experiments confirm that the AS1S2 dodecamer is present as a unique stereoisomer: the head side of the A quartet faces the tail side of the S1 quartet, while the head side of the S1 quartet faces the tail side of the S2 quartet. Finally, the following dodecamer repetition sequence is observed in the polymer: $[(\text{AS1S2}) (\text{S2S1A})]_n$, wherein two “all-*anti*” quartets A and two “all-*syn*” quartets S2 are close together, arranged in a tail-to-tail and a head-to-head orientation, respectively (**Figure 2.1.3**).

It should be noted that the stereochemistry of AS1 arrangement is similar to that reported for C_4 -symmetric octamer $\text{LG}_8 \cdot \text{K}^+$, suggesting that the octamer presumably represents the first step of aggregation. The stereochemical regularity of these columnar polymeric G-aggregates is truly amazing as far as the rotamers around the glycosidic bond within each G-quartet, the repeated sequence of the G-quartets along the columns, and their relative stacking orientation are concerned. Owing to the hetropolar stacking modes of all the contiguous G-dodecamers, the polymer has D_4 symmetry.

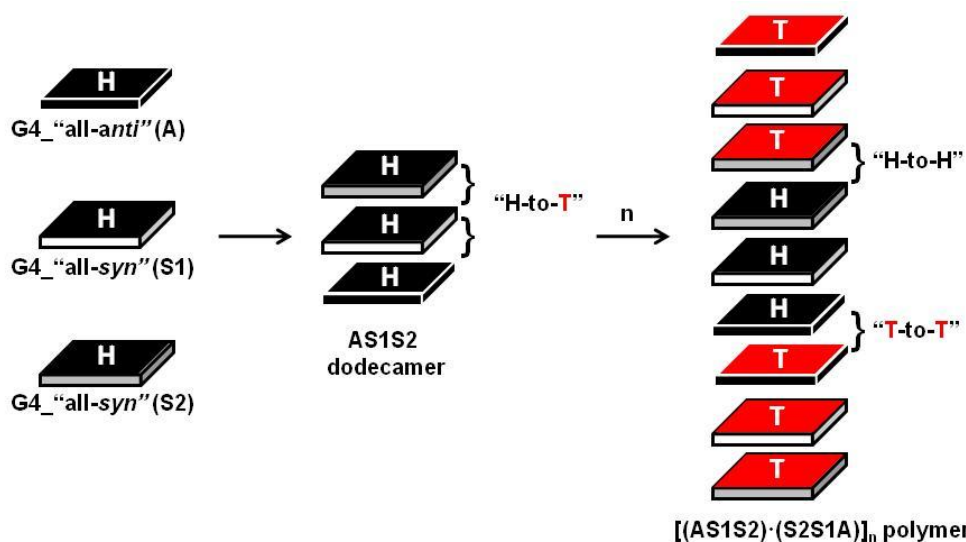


Figure 2.1.3: Formation of $[(AS1S2)(S2S1A)]_n$ polymer, composed of all-anti (A, black), all-syn1 (S1, white) and all-syn2 (S2, grey) quartets.

While dG(C10) forms the K^+ -templated C_4 -symmetric octamer structure or the polymeric assembly $(G_4 \cdot M^+)_n$ in solution, other lipophilic guanosine derivatives (especially those with ribose, as sugar moiety) can give a different stereoregular octamer with a D_4 -symmetry, as described above. For example, in the presence of Na^+ ions N^2 -modified guanosine derivatives, like N^2 -(4-butylphenyl)-2',3',5'-O-triacetylguanosine (**III**), are found to self-associate into discrete octamers with this symmetry, as confirmed by NMR spectra¹³: 1H spectrum reveals only one set of signals, corresponding to a *syn* glycosidic conformation for all eight guanosine molecules in each octamer, while correlation studies demonstrate that the two G-quartets are stacked in a tail-to-tail fashion (**Figure 2.1.2, c.**).

Once confirmed that the assembly has an octameric structure (e.g., by UV-vis, DOSY, or 1H -NMR spectroscopy) it is relatively easy to assign its symmetry to the C_4 or D_4 point group: in fact, while in the former case two sets of signals are observed in the 1H -NMR spectrum (the two G-quartets are diastereotopic), in the latter case only a single set of signals is observed for the two homotopic G-quartets. Furthermore, as shown in the case of G-quadruplex structures (see *Introduction*, chapter 2.1.5), CD is diagnostic of the stacking polarity of two contiguous G-quartets: the tetramers do not stack in register but are rotated with respect to each other to give, in the 230–300 nm region characteristic of the π - π^* transitions of guanine chromophore, a double-signed exciton-like CD signal. This couplet, the sign of which allows the assignment of the stacking helicity (handedness), exhibits opposite signed bands at about 260 and 240 nm for the head-to-tail (C_4 -symmetric) stacking, while both bands are blue-shifted by 20–30 nm in the D_4 -symmetric stacking (**Figure 2.1.4**).

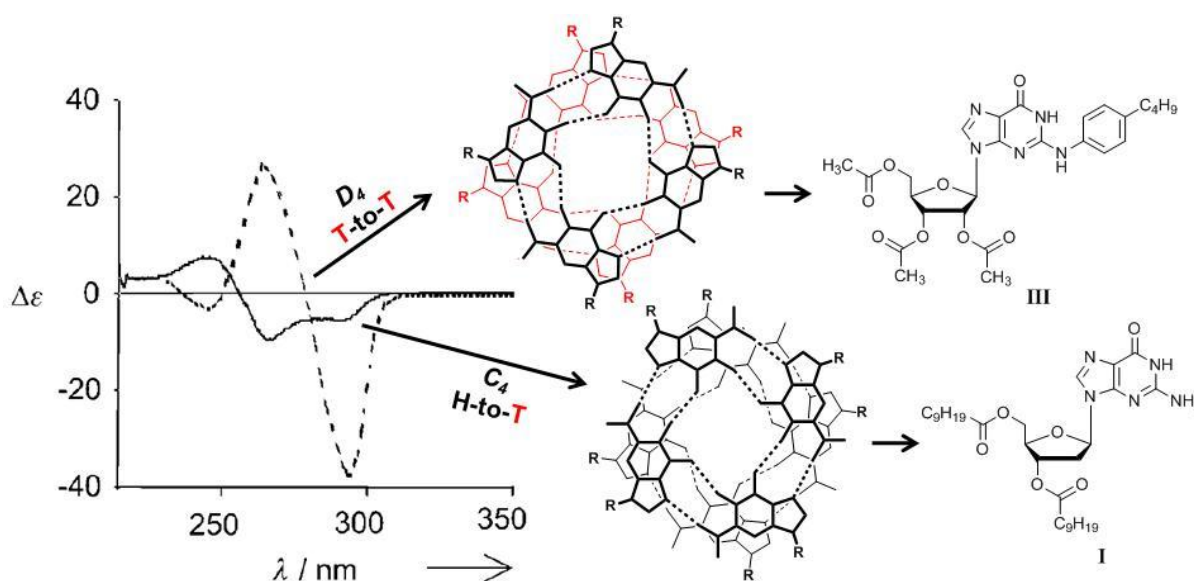


Figure 2.1.4: Comparison between CD spectra of C_4 - (solid line) and D_4 -symmetric (dashed line) octamers $G_8 \cdot M^+$ obtained from **I** and **III**, respectively^{6,14}.

Different metal ions in solution can bring to other types of G_4 -aggregates: the first species detected was an hexadecamer, formed by the lipophilic derivative 5'-*tert*butyldimethylsilyl-2',3'-isopropylidene-guanosine (**II**) in presence of equimolar potassium and cesium picrates. The structure of the hexadecamer $G_{16} \cdot 3K^+ / 1Cs^+ \cdot 4Pic^-$ was characterized by X-ray crystallography¹⁰: two C_4 -symmetric $G_8 \cdot K^+$ octamers are linked together by bifurcated hydrogen bonds between the phenolate oxygen atoms and the two ortho-substituted nitro groups of four picrate anions and to the N^2-H_B amino protons that project from the two "inner" G_4 -quartets. These nucleobase-anion hydrogen bonds give rise to a D_4 -symmetric hexadecamer, consisting in a fully occupied cation channel, with three collinear K^+ ions, located between G -quartet planes, and one Cs^+ ion along the central axis, capping this ion channel because is too large for the cavity between stacked G -quartets, but it can fit above the "outer" G_4 -tetrad (**Figure 2.1.5**, upper part).

Hexadecameric aggregates were detected also in presence of bivalent cations, such as Ba^{2+} , Sr^{2+} , Pb^{2+} . For example, Ba^{2+} stabilizes both in solution and in solid state D_4 -symmetric hexadecamers: bivalent cations coordinates C_4 -symmetric $G_8 \cdot Ba^{2+}$ octamers and two of these are linked together by anion- N^2H_B H-bonds interactions as described above. The higher stability of $G_{16} \cdot 2Ba^{2+} \cdot 4Pic^-$ compared to $G_{16} \cdot 4K^+ \cdot 4Pic^-$ is due to divalent cation which has a greater charge density that held tighter the picrate, stabilizing the hexadecamer; furthermore there is no cation located between the "inner" two G -quartets, minimizing the charge-charge repulsion between cations¹⁵. In addition, in presence of both (D)-guanosine and (L)-

Chapter II: Structure and behaviour of lipophilic guanosines

guanosine, Ba^{2+} seems to provide the enthalpic stabilization needed to overcome the unfavorable entropy associated with enantiomeric self-recognition, leading to homochiral G-hexadecamers (**Figure 2.1.5**, middle part) by strengthening cation-dipole interactions, G-quartet hydrogen bonds, and G-quadruplex-picrate interactions.

Sr^{2+} forms the same aggregates of Ba^{2+} ; adding equimolar barium and strontium picrates to a guanosine solution in CD_2Cl_2 was obtained a 1:1:2 ratio of these hexadecameric aggregates: $\text{G}_{16}\cdot 2\text{Ba}^{2+}\cdot 4\text{Pic}^-$, $\text{G}_{16}\cdot 2\text{Sr}^{2+}\cdot 4\text{Pic}^-$ and the mixed hexadecamer $\text{G}_8\cdot \text{Ba}^{2+}\cdot \text{G}_8\cdot \text{Sr}^{2+}\cdot 4\text{Pic}^-$, as verified by the presence of new four sets of ^1H NMR signals¹⁶. Kinetic stability of these three species was demonstrated by mixing a 1:1 ratio of crystalline $\text{G}_{16}\cdot 2\text{Ba}^{2+}\cdot 4\text{Pic}^-$ and $\text{G}_{16}\cdot 2\text{Sr}^{2+}\cdot 4\text{Pic}^-$: at equilibrium the same statistical distribution (1:1:2) of the three complexes was obtained.

Also the organic anion's structure can determine the stability of guanosine aggregates: a more chelating and basic anion like 2,6-DNP allows an extraordinary kinetic stabilization of hexadecameric species and prevents isomerization product like $\text{G}_8\cdot \text{Ba}^{2+}\cdot \text{G}_8\cdot \text{Sr}^{2+}\cdot 4\text{Pic}^-$ ¹⁷.

A more recent and detailed study underlines how guanosines assembly can be tuned by controlling the Coulombic energy associated with the separation of ion pairs in the solvent environment¹⁸. For example, small and non-coordinating anions, such as PF_6^- or BF_4^- , favoured the growth of the G-quadruplexes, while the use of bulky (BPh_4^-) anions that cannot approach so close to the complex resulted in the formation of smaller species. In addition, more polar solvents, which can solvate the dissociated anion more efficiently, favor the formation of larger assemblies: in the case of **II**, 16mers are formed in THF (dielectric constant, $\epsilon_s = 7.8$), while 24mers in acetone ($\epsilon_s = 20.7$); the use of more polar solvents, (ethanol, DMSO) resulted in no complexation, because they are strongly competing solvents for hydrogen bonding (**Figure 2.1.5**, bottom part).

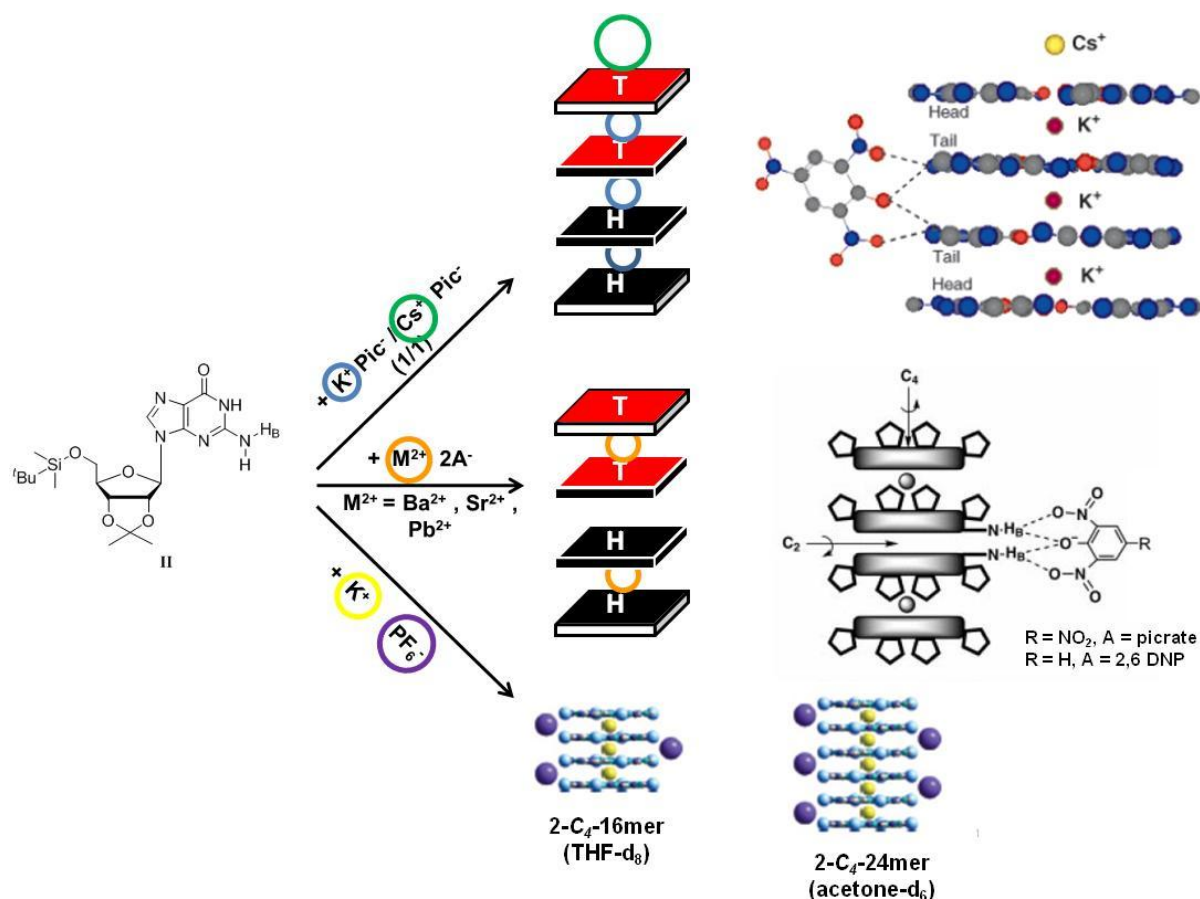


Figure 2.1.5: Aggregates formed by **II** with different cations and solvent: hexadecameric ion channel (upper part, from “Toward Artificial Ion Channels: a Lipophilic G-quadruplex”¹⁰); D_4 -symmetric hexadecamer (middle part, from “Ion-Pair Recognition by Nucleoside Self-Assembly: Guanosine Hexadecamers Bind Cations and Anions”¹⁶); C_4 -symmetric 16-mer and 24-mer (bottom part, from “G-quadruplex self-assembly regulated by Coulombic interactions”¹⁸).

2.2 Self-assembly in the absence of metal ions

All the supramolecular architectures described so far require the presence of a cation (usually an alkali-metal, but also earth-alkali or lanthanide ions) that stabilises the assemblies through dipole–ion interactions. Analogously, even in the absence of metal cations, derivatives **II** undergo an extensive self-assembly mediated by hydrogen bonding between guanine bases: in 1998 our group characterized these aggregates both in solution and in solid state¹⁹. CD spectra, recorded in chloroform at different temperatures and concentrations, showed weak signals, without any exciton pattern, suggesting that no supramolecular chirality was originated by self-assembly of guanosines under these conditions. ¹H-NMR spectra in CDCl₃ show broad signals if compared to the ones recorded in the strongly competing solvent DMSO- d_6 , as expected for largely associated molecules. The existence of oligomeric

Chapter II: Structure and behaviour of lipophilic guanosines

structures in CDCl_3 was supported by ESI mass spectrometry. Moreover, when increasing guanosine concentration (or lowering temperature), progressive deshielding of both the imino N^1H and amino N^2H protons takes place, indicating that the H-bond donor groups of the guanine bases are progressively involved in the self-assembly process. IR spectra lead to the same conclusion. The structure of these aggregates was characterized in the solid state (by X-ray diffraction, MAS (Magic Angle Spinning)-NMR spectroscopy and Atomic Force Microscopy, AFM)^{20,21}, in solution (by NMR spectroscopy and ESI-MS) and at graphite–solution interface (by Scanning Tunneling Microscopy, STM)²².

Two different ribbon-like aggregates, with different patterns of hydrogen bonds, were identified in the solid state and in chloroform solution. The first species (ribbon A, **Figure 2.2.1**, a.), which is stable in the solid state and is detected in solution in (anhydrous) chloroform soon after dissolving the polycrystalline powder, is held together by an intramolecular $\text{N}^2\text{H}–\text{O}^6$ and $\text{N}^1\text{H}–\text{N}^7$ hydrogen bond network. In solution, the ribbon A may slowly undergo a structural transition towards a thermodynamically more stable form (ribbon B, **Figure 2.2.1**, b.) characterized by $\text{N}^1\text{H}–\text{O}^6$ and $\text{N}^2\text{H}–\text{N}^3$ intermolecular cyclic hydrogen bonds: this is normally observed for dialkanoyl derivatives of type **I**. Upon adsorption at the solid–liquid interface, the guanosine supramolecular ribbons B undergo a back rearrangement to the A-type ribbons. In both ribbon-like polymers the glycosydic bonds adopt an *anti* conformation.

It should be noted that the two ribbons possess a different symmetry. As a consequence, while in ribbon B (solution) molecular dipoles cancel each other, ribbon A structure (solid state) has a permanent dipole moment and, remarkably, in the crystal structure ribbons are arranged in a parallel fashion, thus making polar the whole bulk.

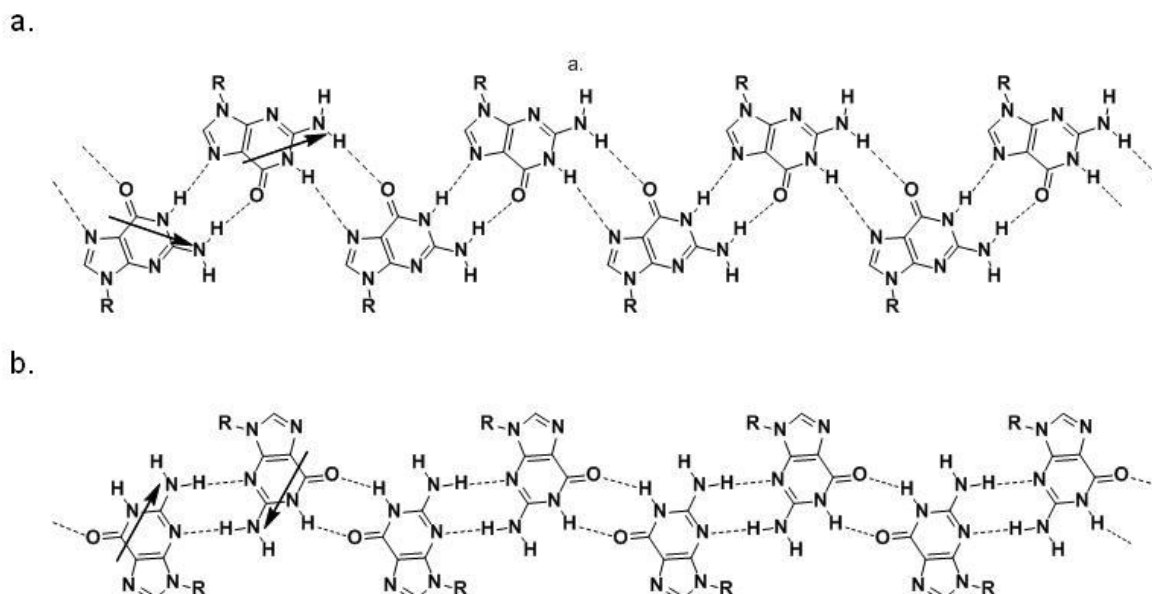


Figure 2.2.1: H-bond pattern of ribbon-like assemblies ribbon A (a.) and ribbon B (b.). Arrows indicate molecular dipoles.

A change in guanosine backbone, for example, introducing a substituent in C⁸, leads to different aggregates. Attachment of a bulky group (4-NMe₂-Ph, SMe, Br) to the guanine 8 position gives a conformationally constrained nucleoside, which adopts a *syn*-glycosidic bond conformation that forces the exocyclic amino group on top of the sugar ring, thus shielding both N³ and one of the N²H protons from hydrogen bonding: thus preventing ribbon formation both in the solid state and in solution. Consequently, the Hoogsteen pairing is the only option available, allowing the formation of “bare” G-quartet structure, without any templation by cations²³ (**Figure 2.2.2, a.**).

After introducing a hydroxylic group in C⁸, the molecule tautomerizes in the more stable 8-oxo-guanosine: the presence of two amide groups opens up new possibilities for the formation of (strong) amide–amide hydrogen bonding pairing and several self-assembled structures, in particular a continuous helical architecture has been characterized (**Figure 2.2.2, b.**) in solution, in the liquid crystalline phases, in the solid state²⁴ and also at solid-liquid interface on graphite, as shown in STM images²⁵.

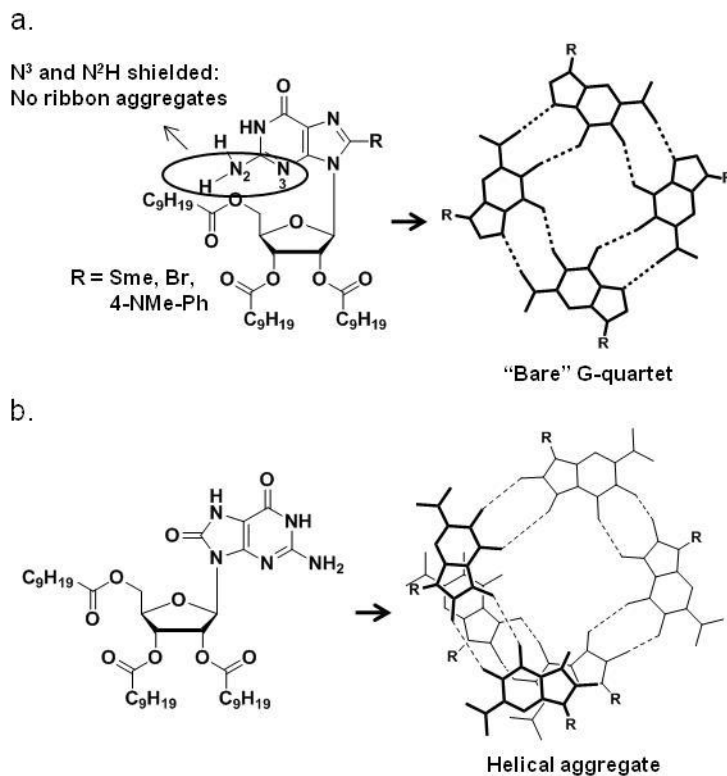


Figure 2.2.2: a. C^8 substituted guanosines which form "bare" G-quartet; b. 8-oxo-guanosine self-assembles in helical aggregates.

3. Guanosine lipophilic assemblies for smart functional materials^{1,26,27}

As shown in the previous chapter, lipophilic guanosines can undergo different self-assembly pathways, typically the ribbons and the cyclic-quartet systems, originating diverse nanoarchitectures. In addition, the easy functionalisation of guanosine in the sugar hydroxyl groups or in the aromatic base (in particular in C⁸) makes it a promising building block for the fabrication of complex architectures with functional units located in pre-programmed positions. The possibility of reversible switching between discrete, highly ordered supramolecular motifs by using external *stimuli* (solvent, presence of ions, light) to control a function at the molecular level is one of the key requirements in the development of “smart” materials.

3.1 From guanosines gels to liquid crystalline mesophases

Low molecular mass gelators of organic liquids are subjects of constant interest. In contrast with their macromolecular counterparts in which covalent bonds are involved, the supramolecular organization of these molecules, which is responsible for the gelling properties, is due to weak molecular forces including hydrogen-bonding, π -stacking and solvophobic effects. As a consequence, the process is reversible and several new applications are possible: for example, the preparation of microcellular organic materials, porous membranes and photoresponsive gels. It may be not trivial to understand the self-assembly process, but, once a type of gelator is discovered and the polymerization process understood, it is possible to design variations of the structure leading to interesting new properties.

Like guanylic acid in water, also LGs are able to form lyomesophases in apolar organic solvents above a critical concentration. This result, which now may seem obvious, was instead surprising, considering that in no case the molecular structure of LGs meets the requirements for liquid crystalline behavior. In every example reported it has been demonstrated that mesophases originated from anisotropic objects, arising from LGs by self-assembly, as the cooperative effect of solvophobic interactions and hydrogen bonding.

Derivative **I**, with two long alkyl chain, is able to form liquid crystal phases both in absence and in presence of alkali metal ions. In absence of metal ions, the gelation process is mediated by the formation of ribbonlike aggregates. Thus, in hydrocarbon solvents, **1** forms a lyotropic

Chapter II: Structure and behaviour of lipophilic guanosines

phase with a 2D square packing, as demonstrated by X-ray diffraction studies, where solvent (hexadecane, heptane) penetrates the structure dissolving long alkyl chain²⁸. In chloroform instead the solvent is not able to penetrate the structure, generating a new different structure, in which the rods, packed in a two-dimensional square cell, are composed of multiple (two to four) stacked ribbons²⁰ (**Figure 3.1.1, a.**).

Potassium picrate was added to a chloroform solution of **1** in 1:4 ratio and, after removing chloroform, heptane was added: microscopy and X-ray diffraction studies were performed while solvent slowly evaporated: the aggregate formed, according to NMR spectroscopy studies, is a columnar polymer ($\mathbf{1}_4 \cdot \text{Kpic}$)_n made of piled G-quartets with an internal channel of K⁺ ions, similar to those observed in water for guanylic acid. Increasing aggregate concentration, the liquid crystalline phase, initially a cholesteric phase, became an hexagonal phase²⁹ (**Figure 3.1.1, b.**).

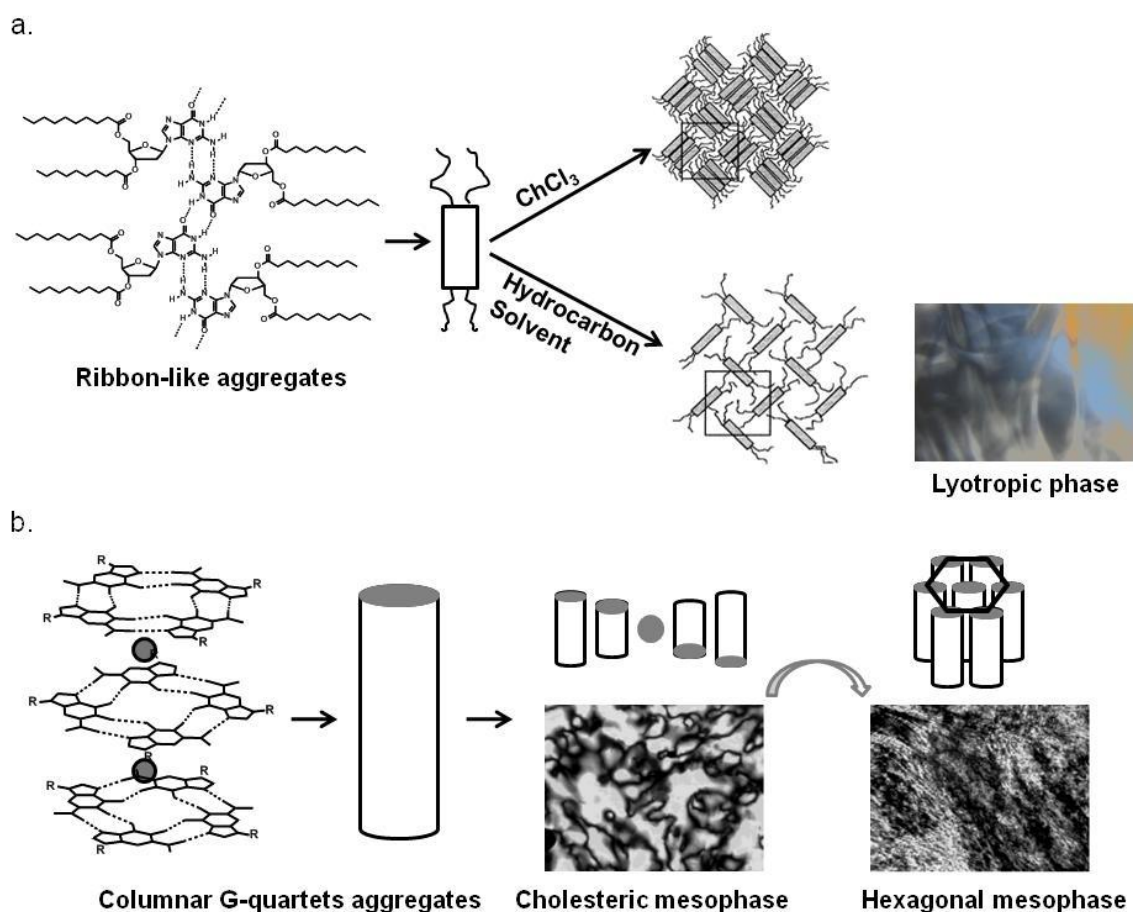


Figure 3.1.1: Different type of liquid crystalline mesophases formed by derivative **I**: in absence of cations (a.) the specie responsible for mesophases is a ribbonlike structure, while with Kpic (b.) the formation of a columnar G-quartet aggregates lead to a cholesteric phase and, increasing **1** concentration, to a hexagonal phase (from “Columnar Lyomesophases Formed in Hydrocarbon Solvents by Chiral Lipophilic Guanosine-Alkali Metal Complexes”²⁹).

3.2 Supramolecular dynamer: switching between assemblies

Reversibility is a hallmark of supramolecular chemistry and lipophilic guanosines represent in this field unique building blocks: in the presence of certain cations, they can form G-quartet-based octamers or columnar aggregates, while in the absence of metal templates, guanosines self-assemble into ribbon-like architectures.

Few years ago, we reported on the tunable interconversion between G-ribbons and G-quartets controlled by sequential addition and removal of cations³⁰ (**Figure 3.2.1**, a.). By addition of 1/8 equivalent of potassium picrate to an initial solution of **1** in CHCl₃, the ribbon-like aggregate **I_n** (B type) is transformed into the octameric complex **I₈·K⁺**. Subsequent addition of 2.5 equiv of cryptand [2.2.2], which offers an efficient complexation of K⁺, yields the cryptate [K⁺ ∩ 2.2.2] and reverts the potassium complex to the ribbon **I_n**. Upon protonation with 1 equiv of triflic acid (HTf) of one of the bridgehead nitrogen atoms of the cryptate, leading to the formation of [H⁺ ∩ 2.2.2], the bound K⁺ can be released and **I₈·K⁺** is regenerated. Adding thereafter 1 equiv of triethylamine (TEA) [H⁺ ∩ 2.2.2] deprotonates; the free cryptand recaptures K⁺, and the G-ribbon **I_n** is formed again. The interconversion may be repeated by sequential addition of acid and base. Circular dichroism (CD) (**Figure 3.2.1**, b.) and ¹H NMR can both be exploited to monitor the ribbon-octamer **I_n** / **I₈·K⁺** interconversion.

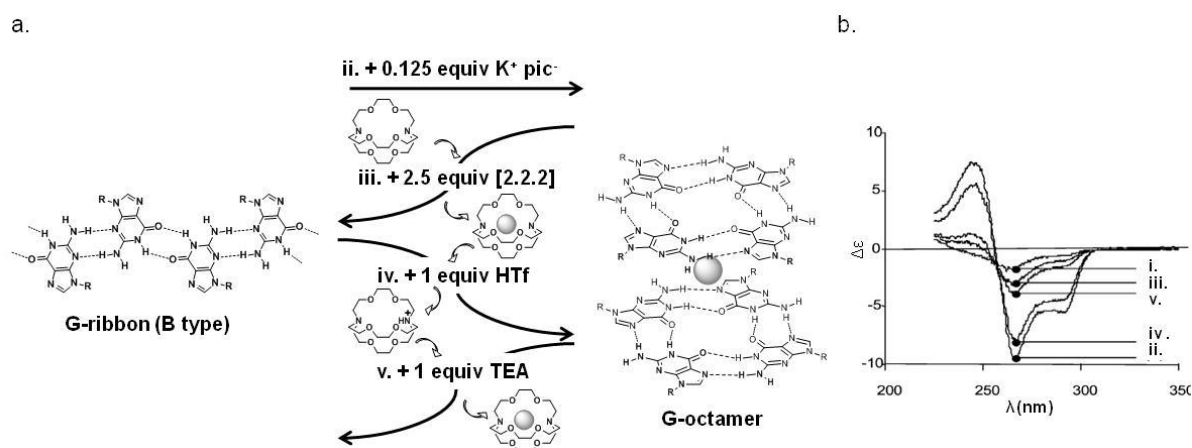


Figure 3.2.1: Switching between ribbon and octameric species mediated by cation addition and removal (a.) and the corresponding CD spectra (b., from “Reversible Interconversion between a Supramolecular Polymer and a Discrete Octameric Species from a Guanosine Derivative by Dynamic Cation Binding and Release”³⁰).

The same process of switching between the ribbon and the G-quartet-based form can be observed not only in solution but also on surfaces using a octadecyl guanine derivative (**IV**):

Chapter II: Structure and behaviour of lipophilic guanosines

the technique employed was STM, Scanning Tunneling Microscopy, and the reversible assembly/reassembly through hydrogen bonding was studied at solid-liquid interface on highly oriented pyrolytic graphite (HOPG).

First a solution of **4** (100 μ M) in 1,2,4-trichlorobenzene (TCB) was dropcasted on HOPG, obtaining monolayer which showed a crystalline structure consisting of ribbon-like architectures. In this 2D crystal, the octadecyl side chains are physisorbed flat on the surface and are interdigitated between adjacent supramolecular ribbons. In situ successive assembly/reassembly cycles were accomplished: upon addition of 10 mM potassium picrate solution in TCB to the initial ribbon-like motif, the G4 supramolecular motif was obtained (**Figure 3.2.2**). Subsequent addition of cryptand [2.2.2] (10 mM in TCB) and HTf (10 mM in TCB) allowed the desired switching, but unfortunately, even in presence of a large excess of triethylamine it was not possible to trigger the formation of ribbons at surfaces. The reproducibility of the submolecular resolution STM imaging of the interconversion of **IV** from ribbons to G4-based architectures requires stringent experimental conditions characterized by an extremely low thermal gradient (below 3 $^{\circ}$ C) and a high control over the concentration of the solutions employed (the concentration of HTf could not exceed that needed to protonate only the nitrogen atoms of cryptand [2.2.2], otherwise only disordered monolayers were obtained).

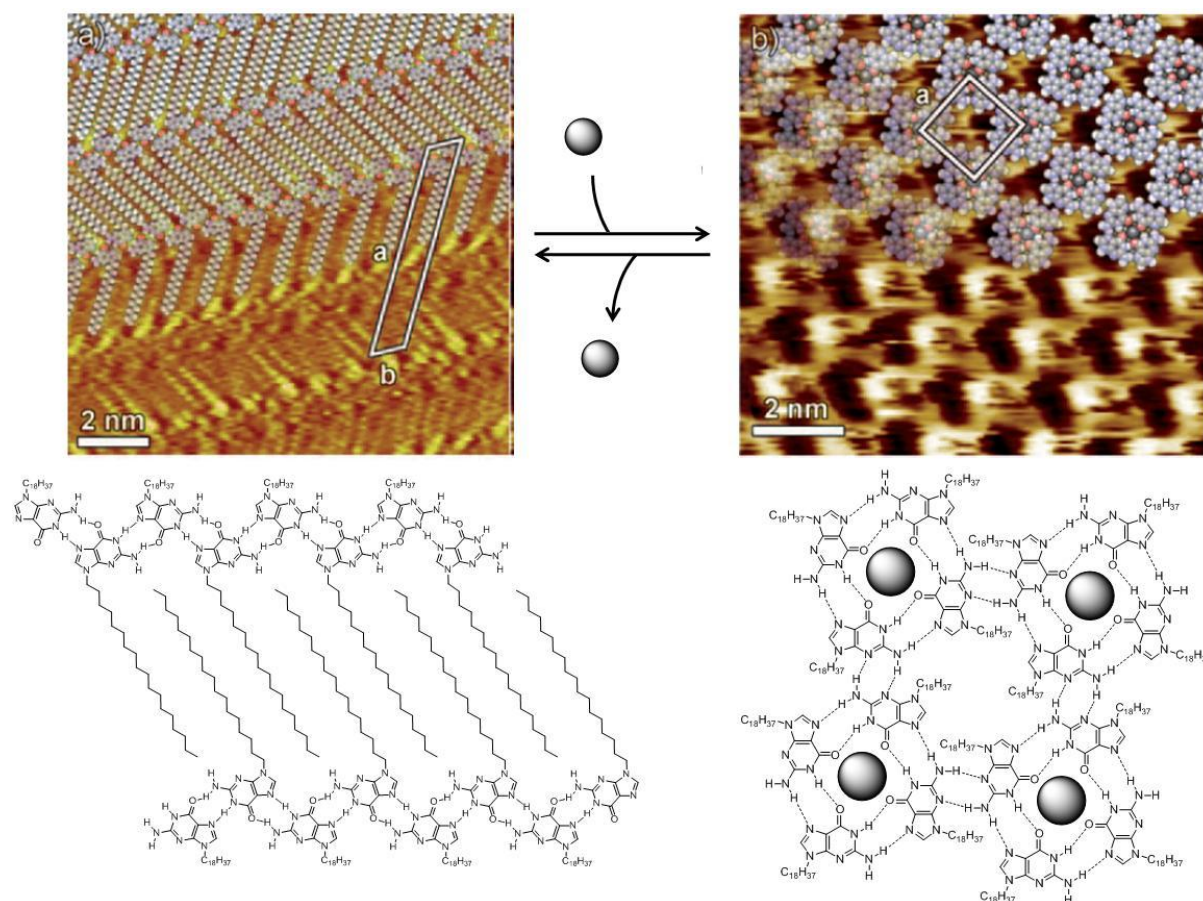


Figure 3.2.2: STM images of monolayers of supramolecular architectures of **IV** at the solid-liquid interface self-assembled from TCB solution; a) ribbonlike structure and b) G4-based architecture (from “Dynamers at the Solid–Liquid Interface: Controlling the Reversible Assembly/Reassembly Process between Two Highly Ordered Supramolecular Guanine Motifs”³¹).

This supramolecular dynamer, besides being of importance as a model system to mimic the formation-annihilation of G-quartet-based architectures, which might be of biological significance in the frame of nucleic acid telomerase, expands the possibilities offered by the scaffolding concept.

3.3 Molecular electronic devices

Molecular electronics is gaining an increasing attention worldwide due to the appealing possibility of realizing cheap and easy-to-fabricate devices that exploit the self-assembly, self-recognition and self-repairing capability of engineered organic or bio-inspired molecules. Self-assembling guanosines are, therefore, promising candidates for fabrication of electronic nanodevices.

Our first attempt, in collaboration with Rinaldi group, was the fabrication of a hybrid (metal–semiconductor–metal, MSM) photodetector using as semiconductor a self-assembled layer of guanosine derivative **I**³². A solution of **I** in chloroform was deposited on SiO₂ substrate between two gold electrodes which were separated by a distance of about 120 nm (**Figure 3.3.1**, a.). After solvent evaporation, AFM images of the substrate confirmed the formation of a ribbon-like aggregate between the two electrodes. Extensive transport and photocurrent experiments, performed on this device, revealed that the self-assembled deoxyguanosine films behave like semiconductors. The experimental *I*–*V* characteristics (plot of current intensity vs. voltage) are in agreement with MSM photodetector characteristics and the curve is also dependent on the illumination conditions: the current increases from sub- μ A level in the dark to sub-mA levels under illumination of a few mW of power (**Figure 3.3.1**, b.).

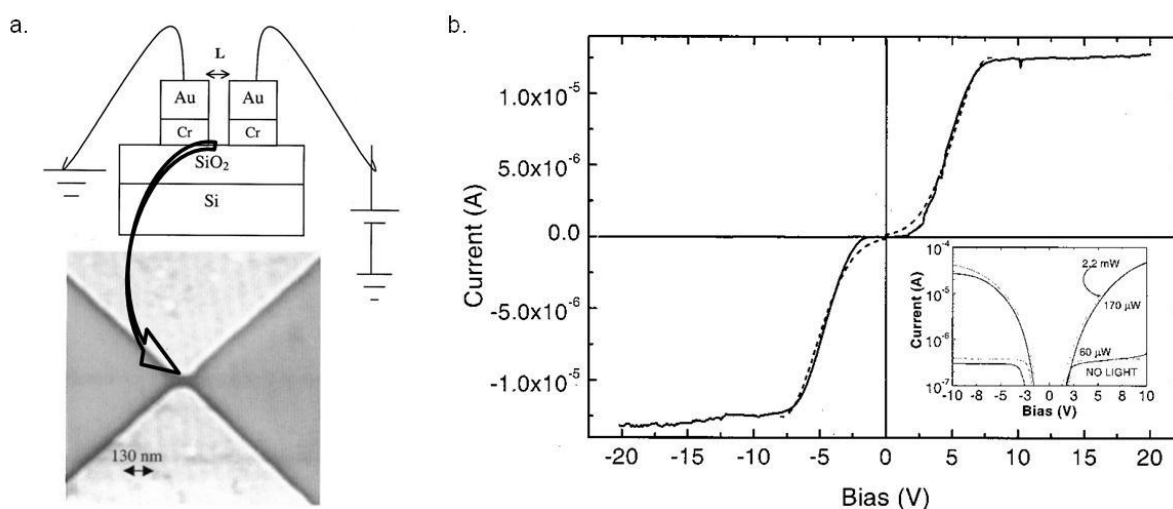


Figure 3.3.1: a. Section of the device used in the experiment and a SEM image of the gold nanoelectrodes fabricated by EBL and lift-off onto a SiO₂ /Si substrate; b. *I*–*V* characteristics of 1-MSM device (*L* = 120 nm) (dark current): the continuous line represents the experimental data while the dashed line is the theoretical one for MSM devices. In the inset several curves are shown at different power illumination conditions (from Photodetectors fabricated from a self-assembly of a deoxyguanosine derivative³²).

Further experiments were performed to understand the conduction proprieties of guanosine films, studying the effect of both different structural modification of guanoses and different electrodes distances³³. Two derivatives were considered, deoxyguanosine **I** and 8-oxo-deoxyguanosine **V**. Solutions of these compounds were deposited between two arrow-shaped Au/Cr (35/8 nm) electrodes on SiO₂ substrates, fabricated by electron beam lithography. AFM images revealed self-assembled structures on substrates: derivative **I**, as seen before, forms an array of ribbons (ribbon A, which has a permanent dipole moment oriented along the ribbon

Chapter II: Structure and behaviour of lipophilic guanosines

axis) aligned on a range of about 100 nm.; derivative **V** instead forms both tetramers and continuous helices, due to the presence of oxygen atom in C⁸ position, with a negligible resulting dipole moment (**Figure 3.3.2**).

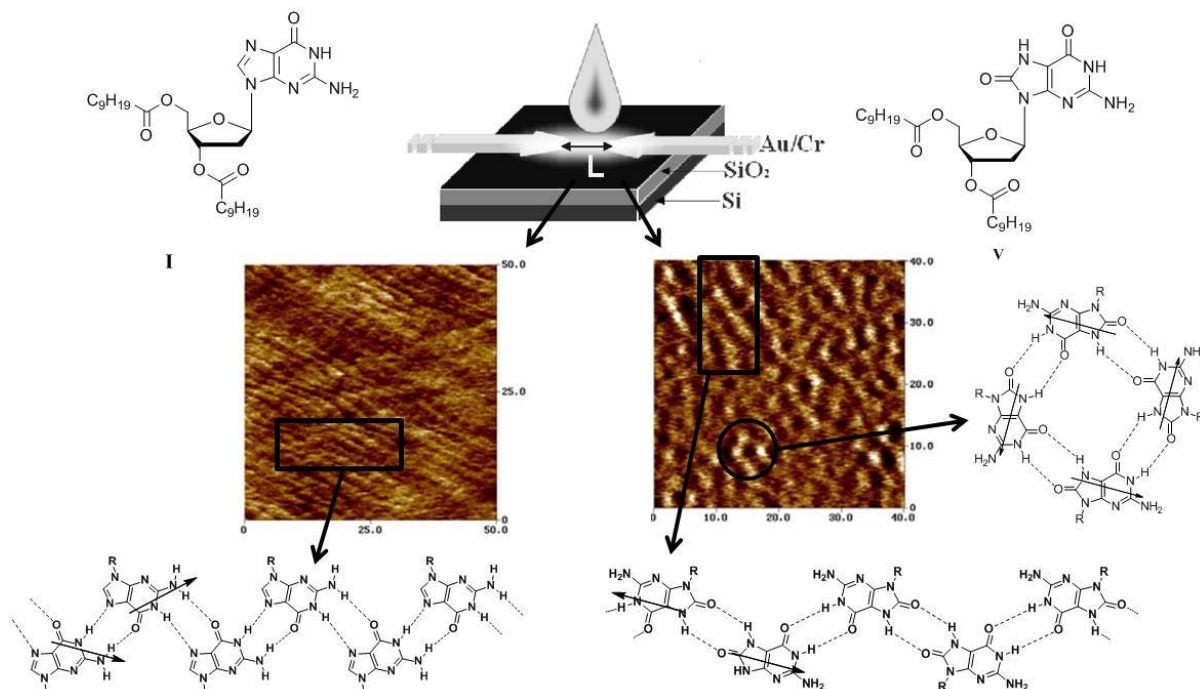


Figure 3.3.2: Scheme of the device (*L* is the distance between the planar electrodes, represented as arrows) and AFM images of LG self-assembled layers on the substrates: on the left, rectangle indicates the ribbon-like structure of **I**, which poses a permanent dipole moment; on the right both ribbon (rectangle) and tetramer (circle) structures can be observed for derivative **V**, leading to a negligible total dipole moment (from “Hybrid molecular electronic devices based on modified deoxyguanosines”³³).

I-V measurements were first performed in devices with a gap between electrodes of 60 nm. Device prepared with **1** showed a clear diode-like behavior, with currents on the order of μA for positive bias and nA for negative bias (**Figure 3.3.3**, a.). This rectifying propriety (asymmetric *I-V* curve) is related to the existence of the strong dipole that originates from ribbon-like structure: as the typical length of an oriented arrays of parallel ribbons (a “nanocrystal”) is approximately 100 nm, as demonstrated by AFM images: for a contact gap of 60 nm or less, only one nanocrystal, and consequently a well-oriented dipole moment, is probed.

Device prepared with derivative **5** also shows rectification properties, but the current density is two orders of magnitude lower than for **1**, with a rather large current for negative bias (10^{-7}A) (**Figure 3.3.3**, b.): this behavior is due to the self-assembling of a mixed phase of tetramers and continuous helices that led to a partial cancellation of dipole moments.

Chapter II: Structure and behaviour of lipophilic guanosines

When the gap in the two-terminal device prepared with **1** is increased to 120 nm, a few nanocrystals of self-assembled guanosine are probed by the electrodes and the total dipole of the sample between the electrodes averages to zero because the nanocrystals are randomly oriented (**Figure 3.3.3, a.**): the device behaves no more like a diode, but like a MSM device, as shown for the photodetector previously described.

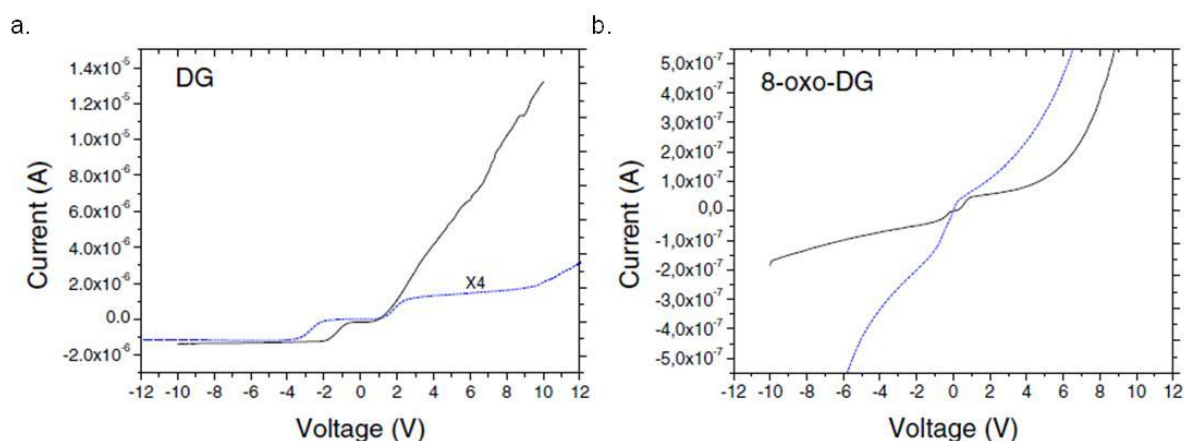


Figure 3.3.3: a.-b.: I - V curves of devices with electrode separations of $L = 60$ nm (solid curve) and $L = 120$ nm (dashed curve) prepared with self-assembled layer of **1** (a.) and of **5** (b.) as semiconductors (from “Hybrid molecular electronic devices based on modified deoxyguanines”³³).

The examples reported demonstrate the possibility of using lipophilic guanosines as semiconductors in two-terminal Hybrid Molecular Electronic (HME). The electrical properties of the active molecular system can be tuned by synthetic modification of molecular structure, self-assembling control and distance variation between the two terminals: derivative **1** behaves like a diode when L is less than 100 nm, and like a MSM device for greater electrodes distance.

The main problem of these systems arises from differences in layer homogeneity due to non-covalent bonding nature of the self-assembly. This leads to a random orientation of the ribbons dipoles between the tips, resulting in different degrees of rectification in different devices. Maximum rectification, and consequently maximum current strength, is obtained when the ribbons are parallel to the tip axis, but in most cases the ribbons are oriented at an arbitrary angle with respect to the tip axis. Comparing several fabricated diodes, some rectified in one direction and others in the opposite direction, and that the rectifying power was not constant.

Owing to its conduction properties, deoxyguanosine **1** was used for fabrication of a field effect transistor (FET), a three terminal device: this device will be discussed in the next chapter.

4. Conclusions

Guanine nucleobases have a high ability to form multiple hydrogen bonds and, possibly, base stacking. These directionally controlled, multiple base–base interactions make the guanine moiety a highly useful structural element for design and construction of geometrically well-defined three-dimensional assemblies. Rapid progress of the guanine-related supramolecular and materials chemistry in recent years, is opening the way to a variety of novel functional materials that consist of geometrically well-defined two- or three-dimensional assemblies of nucleobase-containing molecules. Furthermore, guanine self-assembly is employed in molecular manufacturing, intended as the concept of engineering functional structures at the molecular scale to achieve sub-micro, micro or macro scale objects, with the objective to achieve components and/or systems with predictable and controllable properties.

Chapter II: Structure and behaviour of lipophilic guanosines

Bibliography

- (1) Masiero, S.; Pieraccini, S.; Spada, G. P. In *Molecular Self-Assembly - Advances And Applications*; Li, A., Ed.; Pan Stanford Publishing: 2012, P 93.
- (2) Guschlbauer, W.; Chantot, J.; Thiele, D. *Journal Of Biomolecular Structure & Dynamics* **1990**, 8, 491.
- (3) Bang, I. *Biochem. Z.* **1910**, 26, 293.
- (4) Spada, G.; Carcuro, A.; Colonna, F.; Garbesi, A.; Gottarelli, G. *Liquid Crystals* **1988**, 3, 651.
- (5) Gottarelli, G.; Spada, G. P.; A., G.; Lehn, J. M., Sauvage, J.-P., Hosseini, M. W., Eds.; Pergamon: Oxford, 1996; Vol. 9.
- (6) Gottarelli, G.; Masiero, S.; Spada, G. *Journal Of The Chemical Society-Chemical Communications* **1995**, 2555.
- (7) Gottarelli, G.; Spada, G. *Chemical Record* **2004**, 4, 39.
- (8) Davis, J.; Tirumala, S.; Jenssen, J.; Radler, E.; Fabris, D. *Journal Of Organic Chemistry* **1995**, 60, 4167.
- (9) Marlow, A.; Mezzina, E.; Spada, G.; Masiero, S.; Davis, J.; Gottarelli, G. *Journal Of Organic Chemistry* **1999**, 64, 5116.
- (10) Forman, S.; Fettingner, J.; Pieraccini, S.; Gottarelli, G.; Davis, J. *Journal Of The American Chemical Society* **2000**, 122, 4060.
- (11) Manet, I.; Francini, L.; Masiero, S.; Pieraccini, S.; Spada, G.; Gottarelli, G. *Helvetica Chimica Acta* **2001**, 84, 2096.
- (12) Mezzina, E.; Mariani, P.; Itri, R.; Masiero, S.; Pieraccini, S.; Spada, G.; Spinuzzi, F.; Davis, J.; Gottarelli, G. *Chemistry-A European Journal* **2001**, 7, 388.
- (13) Martic, S.; Liu, X.; Wang, S.; Wu, G. *Chemistry-A European Journal* **2008**, 14, 1196.
- (14) Graziano, C.; Masiero, S.; Pieraccini, S.; Lucarini, M.; Spada, G. *Organic Letters* **2008**, 10, 1739.
- (15) Shi, X.; Fettingner, J.; Davis, J. *Journal Of The American Chemical Society* **2001**, 123, 6738.
- (16) Shi, X.; Fettingner, J.; Davis, J. *Angewandte Chemie-International Edition* **2001**, 40, 2827.
- (17) Shi, X.; Mullaugh, K.; Fettingner, J.; Jiang, Y.; Hofstadler, S.; Davis, J. *Journal Of The American Chemical Society* **2003**, 125, 10830.

Chapter II: Structure and behaviour of lipophilic guanosines

- (18) Gonzalez-Rodriguez, D.; Van Dongen, J.; Lutz, M.; Spek, A.; Schenning, A.; Meijer, E. *Nature Chemistry* **2009**, *1*, 151.
- (19) Gottarelli, G.; Masiero, S.; Mezzina, E.; Spada, G.; Mariani, P.; Recanatini, M. *Helvetica Chimica Acta* **1998**, *81*, 2078.
- (20) Giorgi, T.; Grepioni, F.; Manet, I.; Mariani, P.; Masiero, S.; Mezzina, E.; Pieraccini, S.; Saturni, L.; Spada, G.; Gottarelli, G. *Chemistry-A European Journal* **2002**, *8*, 2143.
- (21) Pham, T.; Griffin, J.; Masiero, S.; Lena, S.; Gottarelli, G.; Hodgkinson, P.; Fillip, C.; Brown, S. *Physical Chemistry Chemical Physics* **2007**, *9*, 3416.
- (22) Lena, S.; Brancolini, G.; Gottarelli, G.; Mariani, P.; Masiero, S.; Venturini, A.; Palermo, V.; Pandoli, O.; Pieraccini, S.; Samori, P.; Spada, G. *Chemistry-A European Journal* **2007**, *13*, 3757.
- (23) Sessler, J.; Sathiosatham, M.; Doerr, K.; Lynch, V.; Abboud, K. *Angewandte Chemie-International Edition* **2000**, *39*, 1300.
- (24) Lena, S.; Cremonini, M.; Federiconi, F.; Gottarelli, G.; Graziano, C.; Laghi, L.; Mariani, P.; Masiero, S.; Pieraccini, S.; Spada, G. *Chemistry-A European Journal* **2007**, *13*, 3441.
- (25) Giorgi, T.; Lena, S.; Mariani, P.; Cremonini, M.; Masiero, S.; Pieraccini, S.; Rabe, J.; Samori, P.; Spada, G.; Gottarelli, G. *Journal Of The American Chemical Society* **2003**, *125*, 14741.
- (26) Lena, S.; Masiero, S.; Pieraccini, S.; Spada, G. *Chemistry-A European Journal* **2009**, *15*, 7792.
- (27) Masiero, S.; Gramigna, L.; Neviani, P.; Perone, R. C.; Pieraccini, S.; Spada, G. *P. International Review Of Biophysical Chemistry (I.Re.Bi.C.)* **2011**, *2*.
- (28) Gottarelli, G.; Masiero, S.; Mezzina, E.; Pieraccini, S.; Spada, G.; Mariani, P. *Liquid Crystals* **1999**, *26*, 965.
- (29) Pieraccini, S.; Gottarelli, G.; Mariani, P.; Masiero, S.; Saturni, L.; Spada, G. *Chirality* **2001**, *13*, 7.
- (30) Pieraccini, S.; Masiero, S.; Pandoli, O.; Samori, P.; Spada, G. *Organic Letters* **2006**, *8*, 3125.
- (31) Ciesielski, A.; Lena, S.; Masiero, S.; Spada, G.; Samori, P. *Angewandte Chemie-International Edition* **2010**, *49*, 1963.
- (32) Rinaldi, R.; Branca, E.; Cingolani, R.; Masiero, S.; Spada, G.; Gottarelli, G. *Applied Physics Letters* **2001**, *78*, 3541.

Chapter II: Structure and behaviour of lipophilic guanosines

(33) Rinaldi, R.; Maruccio, G.; Biasco, A.; Arima, V.; Cingolani, R.; Giorgi, T.; Masiero, S.; Spada, G.; Gottarelli, G. *Nanotechnology* **2002**, *13*, 398.

*Chapter III: Liponucleoside thin films: the
special behaviour of guanosine*

1. Introduction^{1,2}

Langmuir–Blodgett (LB) film methods are perhaps the earliest example of what is now called ‘supramolecular assembly’, providing the opportunity to exercise molecular level control over the structure of organic thin films. In this method, a single layer of molecules is first organized on a liquid surface, usually water, before being transferred onto a solid support to form a thin film with the thickness of a constituent molecule. If the process is repeated, multiply layered films can be prepared, with a control over the orientation and placement of molecules that are difficult to achieve otherwise. The layer of molecules on a liquid surface is termed a *Langmuir monolayer* and after transfer it is called a *Langmuir–Blodgett film*. LB films have been explored for applications that include electronics, optics, microlithography, and chemical sensors, as well as biosensors or biochemical probes^{3,4}.

The technique is named after Irving Langmuir and Katharine Blodgett, researchers at the General Electric Company in the first half of the twentieth century. Langmuir, awarded the Nobel Prize for Chemistry in 1932 for his studies of surface chemistry, used floating monolayers to learn about the nature of intermolecular forces. In the course of his studies, Langmuir developed several new techniques that are by and large still used today in the study of monomolecular films. Together with Langmuir, Katharine Blodgett refined the method of transferring the floating monolayer onto solid supports. In addition to treating many practical details of LB methods, publications and patents by Langmuir and Blodgett cover a number of potential applications including controlling the reflectivity of glass, a step gage for optically measuring the thickness of thin films, submicron mechanical filters, and biosensing.

It was however not until 1965 that Langmuir-Blodgett films received much further attention, when Hans Kuhn studied their spectroscopic properties⁵. His research seemed to initiate increasing interest in the properties of Langmuir-Blodgett films, as since then the number of research groups has been increasing steadily, until in the recent years when the commercial implementation of LB films is getting closer to reality.

1.1 Langmuir-Blodgett films: preparation and characterization

Before considering the preparation of LB films, it is necessary to introduce the fundamental characteristics required for a molecule in order to form a Langmuir monolayer. Suitable compounds are water insoluble and soluble in a volatile solvent like chloroform or benzene;

Chapter III: Liponucleoside thin films: the special behaviour of guanosine

they consist of two parts, a 'head' and a 'tail' part. The 'head' part is a hydrophilic chemical group, typically with a strong dipole moment and capable of hydrogen bonding, like $-\text{OH}$, $-\text{COOH}$, $-\text{NH}_2$ etc. The 'tail' part on the other hand is hydrophobic, typically consisting of a long aliphatic chain. Such molecules, containing spatially separated hydrophilic and hydrophobic regions, are called amphiphiles.

The core of LB films deposition instrument is a Langmuir-Blodgett trough, or Langmuir film balance, containing an aqueous subphase (**Figure 1.1.1, a.**). To form the Langmuir monolayer film, the molecules of interest is dissolved in a volatile organic solvent (chloroform, hexane, toluene etc.) that will not dissolve or react with the subphase. The dilute solution is then minutely placed on the subphase of the LB trough with a micro-syringe. The solvents evaporate quickly and the surfactant molecules spread over the subphase surface in the LB trough. If amphiphile molecules arrive at the air-water interface with its hydrophobic tails pointing towards the air and its hydrophilic group towards water, the initial high energy interface is replaced by lower energy hydrophilic – hydrophilic and hydrophobic – hydrophobic interfaces, thus lowering the total energy of the system. Hence, the molecules at the interface are anchored, strongly oriented normal to the surface and with no tendency to form a layer more than one molecule thick.

In order to control and monitor the surface pressure, (π , i.e. the reduction of surface tension below that of clean water), movable barriers intercepting the air-water interface are allowed to move to compress or expand the surface film. Wilhelmy plate arrangement is used to measure the surface pressure: in this method a small piece of hydrophilic material, usually filter paper, intercepts the air-water interface and is supported from the arm of an electronic microbalance interfaced with a computer. The force exerted is directly proportional to the surface tension.

The measurement of surface pressure (π) as a function of area per molecule (A) in the monolayer films is known as the isotherm characteristic (**Figure 1.1.1, b.**). This characteristic is easily obtained and can give useful information about the mono-molecular films at the air-water interface. In a typical isotherm measurement, a monolayer is organized under compression, starting from a two dimensional gas phase (G) moving through a liquid expanded phase (LE) to a fully organised condensed phase (C). In the gas phase the molecules are not interacting with each other. When the surface area is decreased the molecules become more closely packed and start to interact with each other, with a transition to an initial LE and then to a condensed phase. In some cases a two phase coexistence can be noticed. In the condensed phase the molecules are completely organized and the surface pressure increases

dramatically. At the maximum surface pressure the collapse point (π_c) is reached after which the monolayer packing is no longer controlled.

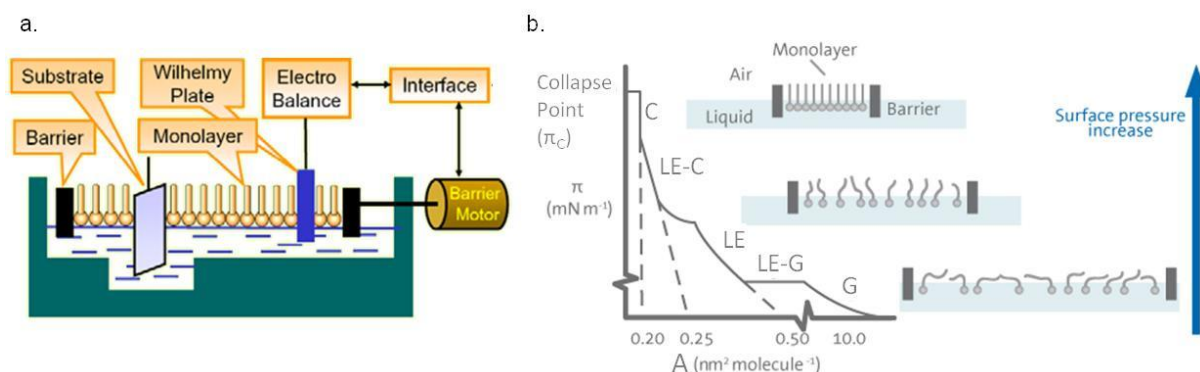


Figure 1.1.1: a. Langmuir Blodgett through schematic representation (from “Langmuir-Blodgett Films a unique tool for molecular electronics”²); b. *Surface pressure-area isotherms of a Langmuir film and molecules in different phases* (from “Langmuir Film”⁶).

The monolayer Langmuir film (**Figure 1.1.2, i.**) can be transferred off the water subphase onto a solid support (glass, silicon, mica or quartz etc), obtaining a so called ‘Langmuir–Blodgett film’. In principle the Langmuir-Blodgett deposition method simply consists of dipping and pulling vertically a solid substrate through the coating monolayer at controlled and low rate (1 – 5 mm/min) (**Figure 1.1.2, ii.**). The surface pressure must be kept constant at a desired value: for film deposition it is normally chosen to be in the solid like region, but films can be deposited at any pressure. It is also a common practice to coat the substrate with a highly hydrophobic or hydrophilic material. The transfer of monolayer film occurs via hydrophobic interactions between the alkyl chains and the substrate surface or the hydrophilic interaction between the head groups of the molecules and the hydrophilic substrate surface. Subsequent dipping or pulling deposits a second layer on top of the first (**Figure 1.1.2, iii.**) and the process can simply be repeated until the desired number of layers has been deposited (**Figure 1.1.2, iv.**).

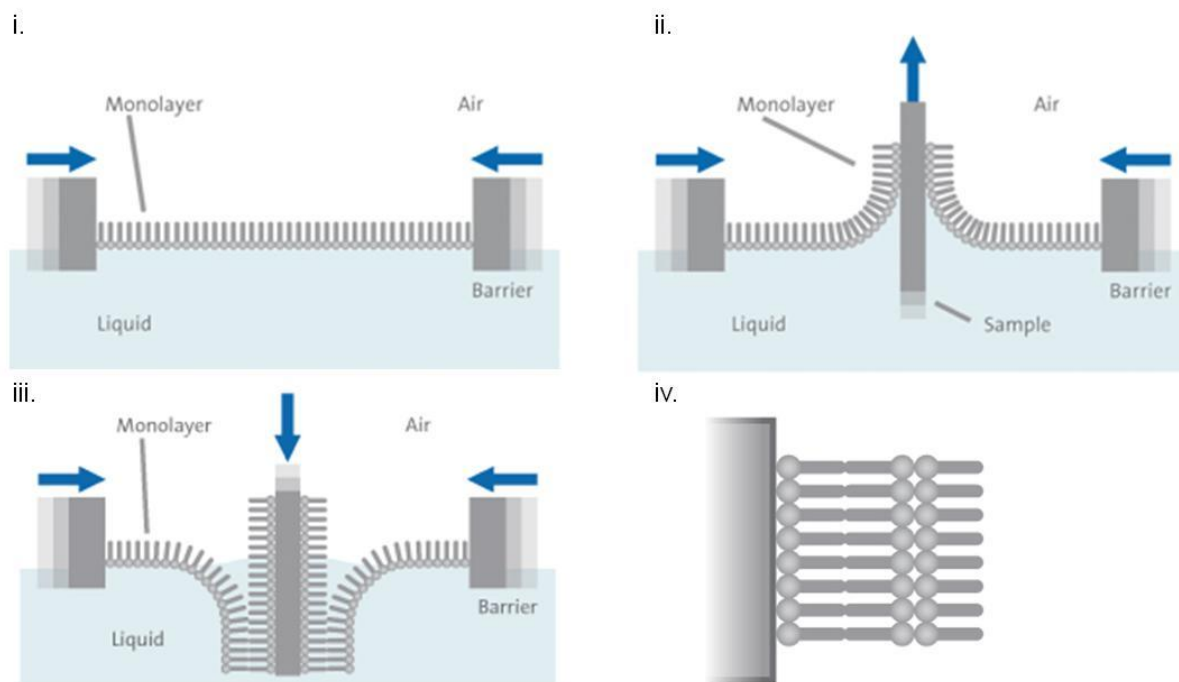


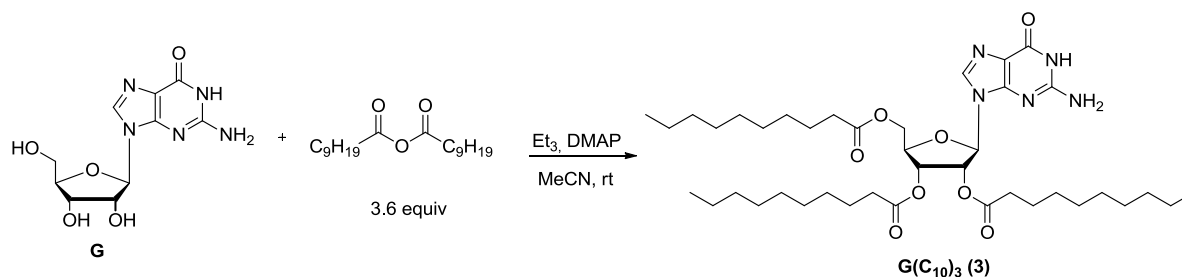
Figure 1.1.2: LB film deposition: i. monolayer compression; ii. Transfer of LB film on the substrate; iii. Second layer deposition; iv. Multiple layer on the substrate (from “Langmuir-Blodgett technique”)⁷.

Many analytical techniques are used to study both Langmuir and transferred films. In addition to the targeted materials properties, film characteristics that are typically of interest are thickness, molecular orientation and packing, film coverage and chemical composition. To characterize Langmuir films, in addition to isotherm characteristics, ellipsometry or X-ray can be employed to determine film thickness. The arrangement of molecules in transferred LB films is observed using AFM technique, while their chemical make-up is determined using for example FTIR, Raman scattering, and UV–visible absorption.

2. Surface structure of Langmuir–Blodgett films of lipophilic guanosine derivatives^{8,9}

As described in Chapter II, surface structures of guanosine nanoribbons were found to possess intriguing charge transfer properties, such as optical rectification and photoconductivity, which make them very promising for applications in nano-electronic devices. One of the major challenges in view of nano-electronics is to attain control of assembly and orientation of the material between the electrodes, which means that appropriate material deposition methods leading to well defined structures has to be found. In particular, the simple drop-casting procedure, which was used in most of the experiments with guanosine derivatives performed until now, has to be replaced by more precise methods. Langmuir–Blodgett (LB) method of manufacturing molecularly ordered films is receiving increased attention as a procedure for preparation of organic and biomolecular electronic devices. To fabricate proper structures, it is imperative to study in detail the formation of different two-dimensional phases on water surface and to investigate the effect of different parameters of the deposition procedure on molecular ordering within the resulting LB films

Few years ago our group, in collaboration with Professor Olenik in Lubiana, studied the different behavior of Langmuir and LB films of guanosine derivatives with one (**1**), two (**2**) and three (**3**) 10-carbon long alkanoyl groups¹⁰. Guanine as “hydrophilic” head and alkyl chains as “hydrophobic” tails assure the amphiphilic character required for films preparation. The synthesis of **1**¹¹ and **2**¹² has been described elsewhere. Derivative **3** was synthesized by direct esterification of the three ribose alcoholic functions with decanoic anhydride in MeCN (Scheme).



Scheme 2.1: Synthesis of G(C₁₀)₃ (3).

For the preparation of Langmuir films, chloroform solutions of these three different guanosines (10⁻³ M) were spread on freshly prepared UV sterilized and deionized water (subphase) in a computer controlled Langmuir-Blodgett trough; a Wilhelmy plate placed in the middle of the

trough was used as the surface pressure sensor. Surface layers were first let to relax for 15 min in non-compressed state to allow solvent evaporation and then isotherms $\pi(A)$ were recorded by compressing the monolayer with a barrier speed of 0.43 cm/min. Recompression to the initial surface area was made with the same speed of the barriers as in the first compression. This procedure was repeated several times.

The resulting isotherms revealed that the number of lipophilic tails attached to guanine nucleobase (**Figure 2.1**, a.) strongly influences the characteristics of Langmuir films. All derivatives display a first ordered phase transition from LE phase and C phase, with a plateau region of phase coexistence that starts with a noticeable kink. Derivative **1**, with only one tail, shows lower collapse pressure and surface area occupied by a single molecule smaller than the other two derivatives; in addition, **1** exhibits irreversible course of the isotherms (**Figure 2.1**, b.), with a significant shift toward smaller surface areas after every compression expansion cycle, while the derivatives **2** (**Figure 2.1**, c.) and **3** (**Figure 2.1**, d.) show nearly perfect reversibility as well as very good reproducibility.

From the values of surface area occupied by a single molecule (A) it is evident that only **1**, whose surface area corresponds to the size of the guanine base, can be packed so closely that extensive intermolecular hydrogen bonding can take place. This can explain the irreversible behavior of the surface–area isotherms observed for this derivative. After first compression, interbase hydrogen bonds are partially formed between the molecules, and this prevents complete dissociation of the monolayer structure during expansion. As a result, the concentration of non-aggregated molecules on the surface is reduced in each compression/recompression cycle and consequently the isotherms are different. For the derivatives with two and three tails (**2** and **3**) intermolecular hydrogen bonding cannot be established due to steric restrictions (values of the molecular surface area strongly increases with increasing number of the tails), so they exhibit a reversible association and dissociation process.

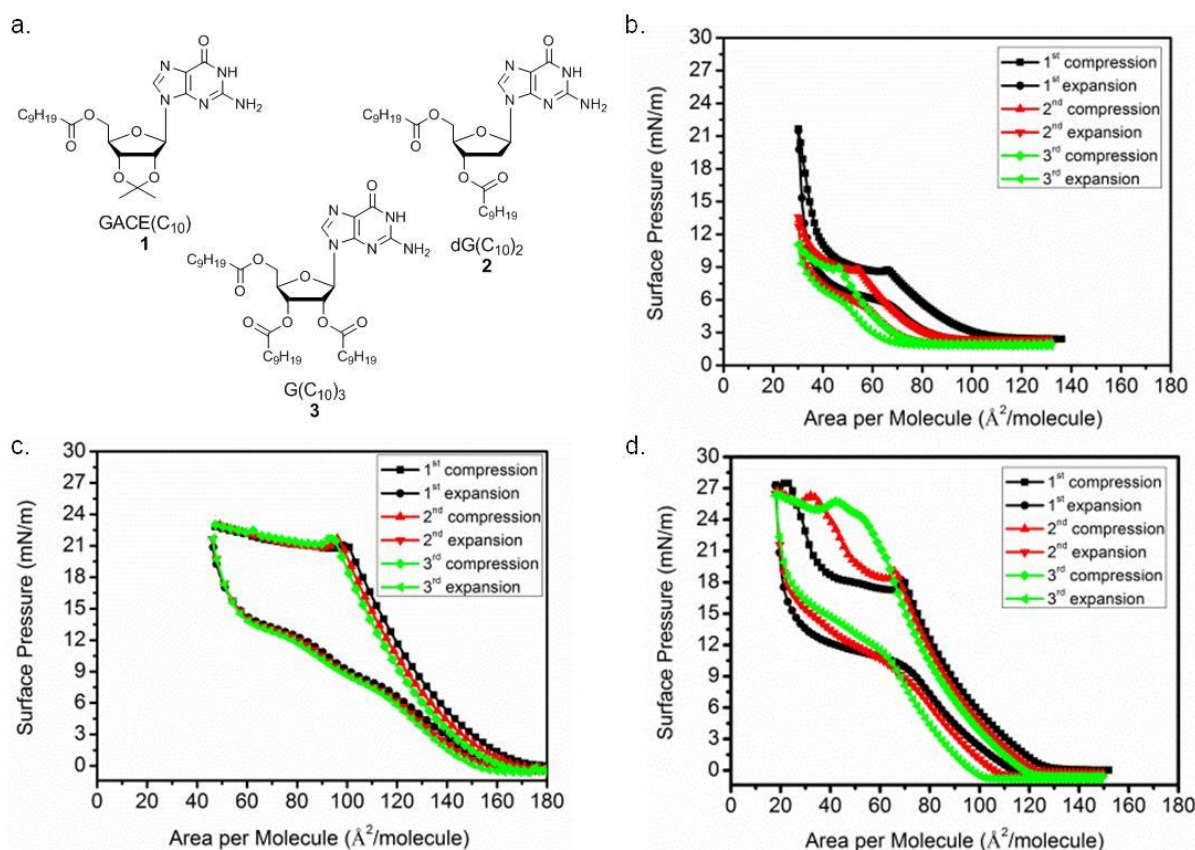


Figure 2.1: (a.) molecular structure of guanosine derivative 1-3; b. $\pi(A)$ isotherms of 1 (a.), 2 (b.) and 3 (c.) (from “Specific behaviour of guanosine in liponucleoside thin films”⁹).

For the preparation of monolayer LB films, clean deionized Millipore water was placed in the bath of the Langmuir–Blodgett trough, then a freshly cleaved muscovite mica plate was dipped into the water by a motorized vertical dipper. Initial Langmuir films were prepared compressing guanosines films to the corresponding critical pressure. After 30 minutes relaxation, the mica plate was lifted from the bath at the rate of 3 mm/min and the adsorbed films were then let to dry in air for 24 hours before recording AFM images (**Figure 2.2**).

Profound differences between surface structures of different derivatives can be immediately noticed. Derivative **1** shows a ribbon-like structures, confirming the hypothesis deduced from isotherm: this ribbon-shaped aggregates have maximal height of around 2.4 nm, corresponding to nearly twice the length of the hydrocarbon tail, $2l_c = 2.6$ nm, which signifies partial formation of bilayer structures. Derivative **2** shows flat terraces of micrometer size with height modifications in steps of around 2.6 nm or some multiple of this value: from the height of these terraces it can be concluded that LB films of the derivative with two tails are actually bilayers. Derivative **3** shows irregular thread-like assemblies with heights of several micrometers (10 nm); the height is also not changing in steps, but continuously, which might

be explained by formation of elongated micellar aggregates, which are laying freely on the surface.

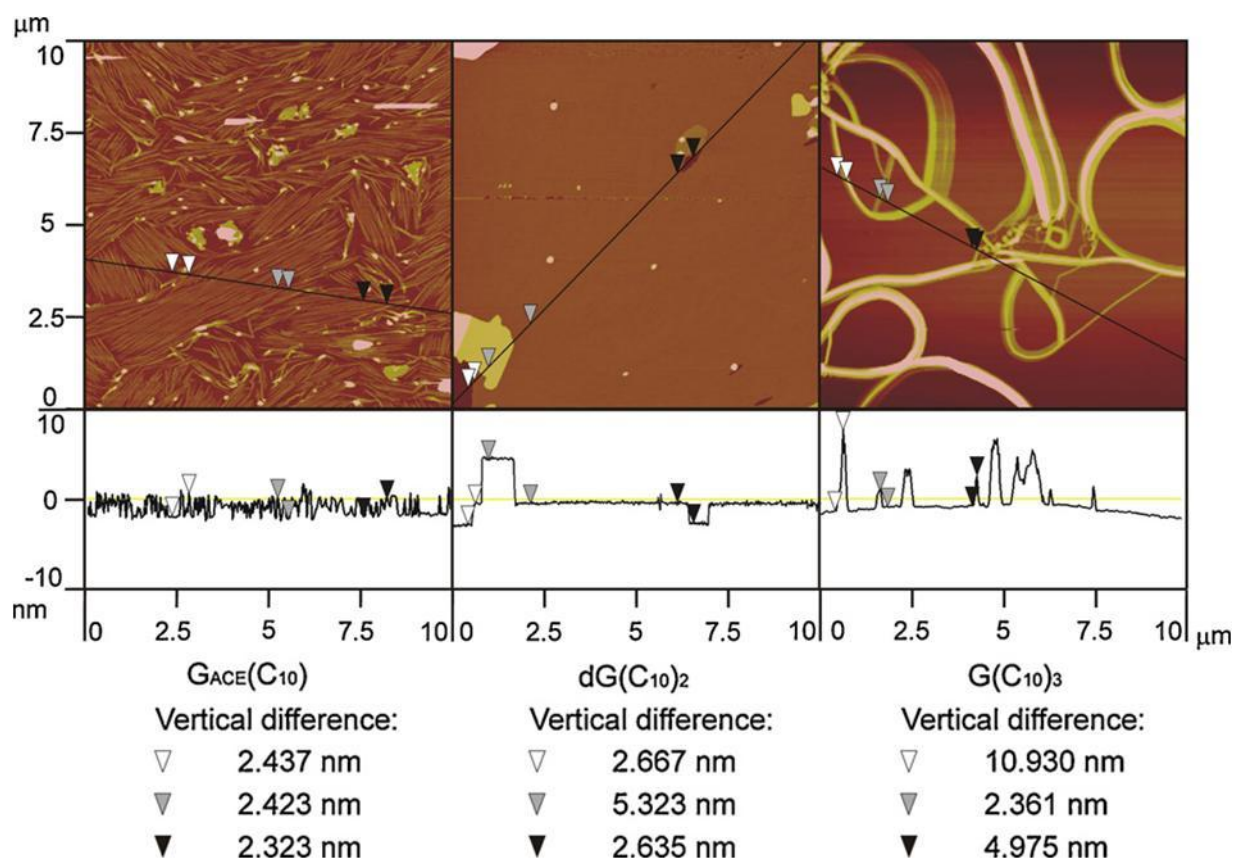


Figure 2.2: AFM images of LB films of $G_{ACE}(C_{10})$ (1, left), $dG(C_{10})_2$ (middle, 2), and $G(C_{10})_3$ (right, 3) deposited on muscovite mica. Vertical cross-sections along the marked lines are reported below each image. The values displayed at the bottom are vertical distances between the markers of the same colour (from “Surface structure of Langmuir–Blodgett films of lipophilic guanosine derivatives”¹⁰).

The large differences between the surface morphologies of the transferred films can be attributed to surface interaction between the hydrophilic mica surface and the deposited monolayer¹³. Due to this interaction, similar behaviour of the $\pi(A)$ isotherms does not necessarily mean also similar quality of the LB films. These findings are in agreement with the results of recent work of Jin at al., who studied lipid derivatives of acyclovir with one and two 18-carbon long hydrocarbon tails and reported that double-chained derivative formed rigid surface layers, while single-chained derivative formed loose structures^{14,15}.

From the point of view of possible applications in nanotechnology, the G-derivative with two tails seems to be most promising for applications requiring homogeneous films with well defined and tunable thickness. It forms relatively homogeneous LB films with a regular terrace-like morphology, preserved also in multilayer structures. Derivative 3 is likely

Chapter III: Liponucleoside thin films: the special behaviour of guanosine

unsuitable for applications, as its LB film structures are very irregular and practically cannot be controlled. The ribbon-like structures formed by the derivative **1** are on the other hand interesting for applications requiring wire-like surface architectures, such as various interconnects and orientation-sensitive elements. Its properties might be further improved by developing appropriate methods leading to alignment of the ribbons along a predetermined direction. In addition to this, intermolecular hydrogen bonding, which might occur in Langmuir films of this derivative, provides additional possibility for tuning the properties of its LB film structures. The tuning can be achieved either by adding assembly stimulating ions to the water subphase or by dilution of the material with some other lipophilic molecules.

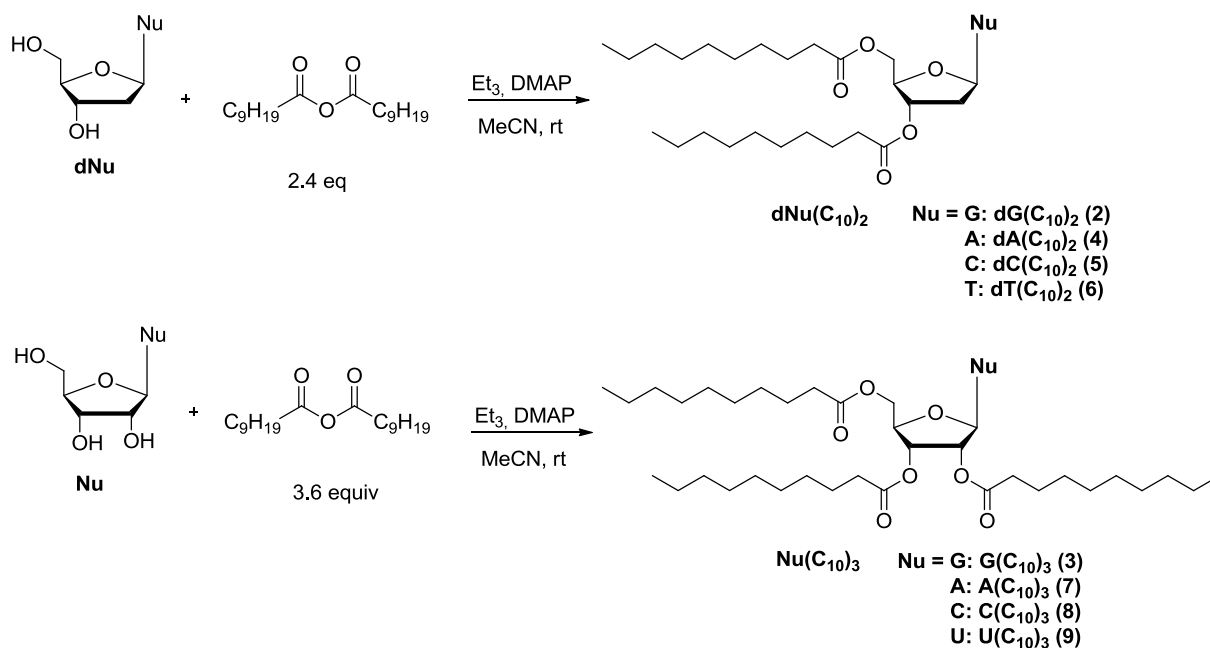
3. Liponucleoside thin films⁹

After studying different guanosine LB films, it has been investigated the surface assembly of lipophilic nucleosides having the two or three lipophilic tails, but incorporating different nucleobases in their headgroups. The emphasis is on analysis of monomolecular layers (Langmuir films) formed at the air–water interface. In addition, some comparison is made with films (LB films) transferred from the water surface onto a mica substrate. The compounds investigated are derivatives of deoxynucleosides (containing guanine (G, **2**), adenine (A, **4**), cytosine (C, **5**) or thymine (T, **6**) nucleobase, respectively) with two 10-carbon long alkanoyl tails and derivatives of nucleosides (containing G (**3**), A (**7**), C (**8**) or uracil (U, **9**) nucleobase, respectively) with three 10-carbon long alkanoyl tails.

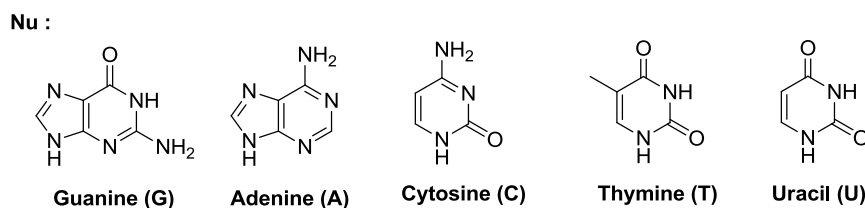
3.1 Synthesis of liponucleosides

The synthesis of the liponucleosides has been carried out in the same fashion described for derivative **3**, by direct esterification of the (deoxy)ribose alcoholic functions with decanoic anhydride in acetonitrile (MeCN) (**Scheme 3.1.1**), and is described in the experimental section. Depending on nucleoside, purification through column chromatography or crystallization or both allowed the obtainment of analytically pure products.

a.



b.



Scheme 3.1.1: a. Synthesis of deoxynucleosides with two 10-carbon long alkanoyl tails 2, 4-6 and of nucleoside with three tails 3, 7-9; b. different types of nucleobases.

3.2 Results

3.2.1 Langmuir films isotherms

Following the procedure used for guanosine derivatives **1-3**, Langmuir films of liponucleosides were prepared from 10^{-3} M solutions of compounds **2-9**, using a LB trough with UV sterilized and distilled water (Millipore) as subphase. After 30 min in non-compressed state to allow solvent evaporation and establishment of the internal equilibrium, surface-pressure versus area isotherms $\pi(A)$ were recorded by compressing a monolayer with a barrier speed of 5 mm/min. Compression/expansion cycles were repeated several times.

From $\pi(A)$ isotherms of derivatives with two decanoyl tails one can immediately notice that the isotherm for deoxyguanosine derivative **2** (**Figure 3.2.1.1**, a.) exhibits significantly different characteristics from the isotherms of derivatives of the other three deoxynucleosides **4-6**. During the first compression cycle **2** displays a first order transition from the liquid

expanded (LE) to the condensed phase (C)¹⁶. A plateau region of phase coexistence starts with a noticeable kink at $\pi \sim 18$ mN/m and $A \sim 65 \text{ \AA}^2$. The onset of the condensed phase appears at $A \sim 40 \text{ \AA}^2$, which corresponds to the minimum molecular area that can be occupied by two alkyl chains¹⁷. A subsequent expansion of the film reveals a considerable hysteresis of the $\pi(A)$ isotherm with a prompt drop of surface pressure taking place at the beginning of the expansion process. This signifies formation of a well-ordered structure with slow and irreversible dissociation mechanism¹⁸. The isotherm of the second compression–expansion cycle (red curve in **Figure 3.2.1.1**, a) at larger surface areas is practically the same as for the first cycle, i.e. only a minor shift towards smaller areas per molecule is observed. This observation indicates a good stability of the monolayer structure, i.e. no material is lost during first compression due to formation of stable aggregates and/or diffusion to the subphase. The following cycles, however, reveal some unusual modifications. The third cycle exhibits an intermediate behavior, while the fourth and further cycles show a shift of the kink and the associated starting of the plateau region towards higher surface pressure ($\pi \sim 25$ mN/m) and smaller area per molecule ($A \sim 45 \text{ \AA}^2$). A transition to the new type of $\pi(A)$ isotherms might be explained by rearrangement of the initial surface assembly to some other surface structure. Additionally, one can notice that in the subsequent cycles the $\pi(A)$ isotherms exhibit significant shifts towards smaller surface areas. The experiment was repeated several times and the transition from one to another type of the $\pi(A)$ isotherms had always been observed, only the consecutive number of the cycle at which it occurred was slightly varying.

The surface pressure of deoxyadenosine derivative **4** during all compression–expansion cycles monotonously increases with decreasing area per molecule (**Figure 3.2.1.1**, b.). During the first compression, the slope $d\pi/dA$ of the $\pi(A)$ curve increases up to $\pi \sim 35$ mN/m and $A \sim 50 \text{ \AA}^2$. Afterwards, for $A < 50 \text{ \AA}^2$, the slope decreases and a plateau region emerges smoothly and continuously. The observed behavior is very similar to the behavior reported for dioleoylphosphatidyl-adenosine exhibiting two considerably longer hydrocarbon tails¹⁹. In contrast to derivative **2**, which shows very different forms of the $\pi(A)$ curve during compression and expansion processes, the deoxyadenosine derivative behaves practically the same during compression and expansion. However, during expansion the $\pi(A)$ curve is significantly shifted towards the lower areas per molecule. The shifts appear also in consecutive compression–expansion cycles. These features imply formation of loose aggregates, which are diffusing into the subphase.

During the compression process deoxycytidine derivative **5** exhibits a very similar $\pi(A)$ isotherm (**Figure 3.2.1.1**, c.) compared to the deoxyadenosine derivative **4**. It also exhibits

similar shifts towards the lower surface areas in subsequent compression–expansion cycles. However, the form of the $\pi(A)$ curve observed during the expansion is notably different from the one observed during the compression. In particular, a prompt drop in surface pressure at the beginning of the expansion process is evident. The behavior of deoxythymidine derivative **6** resembles the behavior of the deoxyadenosine derivative **4** during both the compression and the expansion process, the main difference being the slightly lower maximum values of π and $d\pi/dA$ for **6** (Figure 3.2.1.1, d.).

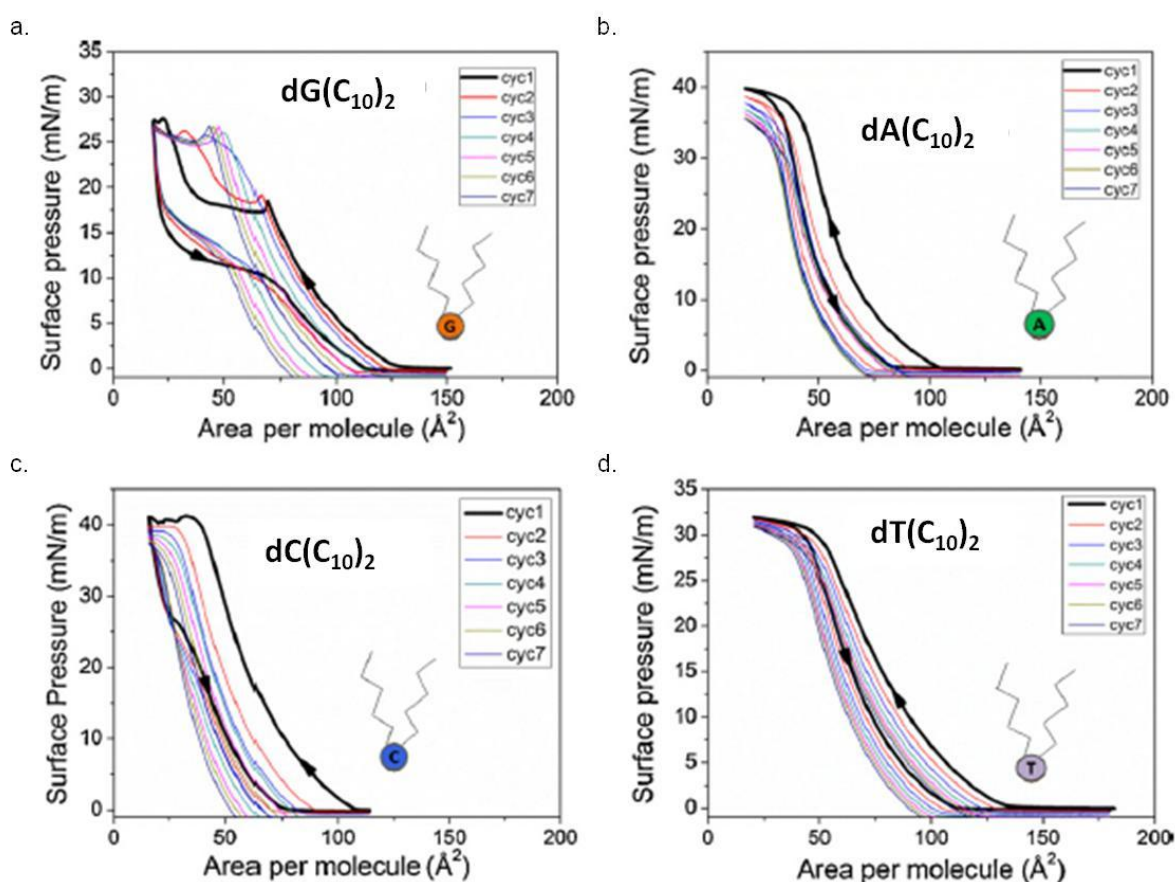


Figure 3.2.1.1: Surface pressure–area isotherms of derivatives with two alkanoyl tails: **2** (a.), **4** (b.), **5** (c.), **6** (d.) (from “Liponucleoside thin films: the special behaviour of guanosine”⁸).

The $\pi(A)$ isotherms of derivatives with three decanoyl tails are shown in **Figure 3.2.1.2**. Also here the isotherm for guanosine derivative **3** exhibits profoundly different features from the isotherms of derivatives of the other three nucleosides (**Figure 3.2.1.2**, a.). For derivative **3** again a notable kink followed by a plateau region of the two-phase coexistence can be observed. The kink appears at $\pi \sim 17$ mN/m and $A \sim 80 \text{\AA}^2$. The onset of the condensed phase again appears at $A \sim 40 \text{\AA}^2$, but the increase of surface pressure is less prominent than for the analogous derivative **2** with two tails. The hysteresis observed between the compressions and

subsequent expansions is very similar as for the derivative **2**, however the reproducibility of the $\pi(A)$ isotherms for the derivative **3** is far better, i.e. no transition to some other type of isotherm takes place. These observations suggest that surface assembly formed by this derivative is very robust and stable.

The above described behavior was not observed for the other liponucleosides with three tails **7**, **8** and **9**, which showed analogous properties among them **Figure 3.2.1.2**, b.-d.). They all exhibit higher maximum surface pressures than the guanosine derivative. They show monotonic transition from the liquid phase to the plateau region. They all also exhibit considerable shifts towards smaller surface areas in consecutive compression–expansion cycles. However, similar to the series of derivatives with two tails, the cytosine derivative **8** exhibits some differences in the form of $\pi(A)$ curves measured during compression and expansion (Figure 3.2.1.2, c.).

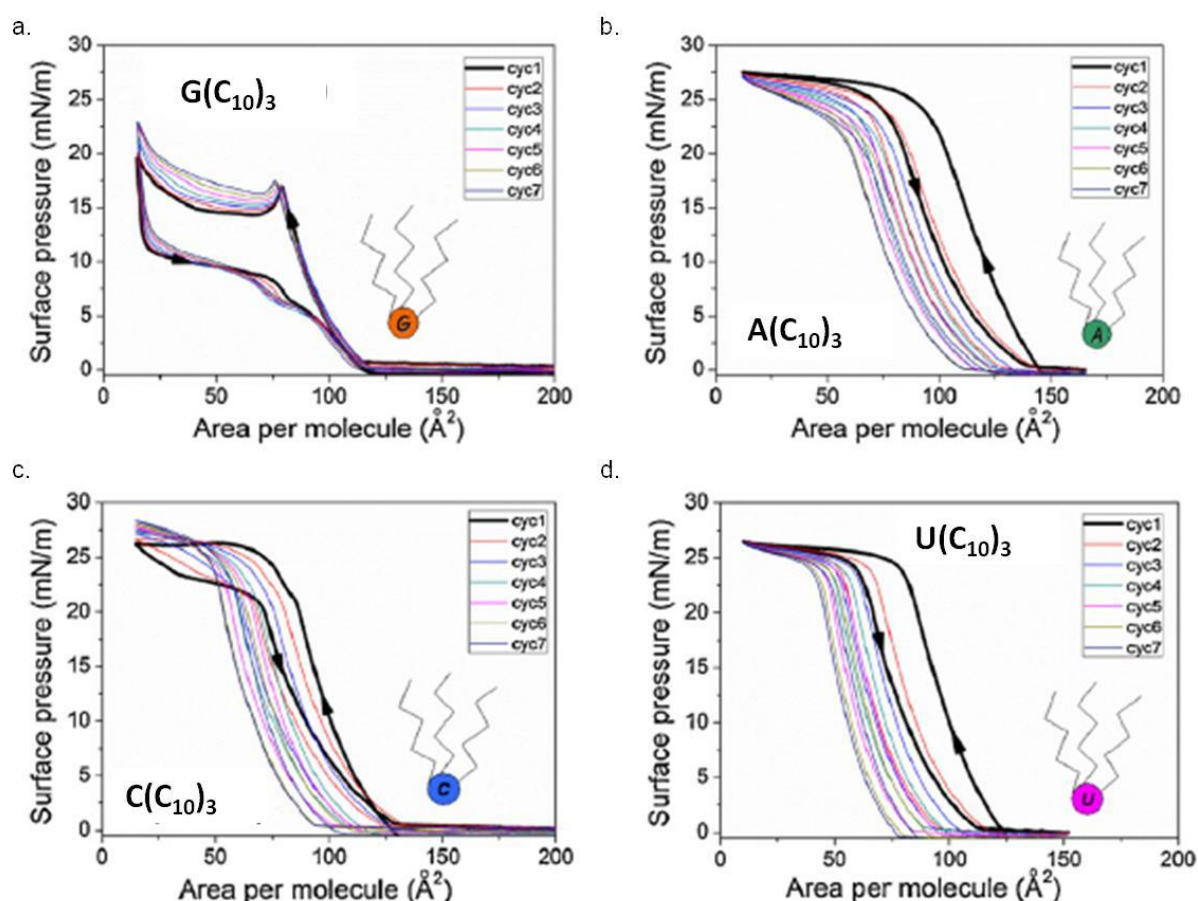


Figure 3.2.1.2: Surface pressure–area isotherms of derivatives with three alkanoyl tails: **3** (a.), **7** (b.), **8** (c.), **9** (d.) (from “Liponucleoside thin films: the special behaviour of guanosine”⁸).

3.2.2 Real time Brewster angle microscopy

A Brewster Angle Microscope (BAM, **Figure 3.2.2.1, a.**) enables the visualization of Langmuir monolayers or adsorbate films at the air-water interface²⁰. It utilizes the fact that when p-polarized light (polarized light with its electric field along the plane of incidence) is guided towards an air-water interface, no reflection occurs at a certain incident angle. This angle, the Brewster angle, is determined by Snell's law and depends on the refractive indices of the materials in the system:

$$\text{Snell's law: } \tan \alpha = n_2 / n_1$$

with α the Brewster angle in radians, n_1 the refractive index of air (≈ 1) and n_2 the refractive index of water (≈ 1.33) (**Figure 3.2.2.1, b.**).

The Brewster angle for the air-water interface is 53° , and under this condition the image of a pure water surface appears black. Addition of material to the air-water interface modifies the local refractive index (RI), and hence, a small amount of light is reflected and displayed within the image. The image displayed contains areas of varying brightness determined by the particular molecules and packing densities across the sampling area. This technique provides a perfect solution for noninvasive imaging of monolayers at the air-water interface: changes of film structure can be observed in real-time during the measurement.

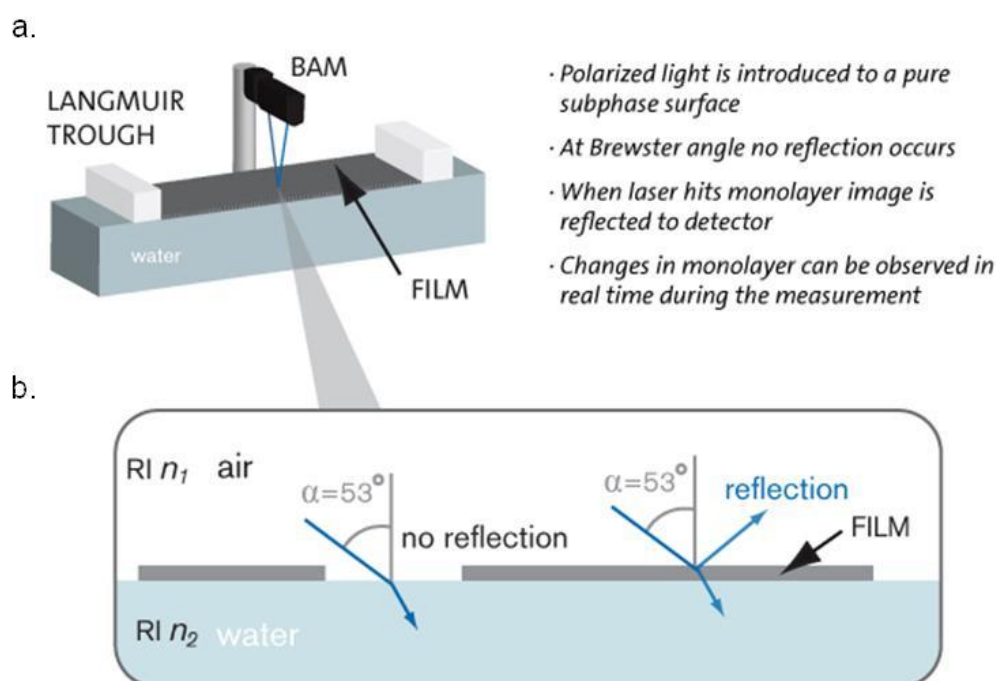


Figure 3.2.2.1: a. A Langmuir-Blodgett trough equipped with a Brewster angle microscope; b. working principle: when p-polarized light is guided towards an air-water interface at Brewster angle (53°), reflection occurs in presence of Langmuir films (from “Brewster Angle Microscopy”²⁰).

BAM images of the surface layer of deoxyguanosine derivative **2** were captured during the first compression, showing LE to C phase transition. At the beginning we observed the liquid expanded phase ($\pi = 15$ mN/m, $A = 75 \text{ \AA}^2$, **Figure 3.2.2.2**, a.), then a two phase coexistence region ($\pi = 17$ mN/m, $A = 65 \text{ \AA}^2$, **Figure 3.2.2.2**, b.). At higher pressure the islands of condensed phase with diameter of about $50 \mu\text{m}$ are clearly visible. With further compression the island fuse together. The observed behaviour is characteristic for first order phase transitions²¹.

In contrast to the deoxyguanosine derivative, BAM images of deoxyadenosine derivative **4** look very similar in the entire investigated range of the $\pi(A)$ isotherm (**Figure 3.2.2.2**, c.-d.). Even when a plateau region is approached ($\pi = 36$ mN/m, $A = 40 \text{ \AA}^2$, **Figure 3.2.2.2**, d.), no significant new structural details or modifications can be observed. Such a behavior is in agreement with a smooth and monotonic form of the $\pi(A)$ isotherm and signifies a 2nd order phase transition.

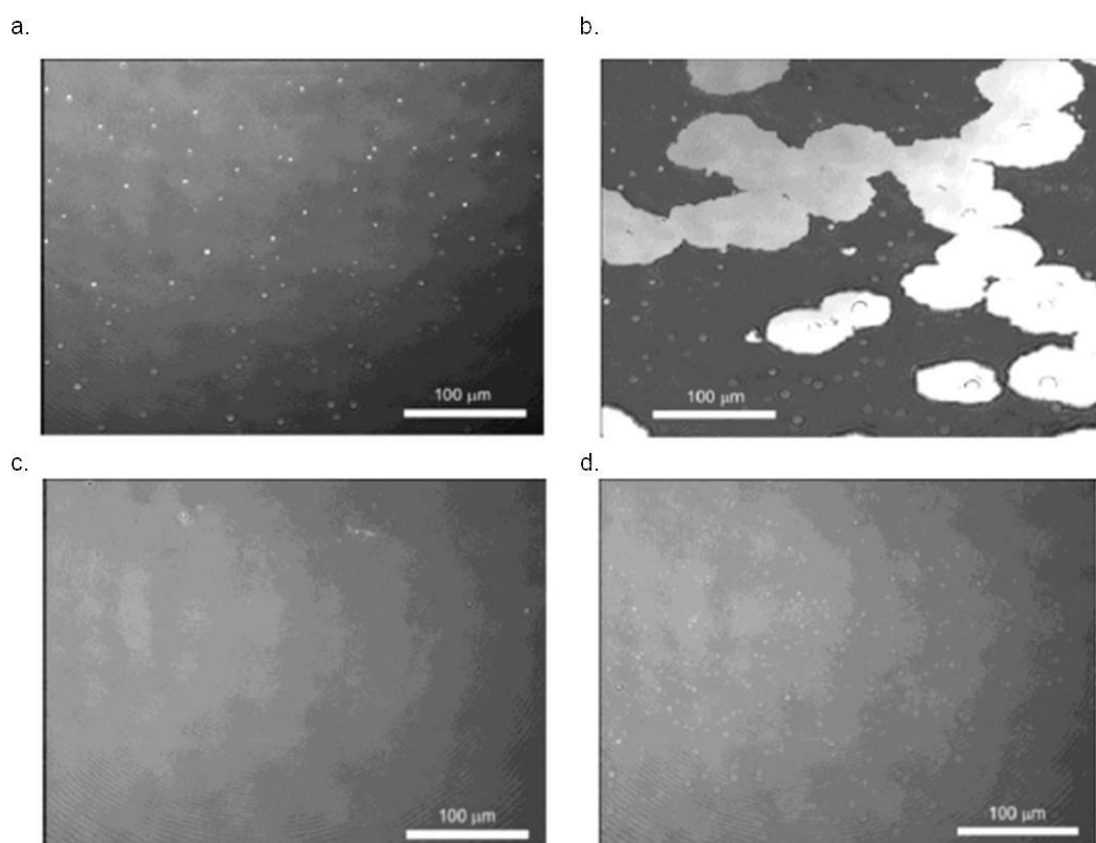


Figure 3.2.2.2: BAM images of Langmuir films: deoxyguanosine **2** just before ($\pi = 15$ mN/m, $A = 75 \text{ \AA}^2$, a.) and just after ($\pi = 17$ mN/m, $A = 65 \text{ \AA}^2$, b.) the kink in the $\pi(A)$ isotherm; deoxyadenosine **4** at lower ($\pi = 17$ mN/m, $A = 60 \text{ \AA}^2$, c.) and at higher surface pressure ($\pi = 36$ mN/m, $A = 40 \text{ \AA}^2$, d.) (from “Liponucleoside thin films: the special behaviour of guanosine”⁸).

3.2.3 Atomic force microscopy of films transferred to mica surface

LB monolayers were prepared as described previously: Langmuir films of nucleosides, compressed at desired pressure, were transferred onto freshly cleaved mica substrates, which were lifted from the bath at the rate of 3 mm/min. The film transfer was measured by the transfer ratio, which is defined as the ratio of the decrease in Langmuir monolayer surface area divided by the area of the solid support which has been coated³. The transfer ratio for the film **2** was 1.25 ± 0.06 , while for the less stable deoxyadenosine **4** film was 2.9 ± 1.2 . This is in agreement with the stability predictions from measurements of Langmuir films at the air-water interface.

The images were recorded at least 24 h after the LB deposition. One can notice that deoxyguanosine **2** produces a monolayer film with a relatively good surface coverage (**Figure 3.2.3.1, a.**). Dark patches, which correspond to the pristine mica surface, are relatively rare. In the right upper part of the image a small region coated with a multilayer film can be seen. The thickness of the monolayer is about 2.9 nm. This is much larger than the length of decanoic acid ($L_t \sim 1.3$ nm) and also significantly larger than the maximum dimension of the entire liponucleoside molecule ($L \sim 2.2$ nm) which signifies a formation of the bilayer surface structure¹⁰.

The quality of the deoxyadenosine **4** LB film is much worse (**Figure 3.2.3.1, b.**). Most of the deposited material appears in the form of large globular aggregates with the height of several tens of nanometers. In-between some patches of the film with the thickness of about 2.2 nm can be found. These observations indicate formation of droplet-like 3D structures. Such structures are soluble in water, which can explain a considerable loss of material detected in subsequent compression and expansion cycles on Langmuir films.

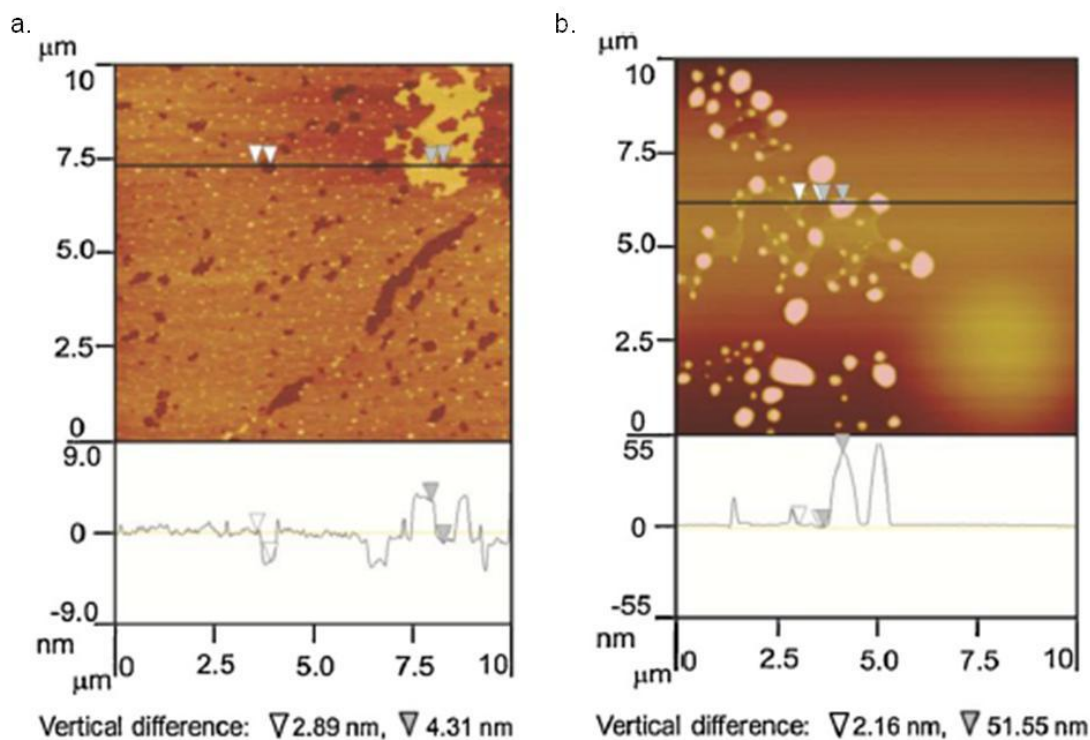


Figure 3.2.3.1: AFM images of Z-type LB films transferred onto freshly cleaved mica surface: a. deoxyguanosine **2** transferred at $\pi = 15$ mN/m; b. deoxyadenosine **4** transferred at $\pi = 25$ mN/m (from. Liponucleoside thin films: the special behaviour of guanosine⁸).

3.3 Discussion

Investigations of surface layers of different liponucleoside compounds reveal that the phase transition from the liquid analogue to the solid analogue phase in these materials can span the entire range from the profoundly first order to the continuous second order transition. The nature of the transition depends on the molecular structure and on the temperature²². Rädler et al. investigated a series of monoalkylated nucleotides with G, A, U and C head-groups and reported that isotherms of the guanosine analogue showed a unique phase behaviour²³. Our measurements on dialkylated deoxynucleosides and trialkylated nucleosides match very well with their findings. Similar to their results, we also observed that for the guanosine derivatives a well-expressed transition to the condensed phase occurs, while derivatives of all other nucleotides exhibit rather insignificant or absent condensed phase. These observations signify that guanine head-group provides the best support for compact and stable molecular packing in Langmuir films.

When comparing our results with the results of experiments on nucleolipid and phospholipid materials performed at different temperatures, one can notice that the form of $\pi(A)$ isotherms observed for guanosine derivatives in general corresponds to the typical low temperature

Chapter III: Liponucleoside thin films: the special behaviour of guanosine

behaviour, while the form of the $\pi(A)$ curves obtained for other nucleoside derivatives corresponds to the typical high temperature behavior^{17,24}. This additionally supports our hypothesis that molecular packing of guanine-based nucleolipids is optimal.

The question that naturally arises is, whether the observed unique behavior of guanosine derivatives in Langmuir films is based on non-Watson–Crick (Hoogsteen) base pairing typical for guanine assemblies mentioned in Section 1, or is it of some other origin. The surface areas of flat lying purine and pyrimidine nucleobases are around 45 \AA^2 and 35 \AA^2 , respectively^{25,26}, while the starting of the plateau region of the first order phase transition in surface layer of guanosine derivatives is observed at much larger areas per molecule (65 \AA^2 , 80 \AA^2). Consequently, it cannot be attributed to the interaction between the headgroups, but to the assembling of the hydrocarbon tails.

For phospholipid materials it is known that derivatives with only 10-carbon long tails are on the lower limit of their capability to form stable Langmuir films at room temperature²⁷, so a relatively good stability of the films investigated in our study should originate from the hydrophilic properties of the headgroups. The hydrophilic strength depends on the water solubility of the headgroup and on its polarity. The carboxyl groups and ribose are present in all the investigated derivatives, so the observed differences should be attributed to nucleobases. Adenine and thymine possess a multipolar charge distribution with molecular dipole moment of about $3D$, while guanine and cytosine exhibit a profoundly dipolar-type of charge arrangement with molecular dipole moment of about $6D$ ²⁸. These differences can be the reason for the liquid-like nature of Langmuir films of adenosine, thymidine and uridine derivatives and a relatively better stability of the films of cytidine and especially of guanosine derivatives.

In addition to this, guanine and its nucleosides are special because their solubility in water is more than one order of magnitude lower than the solubility of other nucleobases and their nucleosides^{29,30}. The low solubility of guanine head group provides a good hydrophilic balance to the low hydrophobicity of the decanoyl tails, which is to our opinion the main reason why guanosine derivatives are capable of forming stable surface films, while other derivatives form less stable surface layers and exhibit a tendency to diffuse into the subphase. At smaller surfaces areas, i.e. in the condensed phase, also hydrogen bonding between the headgroups definitely comes into play³¹. However, this bonding is to our opinion not crucial for the main differences in the self-assembling properties observed in our study. This view is supported by the results of experiments reported by Wang et al., who studied mixed films of monoalkylated guanine and cytosine²⁶. They detected that Watson–Crick base pairing takes

Chapter III: Liponucleoside thin films: the special behaviour of guanosine

place in the mixed films, however a general form of the $\pi(A)$ isotherm was only slightly perturbed with respect to the isotherms of the pure compounds. Nevertheless, to further elucidate the effect of hydrogen bonding on the behaviour of the $\pi(A)$ isotherms, measurements on mixed monolayers (G and C, G and T, A and T) are in progress and will be reported in a separate paper.

4. Conclusions

Our results show that guanine acting as a head-group in nucleoside molecules induces the formation of very stable Langmuir films at the air–water interface. These molecules exhibit the form of surface-pressure versus area isotherms that is typically found for phospholipid materials. The other analogous nucleosides exhibit considerably less stable films, exhibiting liquid-like isotherms. We suggest that the main reason for the specific behavior of guanine derivatives at large surface areas ($A > 60 \text{ \AA}^2$) is optimal hydrophilic balance of the guanine headgroup to the lipophilic moieties used in our study, and not intermolecular hydrogen-bonding between the headgroups. However, our results do not allow us to make the final conclusion about it, as none of the techniques used in our study is directly sensitive to the formation of hydrogen bonding. In this respect the use of IR spectroscopy techniques, such as for instance the ATR–FTIR, can bring crucial additional information. Computational modeling of molecular properties and experiments with different type of lipophilic groups are also needed to further clarify the phenomenon.

One of the properties, that also might decrease the importance of the hydrogen-bonding, is π – π stacking. It is known that isolated nucleobases prefer π – π stacking in water. The π – π stacking was also found in the interfacial assembly of a monoalkylated guanine moiety and was explained by tilted orientation of the guanine headgroup²⁶.

Another problem that needs further investigations is also transfer of the films from air–water interface onto solid surfaces and molecular arrangement in LB films. The formation of good quality LB films of guanosine derivatives on mica surface is in agreement with the observation of their stable film formation at the air–water interface. However, the measured thickness of the films is quite different from the expected thickness for a monomolecular layer. This signifies rearrangements of the molecular assembly during the transfer process, which is very likely induced by surface interaction with the substrate.

Bibliography

- (1) Talham, D.; Yamamoto, T.; Meisel, M. *Journal of Physics-Condensed Matter* **2008**, *20*.
- (2) Hussain, S.; Bhattacharjee, D. *Modern Physics Letters B* **2009**, *23*, 3437.
- (3) Petty, M. C.; Cambridge University Press: Cambridge, 1996.
- (4) Roberts, G. G.; Plenum, New York, 1990.
- (5) Kuhn, H.; Mobius, D.; Bucher, H. In *Physical Methods of Chemistry Part IIIB*; Rossiter, A. W. a. B., Ed.; Wiley: New York, 1972; Vol. 1, p 577.
- (6) <http://www.ksvnima.com/applications/glossary/langmuir-film>.
- (7) <http://www.ksvnima.com/technologies/langmuir-blodgett-langmuir-schaefer-technique>.
- (8) Coga, L.; Ilc, T.; Devetak, M.; Masiero, S.; Gramigna, L.; Spada, G.; Drevenšek-Olenik, I. *Colloids and Surfaces B-Biointerfaces* **2013**, *103*, 45.
- (9) Čoga, L.; Devetak, M.; Masiero, S.; Spada, G. P.; Drevenšek-Olenik, I. In *Guanine quartets. Structure and application*; RSC publishing: 2013, p 154.
- (10) Devetak, M.; Masiero, S.; Pieraccini, S.; Spada, G.; Copic, M.; Olenik, I. *Applied Surface Science* **2010**, *256*, 2038.
- (11) Giorgi, T.; Grepioni, F.; Manet, I.; Mariani, P.; Masiero, S.; Mezzina, E.; Pieraccini, S.; Saturni, L.; Spada, G.; Gottarelli, G. *Chemistry-a European Journal* **2002**, *8*, 2143.
- (12) Gottarelli, G.; Masiero, S.; Spada, G. *Journal of the Chemical Society-Chemical Communications* **1995**, 2555.
- (13) Samori, P.; Pieraccini, S.; Masiero, S.; Spada, G.; Gottarelli, G.; Rabe, J. *Colloids and Surfaces B-Biointerfaces* **2002**, *23*, 283.
- (14) Jin, Y.; Qiao, Y.; Li, M.; Ai, P.; Hou, X. *Colloids and Surfaces B-Biointerfaces* **2005**, *42*, 45.
- (15) Jin, Y.; Qiao, Y.; Hou, X. *Applied Surface Science* **2006**, *252*, 7926.
- (16) Berndt, P.; Kurihara, K.; Kunitake, T. *Langmuir* **1995**, *11*, 3083.
- (17) Ahlers, M.; Ringsdorf, H.; Rosemeyer, H.; Seela, F. *Colloid And Polymer Science* **1990**, *268*, 132.
- (18) Gambut, L.; Chauvet, J.; Garcia, C.; Berge, B.; Renault, A.; Riviere, S.; Meunier, J.; Collet, A. *Langmuir* **1996**, *12*, 5407.

Chapter III: Liponucleoside thin films: the special behaviour of guanosine

- (19) Berti, D.; Franchi, L.; Baglioni, P.; Luisi, P. *Langmuir* **1997**, *13*, 3438.
- (20) <http://www.ksvnima.com/technologies/brewster-angle-microscopy>.
- (21) DeVries, C. A.; Haycraft, J. J.; Han, Q.; Noor-e-Ain, F.; Raible, J.; Dussault, P. H.; Eckhardt, C. J. *Thin Solid Films* **2011**, *519*, 2430.
- (22) Rosemeyer, H. *Chemistry & Biodiversity* **2005**, *2*.
- (23) Radler, U.; Heiz, C.; Luisi, P.; Tampe, R. *Langmuir* **1998**, *14*, 6620.
- (24) Duncan, S.; Larson, R. *Biophysical Journal* **2008**, *94*, 2965.
- (25) Modeling by Dr. Omar Pandoli, university of Ferrara (Italy), using utility Chem3D, Cambridge Soft Corp., Cambridge, MA, USA, private communication.
- (26) Wang, Y.; Du, X.; Miao, W.; Liang, Y. *Journal of Physical Chemistry B* **2006**, *110*, 4914.
- (27) Yun, H.; Choi, Y.; Kim, N.; Sohn, D. *Bulletin of the Korean Chemical Society* **2003**, *24*, 377.
- (28) Bloomfield, V. A.; Crothers, D. M.; Tinoco Jr, I. T. J. *Nucleic Acids: Structures, Properties, and Functions* Sausalito, CA, 2000.
- (29) Herskovits, T. T.; Harrington, J. P. *Biochemistry* **1972**, *11*, 4800.
- (30) Devoe, H.; Wasik, S. P. *J. Solution Chem.* **1984**, *13*, 51.
- (31) Israelachvili, J. *Intermolecular & Surface Forces*; Academic Press: London, 1992.

*Chapter IV: Functionalized guanosines for
organic electronic devices*

1. Organic semiconductor for Field-Effect Transistor (FET)^{1,2}

A field-effect transistor (FET) is an electronic device that amplifies and switches electrical signals. The development of metal–oxide–semiconductor field-effect transistors (MOSFETs) and integrated circuits (microprocessors) has forever changed our everyday lives since their invention more than 50 years ago. Today, we are facing a new technological evolution that could possibly have a similar impact on our lives: the emergence of flexible and printed electronics. Among them, organic field-effect transistors (OFETs) have been conceptualized and developed over the past two decades. The advantages of organic systems include: vapor/solution phase fabrication and good compatibility with different substrates, including flexible plastics, and opportunities for structural tailoring. This trend is driven by the demand for inexpensive, large area, flexible devices processed at far lower substrate temperatures than Si chips.

1.1 OFET: working principles

The most common OFET device configuration is that of a thin-film transistor, in which a thin film of the organic semiconductor is deposited on top of a dielectric insulator with an underlying gate (G) electrode. Charge-injecting source-drain (S-D) electrodes providing the contacts are defined either on top of the organic film (top-contact configuration) or on the surface of the FET substrate prior to deposition of the semiconductor film (bottom-contact configuration). Minimal current between S and D electrodes is measured when no voltage is applied between the G and S electrodes (device ‘off’ state).

A positive gate voltage (V_g) for example will induce negative charges that were injected from the grounded electrodes (electrons) at the insulator/semiconductor interface. For negative V_g , positive charges (holes) will be accumulated. The number of accumulated charges is proportional to V_g and the capacitance (C_i) of the insulator. However, not all induced charges are mobile and will thus contribute to the current in a field-effect transistor. Deep traps first have to be filled before the additionally induced charges can be mobile. That is, a gate voltage has to be applied that is higher than a threshold voltage (V_{Th}), and thus, the effective gate voltage is $V_g - V_{Th}$. When a small source-drain voltage is applied (V_{ds}) the current flowing through the channel is directly proportional to V_{ds} : this is the linear regime (**Figure 1.1.1, a.**), as shown in transistor output characteristic curve (source-drain current I_{ds} at increasing V_{ds} for different constant V_g). When the source-drain voltage is further increased, a point $V_{ds,sat} = V_g -$

V_{Th} is reached, at which a saturation regime begins: further increasing the source-drain voltage ($V_{ds} > V_{ds, sat}$) will not substantially increase the current but the current saturates at a level $I_{ds, sat}$ ³ (**Figure 1.1.1, a**).

The other curve which describes an OFET is the transfer characteristic (I_{ds} versus V_g at constant V_{ds}). In the linear regime there is a direct proportionality of I_{ds} to V_g and of its gradient to the mobility (μ , the field-effect carrier mobility of the semiconductor); most semiconductors, however, show gate voltage dependent mobilities, and thus, the curve shape may deviate from being linear (**Figure 1.1.1, b**). In the saturation regime the square root of I_{ds} should be linearly dependent on the V_g , and its gradient is proportional to the mobility; extrapolating the linear fit to zero yields the threshold voltage V_{Th} (**Figure 1.1.1, c**). From transfer characteristic one can extract the on/off ratio, which is the ratio of the drain current in the on-state at a particular gate voltage and the drain current in the off-state (I_{on}/I_{off}). For clean switching behavior of the transistor, this value should be as large as possible.

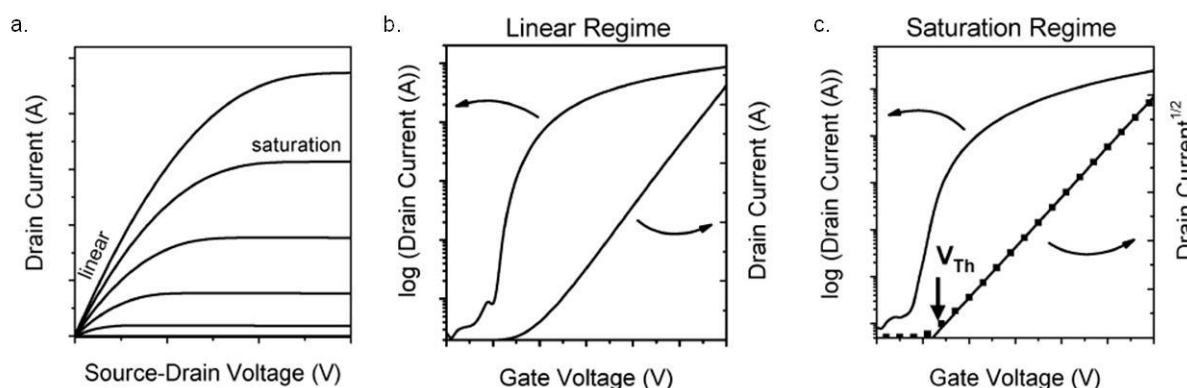


Figure 1.1.1: Representative current-voltage characteristics of an n-channel organic field-effect transistor: output characteristics (a.) indicating the linear and saturation regimes; transfer characteristics in the linear regime ($V_d \ll V_g$, b.) and in the saturation regime ($V_{ds} > (V_g - V_{Th})$, c.), indicating the threshold voltage V_{Th} (from ‘Electron and Ambipolar Transport in Organic Field-Effect Transistors’³).

When an OFET is active, upon the application of negative gate and drain voltage (V_g and V_{ds}), the organic material is said to be *p*-channel since holes are the majority charge carriers. On the other hand, when a positive S-D current (I_{ds}) is observed upon the application of positive V_g and V_{ds} , the semiconductor is *n*-channel since the electrons are mobile (**Figure 1.1.2**). In a few cases, OFETs operate for both V_{SG} and V_{SD} polarities and the semiconductor is said to be ambipolar.

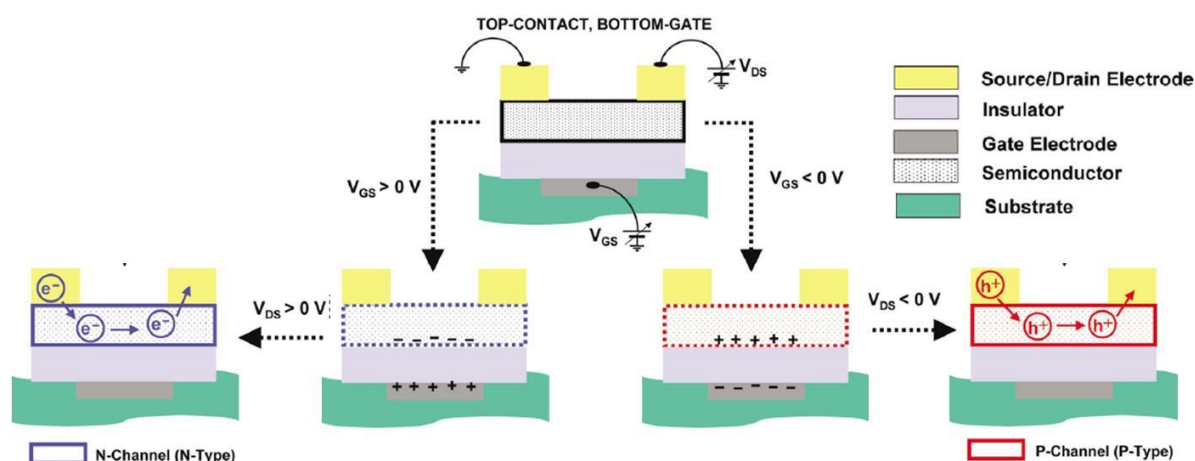


Figure 1.1.2: Schematic of p- and n-channel thin-film transistor operation (from ‘Semiconductors for organic transistors¹’).

1.2 Organic semiconductors

To achieve acceptable performance, organic semiconductors must satisfy general criteria relating both the injection and current-carrying characteristics, in particular: (i) the highest occupied/lowest unoccupied molecular orbital (HOMO/LUMO) energies of the individual molecules (perturbed by their placement in a crystalline solid) must be at levels where holes/electrons can be induced at accessible applied electric fields; (ii) the crystal structure of the material must provide sufficient overlap of frontier orbitals to allow efficient charge migration between neighboring molecules; (iii) the solid should be extremely pure since impurities act as charge carrier traps; (iv) the molecules should be preferentially oriented with the long axes approximately parallel to the FET substrate normal since the most efficient charge transport occurs along the direction of intermolecular π - π stacking; and (v) the crystalline domains of the semiconductor must cover the area between the S and D contacts uniformly, hence the film should possess a single crystal-like morphology.

Organic semiconductors, both small molecules and polymers, consist usually in π -conjugated systems; the structure of this system is made of a conjugated core (backbone), heteroatoms, substituents (electron donating or withdrawing) and side chains (i.e., solubilizing groups). The conjugated core (backbone) determines most of the electronic properties (e.g., energy level and band-gap, inter/intramolecular interaction, and solubility) and influences molecular packing. Heteroatom replacement is an effective way to tune electronic properties, solubility and molecular packing. Core substitution also affects electronic properties, solubility and molecular arrangements. Side chains are usually incorporated to impart solubility, while they may also impact electronic properties in the solid state by changing molecular packing structures (**Figure 1.2.1, a.**).

Chapter IV: Functionalized guanosines for organic electronic devices

Packing mode of the organic semiconductors becomes very important for the analysis of the charge transport between molecules; lamellar packing (2-D π -stacking) is believed to be the most efficient for charge transport because it transports the charge carriers through an almost straight line (namely, the shortest route). As mentioned before, ideally the organic molecules should pack along the current direction in the conducting channel, adopting a so called edge-on orientation⁴, which maximizes charge transport along π - π stacking direction (**Figure 1.2.1**, b.).

Typical acenes and fused arenes of aromatic hydrocarbons as seen in **Figure 1.2.1**, c. show ideal transistor behavior when employed in OFETs (**Figure 1.2.1**, c). Their π -conjugated systems are similar to that of single layer of graphite, that is, graphene, to date the aromatic compound with the highest charge mobility, fundamental for conduction. One of the most studied system is pentacene (**P5**)⁵: it is commercially available and displays one of the highest hole mobilities for a polycrystalline film. As semiconductor, P5 has good characteristics: charge mobility of $1.5 \text{ cm}^2/\text{Vs}$, on/off current ratio ($I_{\text{on}}/I_{\text{off}}$) $>10^8$ and near-zero threshold were reported by Lin et al⁶.

Another important class of molecular semiconductors is based on the thiophene ring, an electron-rich heterocycle: both the first OFET and the first printed transistor utilized polythiophenes as their semiconducting layers⁷; examples of this class of compounds are reported as small molecules, like sexithiophene (**6T**), as oligomers, (hexyl-substituted thiophene oligomers **DH-6T** and **DH-4T**) and also as polymer (poly(3-substituted thiophene)s **P3HT**). Oligothiophenes have attracted attention since the discovery of OFETs because (i) oligothiophenes facilitate planar structures rather than nonplanar structures as it occurs in oligophenyls (planar structures are possible under particular conditions), (ii) it is much easier to modify thiophene than benzene rings and (iii) they have good solubility and processability.

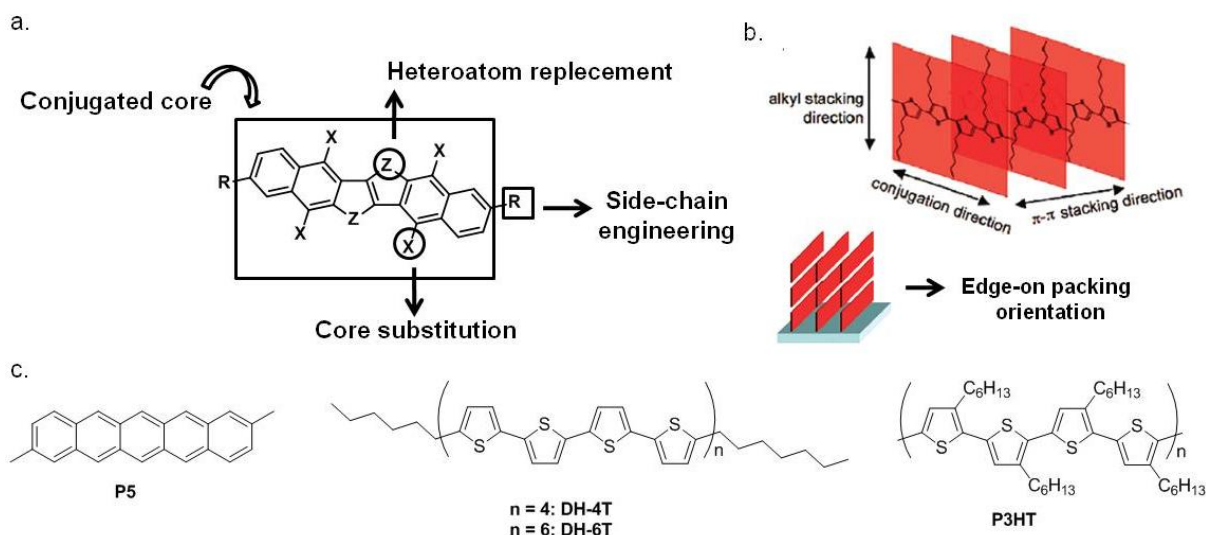


Figure 1.2.1: a. Possible charge transport mechanisms and edge on orientation in crystalline polymer films (from ‘Semiconducting π -Conjugated Systems in Field-Effect Transistors: A Material Odyssey of Organic Electronics⁴’). b. Illustration of a π -Conjugated System (from ‘Integrated Materials Design of Organic Semiconductors for Field-Effect Transistors²’); c. examples of organic semiconductor molecules.

2. Guanosine derivatives as semiconductors in field effect transistors

2.1 Guanosine-based OFET

As described in Chapter II, deoxyguanosine dG(C₁₀)₂ ribbon aggregates showed conduction properties once deposited between two electrodes in a two-terminal Hybrid Molecular Electronic device: depending on the distance between electrodes, this device behaves like a diode if the distance is less than 100 nm, or like a MSM device for greater electrodes distance. dG(C₁₀)₂ was employed also as active layer in a field effect transistors⁸. The prototype structure investigated here is a planar metal-insulator-metal nanojunction, consisting of two arrow-shaped metallic electrodes facing each other and connected by the supramolecular structures, and a third electrode (gate) is deposited on the back of the device. The use of self-assembled molecules as semiconductor is a way to control the formation of a highly ordered layers using a bottom-up approach, a huge improvement compared to devices obtained with disordered molecular layers or single molecules with tremendous interconnection problems.

The hybrid nanodevices were fabricated by room-temperature cast deposition. Transport experiments were performed by changing the gate voltage (V_g) in order to investigate its influence on the current (I_{ds}) between the source and drain electrodes, and to evaluate the response of the nanodevices upon variation of V_g . These I - V curves (**Figure 2.1.1**) are asymmetric, with a rectification ratio (RR) (defined at a fixed drain-source voltage V_{ds} as $RR(V) = I(V)/I(-V)$) of 3. These values suggest that the intrinsic dipole moment is partially preserved in the supramolecular layer connecting the electrodes, and induces an asymmetry in the charge pathway, resulting in a preferential direction for the current flow. In transfer characteristic the current (I_{ds}) at fixed drain-source voltage ($V_{ds} = 2$ in) decreases with V_g as in a p -channel MOSFET (metal-oxide semiconductor FET), where the majority charge carrier are positive (“holes”).

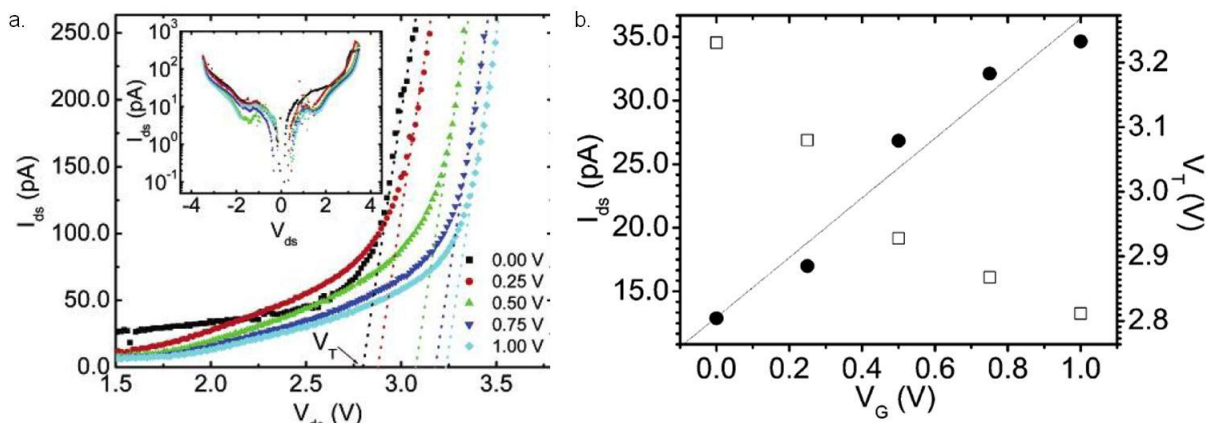


Figure 2.1.1: a. Output characteristics of the three-terminal deoxyguanosine device with an electrode separation of 40 nm. The dashed lines extrapolate V_{Th} for any V_g value. In the box a log plot of the full current-voltage curves at different V_g . b. Left scale: Transfer characteristic (hollow squares) at $V_{ds} = 2.0$ V. Right scale: dependence of V_{Th} (circles) on the gate voltage V_g (from ‘Field Effect Transistor Based on a Modified DNA Base’⁸).

We should point out that our hybrid molecular p-channel MOSFET exhibits some differences with respect to the standard silicon counterpart. In fact, despite the linear dependence of I_{ds} on V_g for a given V_{ds} , the current is quite sensitive to small changes in the drain-source voltage. This suggests that conduction in our device is due to resonant tunneling, requiring an alignment of electronic level of V_g and V_{th} (**Figure 2.1.2**): the voltage threshold for the conduction can be in this way modulated by means of a control gate voltage V_g , an advantage respect to MOSFETs.

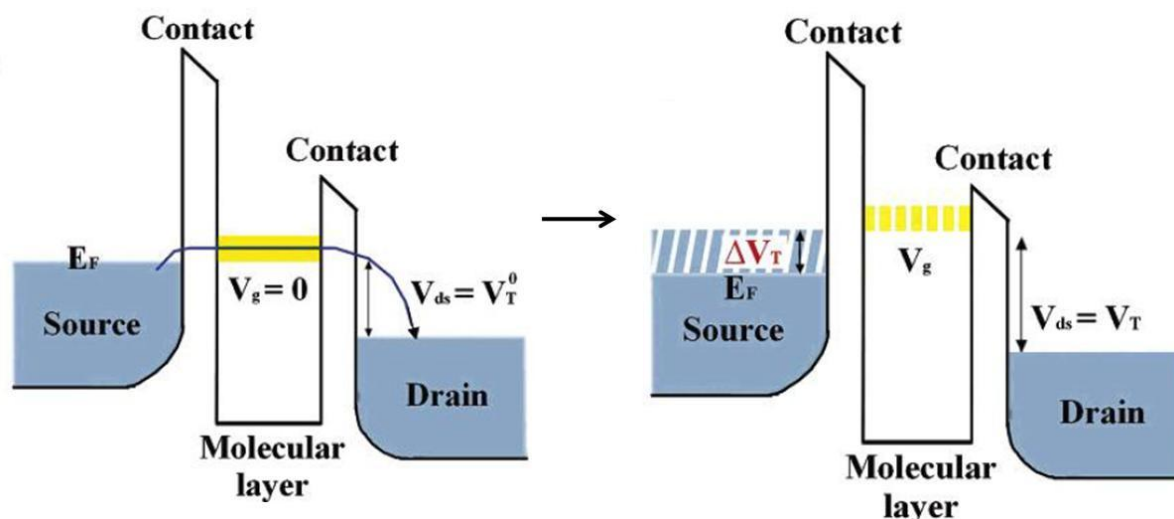


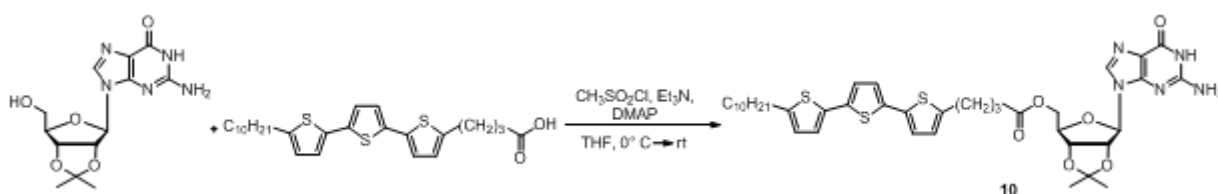
Figure 2.1.2: Resonant tunneling due to level alignment at $V_{ds} = V_{Th}^0$. The yellow bar represents the molecular electronic band at $V_g = 0$. The application of a gate bias V_g induces a shift of the energy bands and an additional ΔV_{Th} between source and drain has to be provided to activate the conduction process (from ‘Field Effect Transistor Based on a Modified DNA Base’⁸).

2.2 Functionalized guanosines: a new challenge

The examples reported of the diode and the OFET exploit the properties originated by guanine moieties ordered in their supramolecular architectures. A step forward is the investigation of new compounds in which guanine acts simply as a scaffold for other functionalities: in p -conjugated systems the control of molecular assembly into well-defined structures on the nanoscale is a key parameter for the improvement of the performances of materials to be used as components in electronic nanodevices, such as solar cells, light-emitting diodes (LEDs), and FETs.

In 2008 our group synthesized an oligothiophene functionalized guanosine: the aim was to drive the formation of a well-defined 2D structure, where oligothiophene functionalities can be directly π - π stacked by taking advantage of guanosine self-assembly. This terthiophene compound, depending on the experimental conditions, can form different ordered H-bonded arrays in solution, including ribbons and quartet-based structures.

The synthesis of guanosine started with the preparation of terthiophene carboxylic acid using a procedure described in literature^{9,10}; esterification of the free 5' position of GACE guanosine by condensation with a mixed anhydride obtained from the prepared acid and methanesulfonyl chloride¹¹ provides the terthiophene-guanosine hybrid in good yields (54%) (**Scheme 2.2.1**).



Scheme 2.2.1: Synthesis of 10.

Comparison between different structures in solution was achieved by registering NMR spectra in DMSO- d_6 , CDCl₃ and THF, and assigning signals through 2D correlated spectroscopy (COSY). In the ¹H NMR spectrum in CDCl₃ at room temperature, peaks are significantly broader than those observed in DMSO- d_6 , a strongly competing solvent for hydrogen bonding: this line-broadening suggests the presence of highly associated species in the former solvent, while DMSO doesn't allow the self-assembly through hydrogen bonding. In particular, signals of groups involved in hydrogen bonding shift downfield: the imino N¹-H and amino N²-H protons, which resonate at 10.71 and 6.54 ppm, respectively, in DMSO- d_6 ,

shift to 11.89 and 6.68 ppm in CDCl₃. In THF-d₈, the imino and amino protons behave analogously to what observed in CDCl₃, but the signals are much narrower all over the spectrum, allowing a easier study of the progressive formation of aggregated species.

In 15mM THF-d₈ solution at room temperature, only the N¹-H proton seems to be involved in H-bonding indicating that the compound exists as a dimer, as observed before for an alkylated guanosine¹². At higher concentrations and/or at lower temperatures, the amino protons are also involved in H-bonding, indicating that extended structures of the ribbon type start to be relevant (**Figure 2.2.1**, a.). The existence of dimeric and oligomeric structures was confirmed by electrospray ionization (ESI) mass spectrometry: derivative **10** was analyzed in positive-ion mode and the spectrum shows the presence of protonated dimers, trimers, and tetramers.

2D nuclear Overhauser effect spectroscopy (NOESY) experiments gave us structural information on the assembled species in solution. The spectrum of a 30 mM solution of **10** in THF-d₈ at 0 °C shows an intermolecular interaction between N²-H and H^{1'}, and a less intense cross peak between N²-H and H^{2'} protons. In addition cross peaks are generated by intermolecular interaction of H⁸ and N²-H with methyl protons of the acetamide ring: it has been shown¹³ that this contact pattern is characteristic of the B-type ribbon-like supramolecular arrangement (**Figure 2.2.1**, b.i.). The spectrum also shows cross peaks between N¹-H and H⁸ and between N²-H and H⁸ signals: this contact pattern is characteristic of the A-type ribbon (**Figure 2.2.1**, b.ii.).

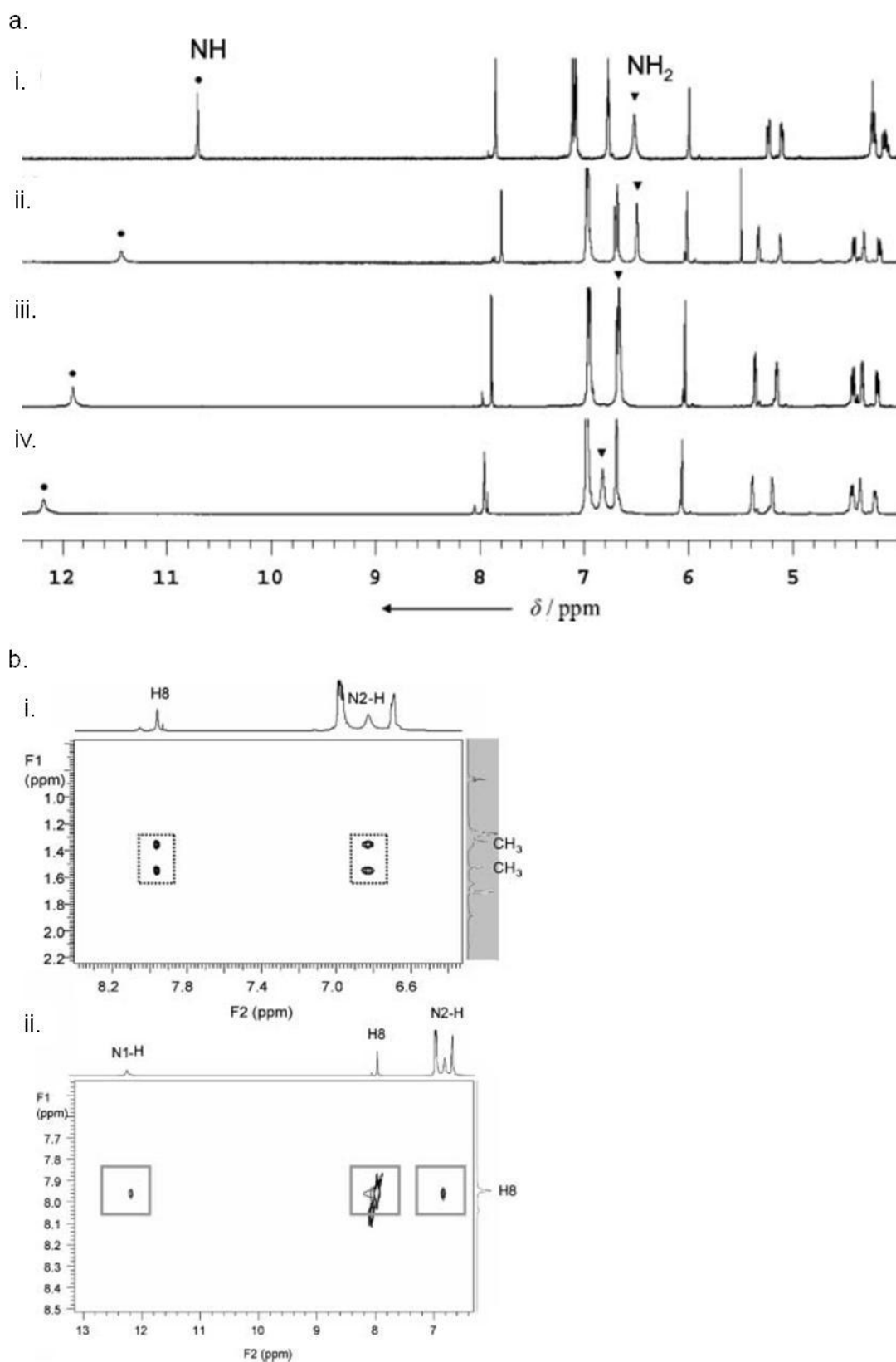


Figure 2.2.1: a. Portions of ^1H NMR spectra for solutions of 10: i. 14mM in DMSO-d_6 , 25 $^\circ\text{C}$; ii. 15mM in THF-d_8 , 25 $^\circ\text{C}$; iii. 30mM in THF-d_8 , 25 $^\circ\text{C}$; and iv. 30mM in THF-d_8 , 0 $^\circ\text{C}$. Triangles and dots mark the amino ($\text{N}^2\text{-H}$) and imino ($\text{N}^1\text{-H}$) protons, respectively. b. Portions of the NOESY spectrum of 30mM in THF-d_8 at 0 $^\circ\text{C}$ (from ‘Guanosine-based Hydrogen-bonded Scaffolds: Controlling the Assembly of Oligothiophenes’¹⁴).

2.2.1 Supramolecular switching triggered by external stimuli

Tuneable interconversion between discrete supramolecular assemblies can be a crucial issue for controlling the properties of the self assembled structures. For this derivative two different kind of switching were proposed: a conversion from ribbons to octameric aggregates fuelled by cation complexation and release, and a variation of supramolecular organization by a proper solvent choice.

As described previously for dG(C10)²⁻¹⁵, controlled sequential addition and removal of K⁺ trigger the ribbon-quartet interconversion of **10** in THF solution; the experiment was followed both by CD spectroscopy and by ¹H NMR.

CD spectrum of **10n** in the region of the intense π - π transitions of the guanine chromophore at ca. 260nm is weak, the stabilization of stacked G-quartet based structures induced by the K⁺ ion introduces a strong negative exciton signal, typical of a D₄-symmetric octameric species. The sequential addition of cryptand, HTf, and TEA, leads to spectra that resemble those of **10n**, **10₈·K⁺** and **10_n** (**Figure 2.2.1.1, a**).

Also ¹H NMR spectra give an unambiguous signature of the ribbon-octamer conversion (**Figure 2.2.1.1, b**): the H⁸ and N¹-H signals at 7.9 and 12.1 ppm, respectively, in **10n** move at 7.4 and 12.5 ppm when the supramolecular complex **10₈·K⁺** is formed. The N²-H signal (at 6.8 ppm in the initial solution) is split in two broad bands at 9.6 (N²-HA) and 6.5 ppm (N²-HB) after KPic addition: This downfield resonance for N²-HA is characteristic of G-quartet formation where this proton is involved in the cyclic H-bonded quartet^{16,17}. The presence of one set of signals confirms the D₄-symmetry for this octameric species.

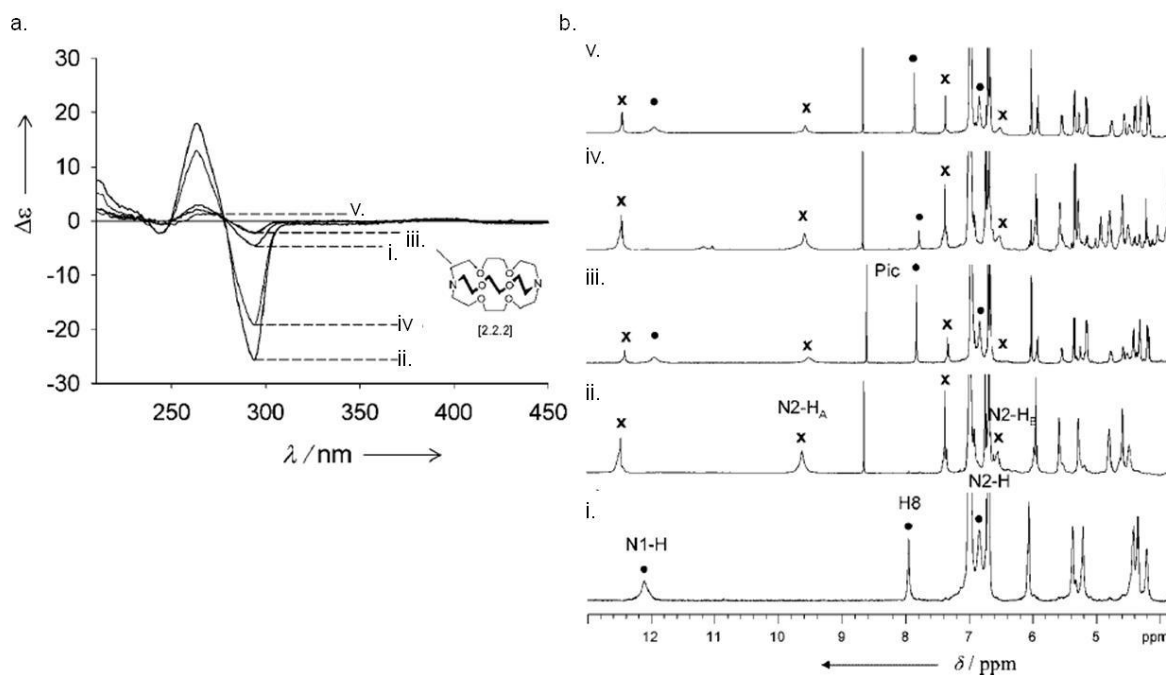


Figure 2.2.1.1: CD (a., 3mM) and ^1H NMR (b., 30mM) spectra of **10** in THF-d^8 at $0\text{ }^\circ\text{C}$. i. Initial solution; ii. after addition of 1/8 eq of K-Pic; iii. after further addition of 5 eq cryptand [2.2.2]; iv. after further addition of 1.3 eq HTf; and v. after further addition of 1 eq TEA. Dots and crosses mark the signals for the ribbon and octamer species, respectively (from ‘Guanosine-based Hydrogen-bonded Scaffolds: Controlling the Assembly of Oligothiophenes’¹⁴).

A change in solvent polarity may affect the supramolecular aggregation of guanosines. Our group reported the different behavior of **10** in the “good” solvent CHCl_3 , where lipophilic guanosine H-bonded structures are typically obtained, and in the more polar acetonitrile (ACN), whose ability to compete with H-bonds tends to disassemble them (“poor” solvent)¹⁸. After testing the stability of both ribbon and octameric species ($\mathbf{10}_8 \cdot \text{K}^+$) in a broad range of guanosine concentration (0.3 mM – 15 mM), a 3 mM solution of **10** was diluted with AcCN to 0.03 mM: a new completely different aggregate emerged from CD and NMR spectra (**Figure 2.2.1.2**, a.). The CD exciton-couplet in the guanine chromophore absorption region disappears, indicating the disassembly of the G-quartet based octameric structure, while an intense quasi-conservative exciton splitting in the 300–450 nm spectral region, characterized by a first negative and a second positive Cotton effect (characteristic change in circular dichroism in the vicinity of an absorption band of a substance), becomes predominant in the CD spectrum¹⁹. This strong bisignate optical activity can be ascribed to (highly) ordered helical packing of (mainly planar) conjugated terthiophene moieties stabilised by π – π interactions, and the negative CD couplet is diagnostic of a left-handed π -stacked assembly.

The intensity of the observed molar CD signal is concentration dependent, thus confirming that it arises from intermolecular interactions.

The solvent-induced switching for $10_8 \cdot K^+$ 0.3 mM was also monitored by 1H NMR spectroscopy, which confirm that the octameric complex disaggregates and that, in the new assembled species, neither imino N^1 -H nor amino protons N^2 -H are involved in intermolecular H-bonding. Additional NOESY studies (Figure 2.2.1.2, b.) revealed NOE cross-peaks between the terthiophene ring protons H^{int} and the methylene hydrogens H^a of the aliphatic chains: since these NOE interactions are not detected in the chloroform solution they are supposed to originate from inter-molecular interactions occurring in the associated species present in $AcCN-d_3/CDCl_3 = 9/1$.

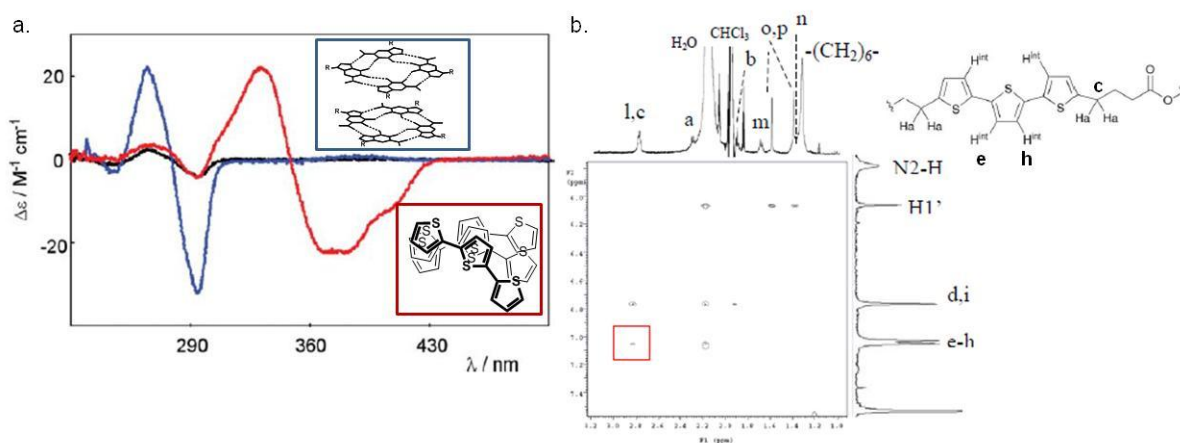


Figure 2.2.1.2: a. CD spectra of 0.3 mM solutions of **10** in $CHCl_3$ (black line), 10_8 -KPic in $CHCl_3$ (blue line) and 10 -KPic in $AcCN/CHCl_3 = 9/1$ (red line). b. NOE interactions between the terthiophene ring protons (e-h) and the methylene hydrogens (c) are observed (from ‘Solvent-induced switching between two supramolecular assemblies of a guanosine–terthiophene conjugate’¹⁸).

A new chiral superstructure has emerged for the guanosine–terthiophene conjugate derivative **10** in $AcCN/CHCl_3 = 9/1$, where the terthiophene chains are π - π stacked in a helicoidal (left-handed) arrangement in the central core and the guanine bases, free from hydrogen bonding, are located at the periphery and exposed to the solvent without any chiral interchromophoric interactions. This structure ($\pi\pi T3$) consists in a H-type aggregate, where the terthiophene backbones are assumed to be almost planar, almost parallel to each other, and packed at the π - π stacking distance. Interacting terthiophenes are rotated counterclockwise with respect to each other, in agreement with the observed exciton type splitting Cotton effects. The twist between the long axis of neighbor molecules in the stack could avoid sterically unfavorable interactions between guanosines (in their *syn* conformation).

In order to get additional information on the self-assembly behaviour of these systems, a careful photophysical characterization was carried out using 0.03 mM solutions. The absorption spectra profiles (**Figure 2.2.1.3**, a.) of solutions of **1**-KPic in the two different solvents in study are quite similar, but in AcCN/CHCl₃ = 9/1 the shoulder around 400–500 nm is more pronounced, indicating a higher degree of π - π stacking interactions between the terthienyl moieties in $\pi\pi$ T3. The peak centered at 360 nm is due both to $\pi\pi$ T3 and the species with non-interacting terthienyl arms (freeT3).

Emissions exciting at two different wavelengths were compared (**Figure 2.2.1.3**, b.): 340 nm (where the absorption of freeT3 is maximum) and 420 nm (where the absorption of $\pi\pi$ T3 species is prevalent). The normalised emission spectra clearly evidence that there are two different peaks, one centred at 440 nm typical of freeT3, and a red shifted one as expected for $\pi\pi$ T3 aggregates. Most interestingly, this last peak, by excitation at 420 nm, is centered at 490 nm in CHCl₃ and at 520 nm in AcCN/CHCl₃ = 9/1: this further red shift of the band is a clear indication of the formation of larger and more conjugated associated species in this latter environment, as expected when increasing π - π stacking interactions between terthiophene fragments. Peaks of both species are always present, but their luminescence intensity ratio and position depend on the excitation wavelength and solvent.

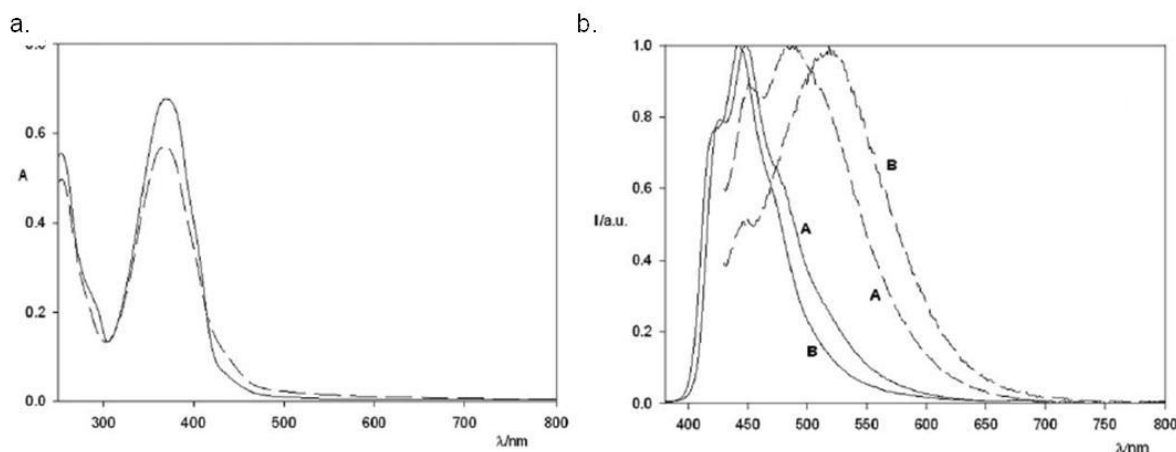


Figure 2.2.1.3: a. Absorption spectra of **10**-KPic in CHCl₃ (solid line) and in AcCN/CHCl₃ = 9/1 (dashed line); b. emission spectra of **10**-KPic in CHCl₃ (A) exciting at 340 nm (solid line), and at 420 nm (dashed line) and of **10**-KPic in AcCN/CHCl₃ = 9/1 (B) exciting at 340 nm (solid line), and at 420 nm (dashed line) (from ‘Solvent-induced switching between two supramolecular assemblies of a guanosine-terthiophene conjugate’¹⁸).

In order to understand the self-assembly on surfaces, fundamental for an organic semiconductor, guanosine **10** was studied by means of scanning probe microscopies (SPMs) and molecular modeling simulations.

2.2.2 Supramolecular studies on surface

Scanning tunneling microscopy (STM) of dry films on HOPG (Highly Oriented Pyrolytic Graphite) shows large domains, extending over hundreds nanometers, each domain being made of parallel lamellae. Within each domain, along the bright lines regularly spaced spots were observed (**Figure 2.2.2.1**, a.): the brightest lines are attributed to the guanine, taking into account the measured line width (around 0.7 nm) is closer to the length of the guanine than that of the terthiophene (around 0.8 nm and 1.2 nm along their long axis, respectively). These lamellae are indeed made of adjacent ribbons arising from H-bonds between guanosines and bright elongated streaks oriented almost perpendicular to the bright lines (distanced of ca. 0.6 nm) are likely to be the oligothiophene or alkyl groups.

Molecular modeling simulations have been used to find whether these structures result from the formation of A-type or B-type ribbon (**Figure 2.2.2.1**, b.). In the **A**-type the terthiophene-decyl groups of adjacent molecules are pointing in opposite directions. The tilt angle between these groups and the H-bond network axis is small (around 30°). In the **B**-type (**Figure S9** right), the guanines are in a staggered configuration and an additional H-bond is possible between the ribose and the guanine, leading to ten possible H-bonds between four molecules. In this case, the terthiophene-decyl groups are nearly perpendicular to the H-bonding network axis, and allows for a planar stack. In the STM images of **Figure 2.2.2**. we only observe the lateral groups almost perpendicular to the bright lines (the guanine H-bond network), which corresponds to the **B**-type network in the molecular modelling.

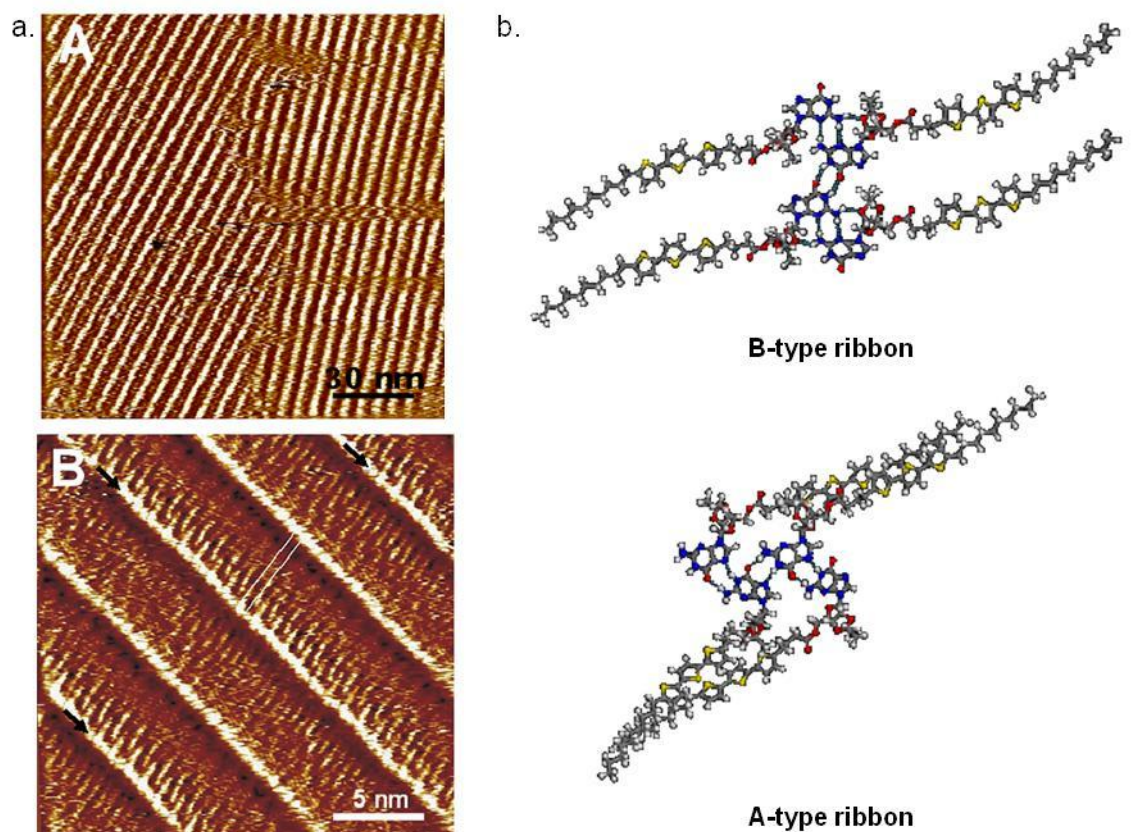


Figure 2.2.2.1: STM images of **10** on highly oriented pyrolytic graphite (HOPG) showing domain of parallel lamellae (A., bright lines); the spots along bright lines show the following unit cell parameters: $a = 0.58 \pm 0.10$ nm; $b = 10.7 \pm 0.3$ nm (2×5.36 nm); angle $\alpha = \pm 97 \pm 2^\circ$ (area = 3.069 nm²). b. Molecular modelling of the two possible H-bonding network for ribbon formation (from ‘Guanosine-based Hydrogen-bonded Scaffolds: Controlling the Assembly of Oligothiophenes’¹⁴).

In this packing configuration, the neighboring terthiophenes of adjacent ribbons are not directly π -stacked because of both the steric hindrance and interdigitation of decyl groups²⁰ (**Figure 2.2.2.2**, a.) and of their propensity to commensurate with the underlying graphite plane: π -type interactions between each oligothiophene and the graphite plane can lead both to parallel or “T-shape” conformations. The fact that we only observed the B-type H-bonding network on graphite is in contrast with previous results on alkylated guanosine derivatives^{12,13}, which show only A-type network on HOPG. The reason could be found in structural differences from previously studied compounds: derivative **10** possesses only one alkyl group (not two) and on the sugar there is an acetonide unit, pointing perpendicularly to the molecule’s main plane. These differences lead to several restrictions that favor the formation of the B-type network.

A ribbon-like morphology for deposits of **10** onto mica substrates was also observed with atomic force microscopy (AFM) (**Figure 2.2.2.2**, b.). The length of the ribbon varies from a

few tens of nanometers in CHCl_3 to a few micrometers in 1,2,4-trichlorobenzene (TCB), a solvent which evaporates slowly. However, the width and thickness of the ribbons are constant: their width ($11.2 \pm 3 \text{ nm}$ or a multiple of this value) fits in size with two parallel H-bonding B-type ribbons, as on graphite; the thickness ($0.6 \pm 0.2 \text{ nm}$) suggests that the ribbons are one-molecule thick structures.

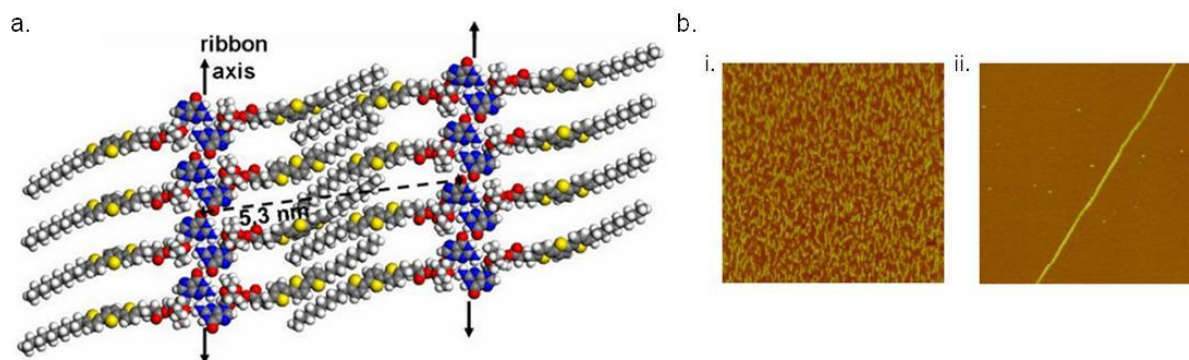


Figure 2.2.2: a. Molecular model of two adjacent B-type ribbons (each made from 8 molecules), fitting the unit cell parameters of the STM images; b. Tapping-Mode AFM images of thin deposits on mica. i. from chloroform solution ($1.5 \mu\text{m}$)²; ii. ($3.5 \mu\text{m}$)² : from 1,2,4-trichlorobenzene (from ‘Guanosine-based Hydrogen-bonded Scaffolds: Controlling the Assembly of Oligothiophenes’,¹⁴).

The formation of straight, parallel ribbons with lengths spanning from hundreds of nanometers to micrometers appears therefore as an intrinsic self-assembly process of **10** during the formation of thin films. This self-assembly is governed by the formation of H-bonds between guanosines that dictates the spatial localization of oligothiophenes, ultimately forming 1D conjugated arrays that may be employed as prototypes of supramolecular nanowires. Significantly the tuneable interconversion between highly ordered motifs fuelled by cation complexation and release or by changing solvent polarity allows the in situ reversible switch of two forms of oligothiophene arrangements.

3. Thiophene functionalized guanosines: a structural investigation

The major problem that emerged from the study of **10** is the distance between adjacent oligothiophene: as shown from molecular models, once the molecules are adsorbed on a solid substrate oligothiophenes are not directly π -stacked. Such a feature renders the system of modest interest for applications in organic electronics. We identified two possible solutions to this problem:

- functionalization of the ribose with at least two oligothiophene moieties (**11**) (**Figure 3.1**) to reduced the distance between terthiophenes of adjacent ribbons;

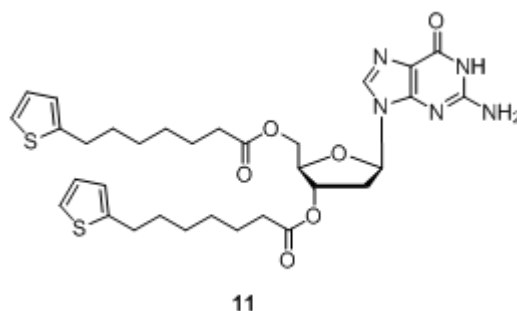


Figure 3.1: Deoxyguanosine **11**

- a good interdigitation and a face-to-face interaction of thiophene moieties, to be achieved with a linker and an alkyl chain of the same length (**12**) or without an alkyl tail (**13**) (**Figure 3.2**).

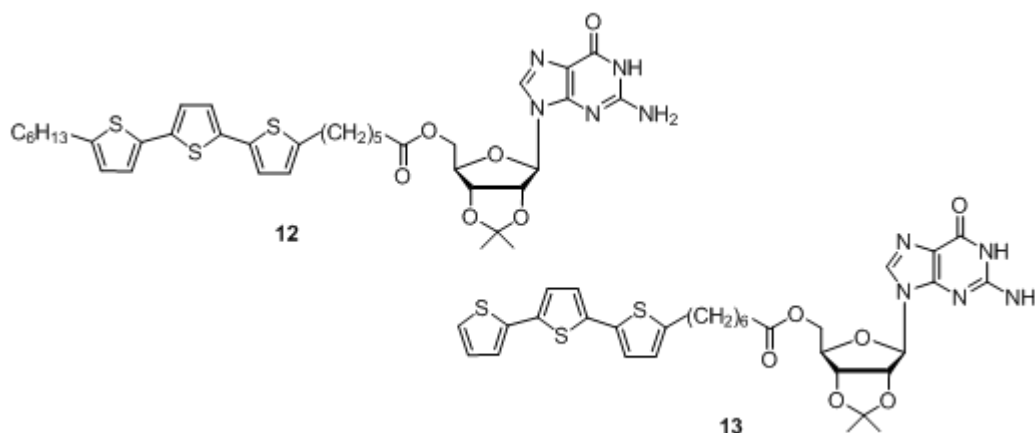


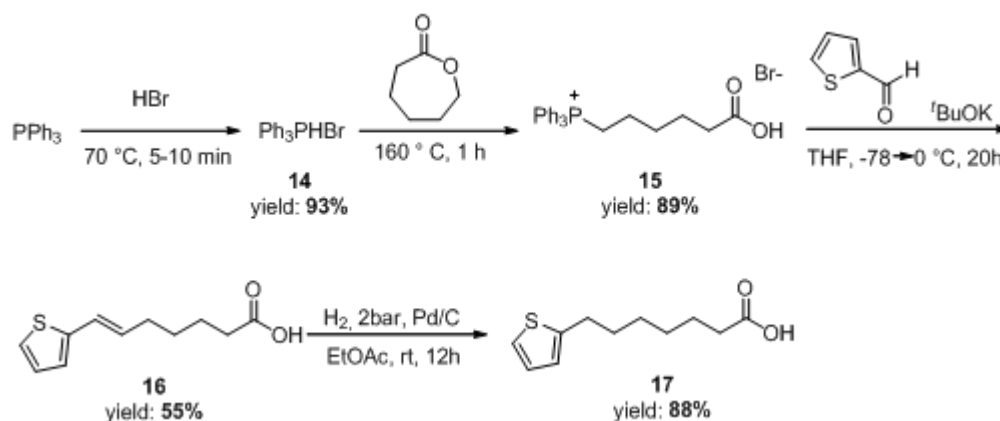
Figure 3.2: GACE **12** and **13**.

3.1 Thiophene disubstitued guanosine

3.1.1 Synthetic procedure

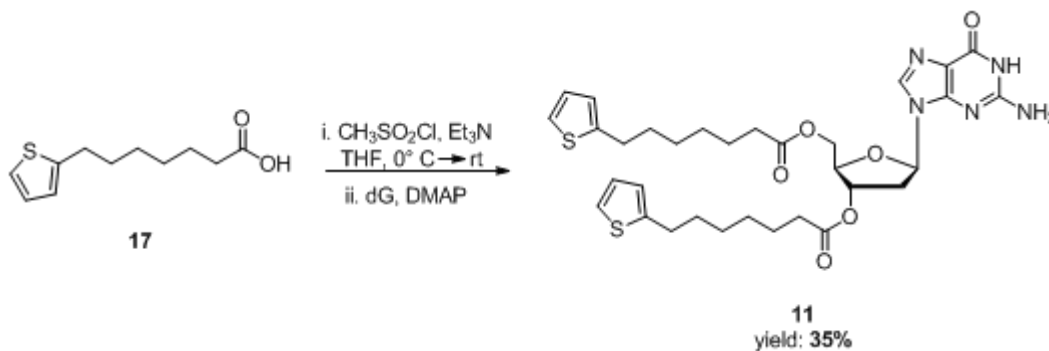
For preliminary studies on supramolecular assemblies in solution and on surface, we prepared a deoxyguanosine with two monothiophene substituents attached to the sugar.

The synthesis of monothiophene acid **17** is reported in **Scheme 3.1.1.1**: after the preparation of 6-(triphenylphosphonium bromide)-hexanoic acid (**15**)²¹ from triphenylphosphonium bromide (**14**)²², a Wittig reaction of this acid with 2-thiophene-carboxyaldehyde provided the unsaturated 7-(thiophen-2-yl)-heptenoic acid (**16**)²³. Subsequent reduction of **16** in a Parr apparatus gave us the desired 7-(thiophen-2-yl)-heptanoic acid (**17**).



Scheme 3.1.1.1: Synthesis of 7-(thiophen-2-yl)-heptanoic acid (**17**).

Esterification of deoxyguanosine with **17** using the mixed anhydride strategy provided compound **11** (**Scheme 3.1.1.2**): after purification with chromatography and crystallization in ethyl acetate the product was obtained as a white powder.



Scheme 3.1.1.2: Synthesis of derivative **11**

Chapter IV: Functionalized guanosines for organic electronic devices

3.1.2 Supramolecular studies in solution

Aggregation of guanosine **11** in chloroform was studied through NMR in order to characterize the ribbon aggregates formed. We report here NMR spectra in DMSO and in CDCl₃ (**Figure 3.1.1.1**): N¹H shifts from 10.65 ppm to 12.12 ppm and its signal is broader in chloroform due to its involvement in hydrogen bonding; there is also line broadening of both H⁸ and N²H₂ signals in CDCl₃. In DMSO there are only three peaks for thiophene hydrogens, while in chloroform there are six signals for those hydrogen: the two thiophene tails of **11** are not equivalent in the more rigid structure of the ribbon aggregate.

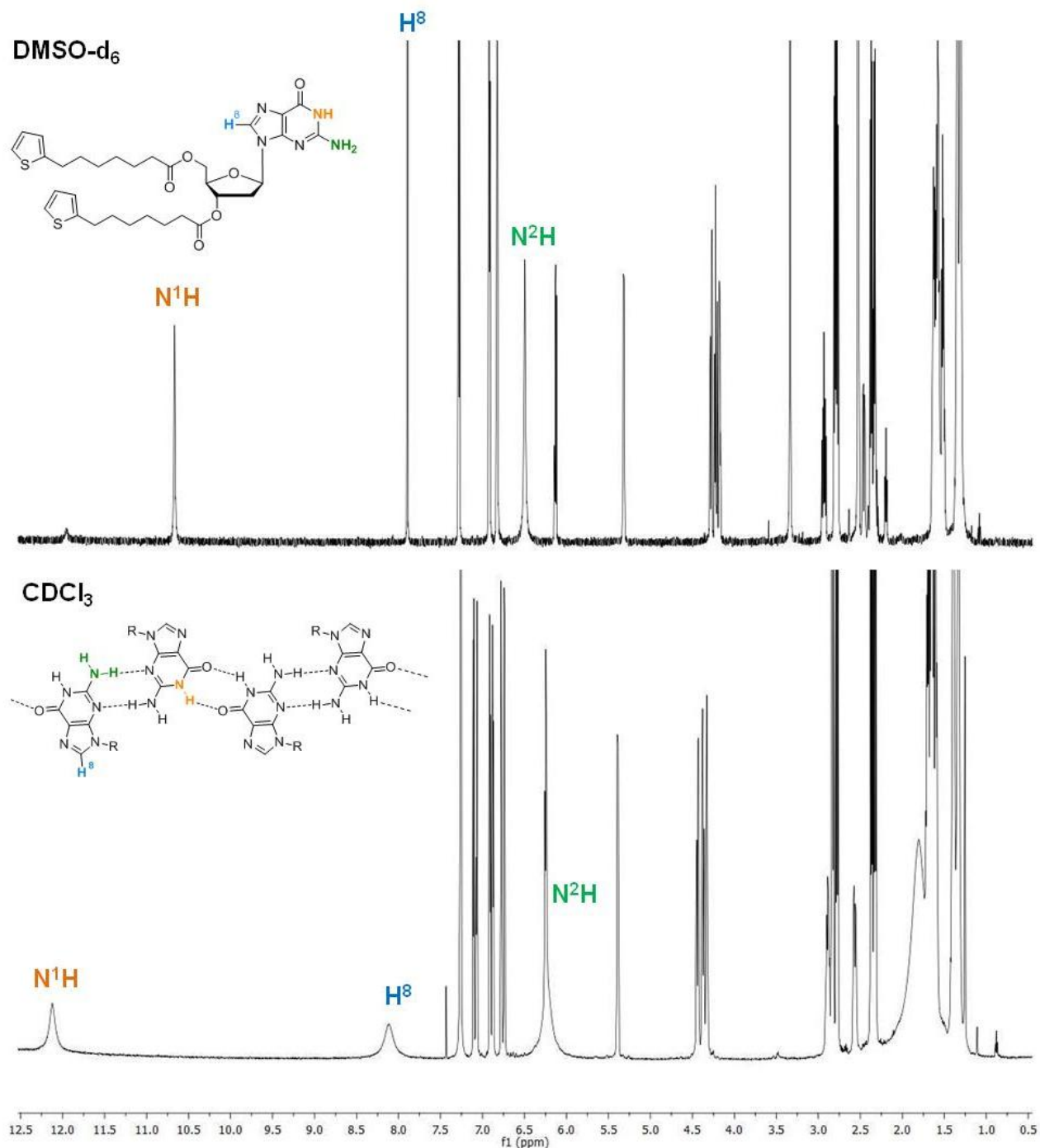


Figure 3.1.1.1: NMR spectra of **11** in DMSO-d₆ (upper part) and in CDCl₃ (bottom).

The spectrum of **11** in the presence of potassium picrate (1/8 equiv.) was registered, but revealed the presence of a mixture of both ribbon and octamer species, confirmed also by CD spectra (**Figure 3.1.1.2**), where the signal of a C₄ symmetric octamer is weaker than expected.

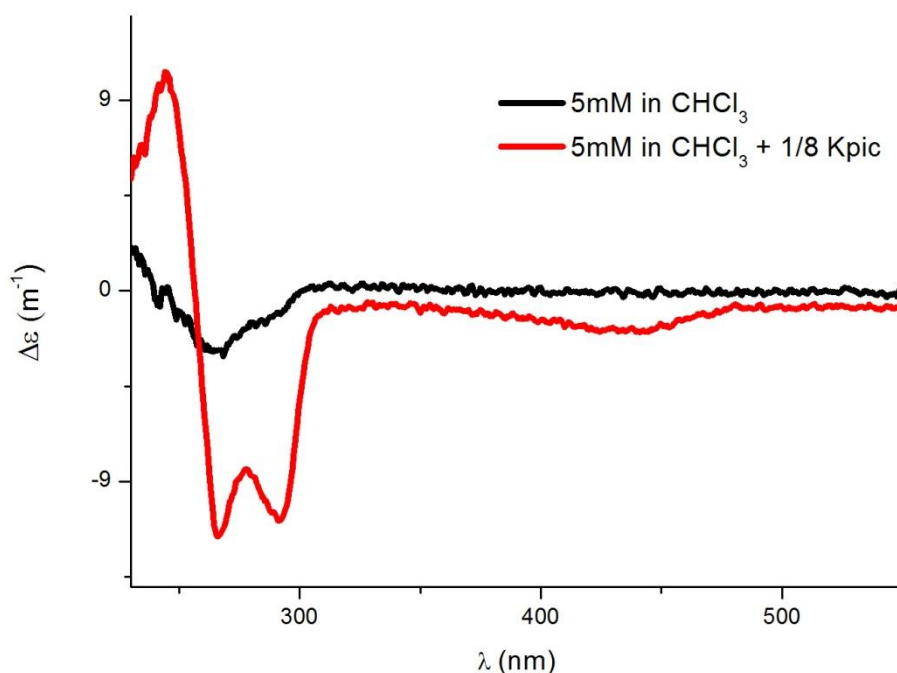


Figure 3.1.1.2: CD spectra of **11** in CDCl_3 (black) and with addition of 0.125 equiv. of Kpic (red).

3.1.3 Aggregation on surface

After studying this derivative in solution, we performed some experiments using STM: this technique, as shown before, could give us information on the supramolecular aggregation on surfaces.

Scanning tunneling microscopy exploits the tunneling current that arises when a bias is applied between a conductive tip and the substrate surface; since this current decreases exponentially with the distance, the tip should be as close as possible to the sample²⁴. During the imaging process, a piezoelectric element ensures the control on x and y directions by applying a voltage, and on z direction by adjusting its vertical position with a feedback loop which keeps the tunneling current constant (**Figure 3.1.3.1, a.**). By scanning the tips across the surface and registering its positions an image of the topographic height of the surface is generated (**Figure 3.1.3.1, b.**).

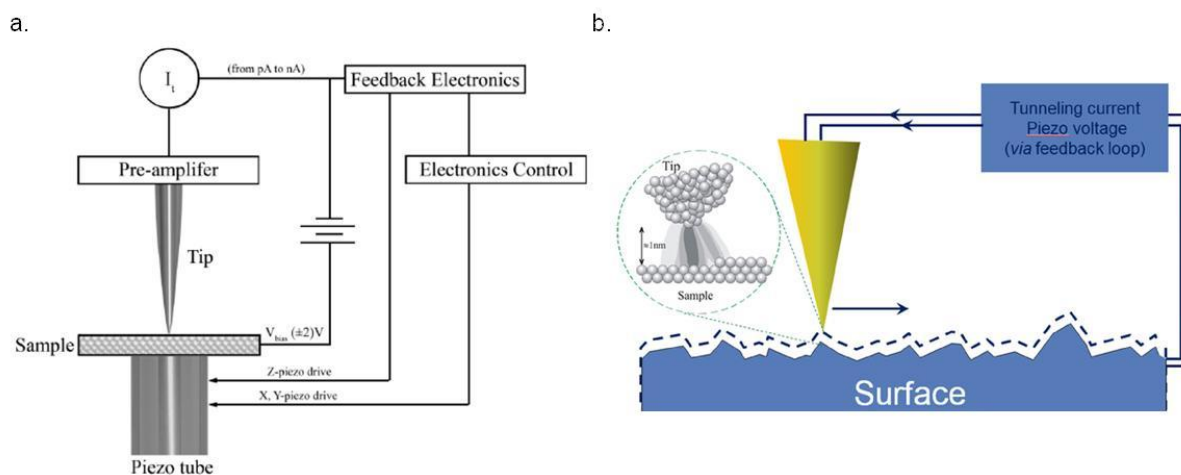


Figure 3.1.3.1: a. Schematic representation of Scanning Tunneling Microscope²⁵; b. Interaction mode between tip and surface.²⁶

The studies of supramolecular assemblies on surfaces are usually carried out at solid-liquid interface²⁷. This feature has many advantages, if compared for example to UHV (Ultra High Vacuum) conditions, such as the dynamic exchange between the molecules adsorbed on the surface and those in the liquid phase (which promotes the self-healing of defects in the self-assembled layers)²⁸, and the possibility of monitoring the *in situ* modification of monolayers by application of external stimuli²⁹ (**Figure 3.1.3.2, b.**). This method provides detailed insight on molecule-molecule and molecule-substrate interactions.

The experiments using compound **15** were performed at solid-liquid interface on a Highly Oriented Pyrolytic Graphite (HOPG) (**Figure 3.1.3.2, a.**). It is a 2D system of stacking graphene sheets in which the overlap of carbon p_z orbitals produces delocalized π electrons lying above and below each benzene ring: this makes graphite a good electrical conductor and a suitable substrate for STM experiments. In addition it is very easy to prepare an homogeneous surface by simply cleaving HOPG surface with an adhesive tape, obtaining a flat surface which is neutral and inert to organic solvents.

A square substrate of HOPG (1 cm x 1 cm) was glued to a metallic magnetic disk, using a silver pigmented conductive coating to electrically connect graphite and the metallic disk. After cleaving the surface twice with a simple adhesive tape, a picture was taken with STM to verify the homogeneity of graphite surface. The measurements were performed using a Veeco scanning tunneling microscope (multimode Nanoscope III, Veeco) by using a scanner A (Veeco), therefore by mapping an area of $1\mu\text{m} \times 1\mu\text{m}$; the tip was mechanically cut from a Pt/Ir wire (90/10, diameter 0.25 mm). The graphite surface was visualized by lowering the bias voltage to 20 mV and raising the current to 65 pA: this image was used as reference for

the following experiments (application of background flattening and correction of the drift) (Figure 3.1.3.2, c.).

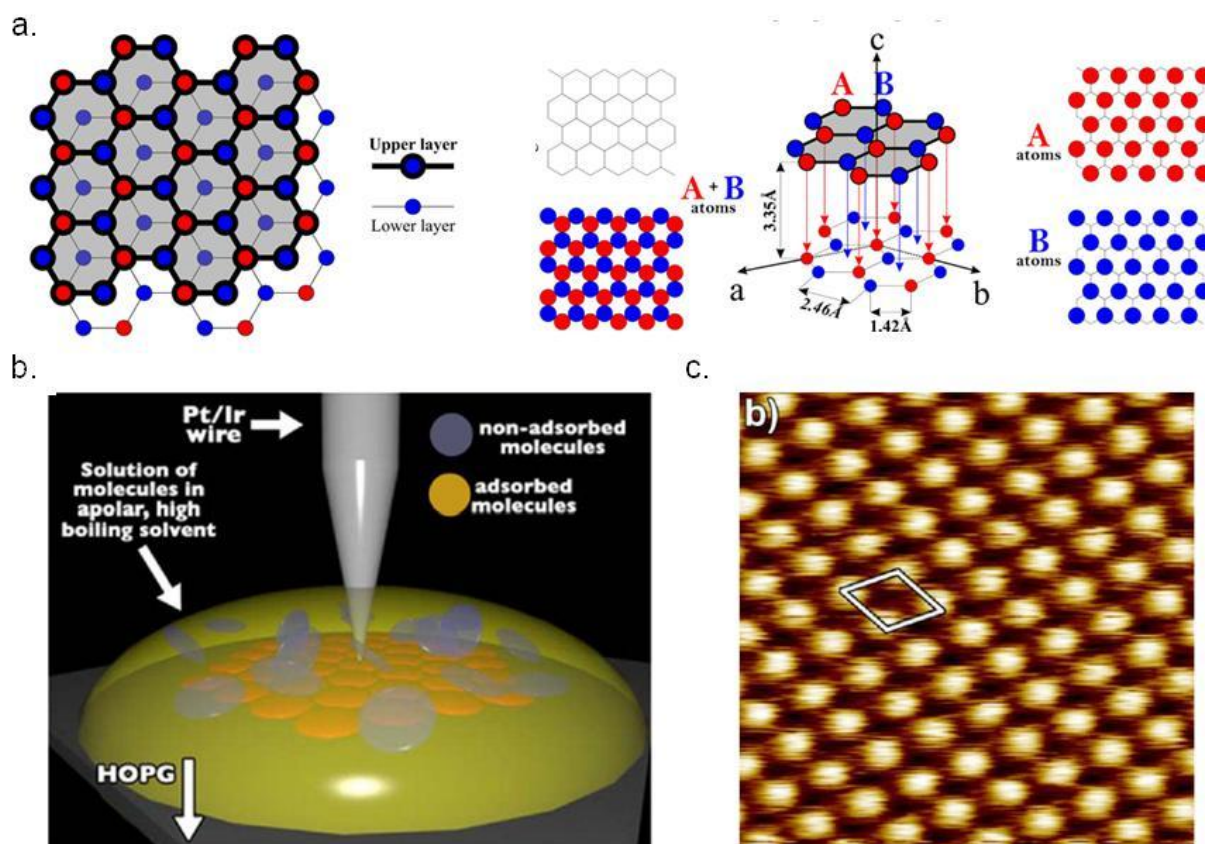


Figure 3.1.3.2: a. Schematic representation of the structure of the bulk hexagonal graphite crystal. The dashed lines show the axes of bulk unit cell. Side insets: top view of the basal plane of graphite and schematic representation of the surface structure (carbon atoms) of graphite most viewed by SPM, where every other atom is enhanced (right-side inset) and viewed under ideal conditions, where every single atom is seen (left-side inset)³⁰. b. Principle of STM at solid-liquid interface²⁵. STM image of HOPG (3x3 nm), with unit cell $a = 0.246 \text{ nm}$ ²⁵.

A solution of compound **11** was prepared by dissolving it in 50 μL of hot dimethylsulfoxide (DMSO at 90 $^{\circ}\text{C}$) and diluting that solution with 1,2,4-trichlorobenzene (TCB) to reach a concentration of 1 mM: TCB is a good solvent for STM because of it is apolar (dielectric constant, ϵ : 2.24) and has a high boiling point, which allows one to measure for several hours with the tip immersed in the solution. A drop of this solution (4 μL) was deposited on HOPG placed on the piezoelectric support of the instrument; STM imaging was carried out in constant height mode yet without turning off the feedback loop, to avoid tip crashes. In this case big agglomerates were found on the surface.

The mother solution of 1 mM was then diluted to 100 μM with TCB and warmed at 60-70°C to improve the solubility, repeating the experiment with the less concentrated solution. The STM images were recorded only after achieving a negligible thermal drift. The images showed that **11** forms ordered structures on the surface: we can recognize domains of parallel lamellae, and we first thought that the bright lines are guanosines that self-assemble through hydrogen bonding in ribbon-like aggregates, as we found for other guanosine derivatives. But, taking into account the measured line width, it seems that also thiophenes form ribbon architectures due to π -stacking interactions: these ribbons are brighter than the guanosine ribbons. Only a thiophene substituent is adsorbed on surface, while the other is perpendicular to it: we can see from STM images an empty space (dark voids) between two thiophene tails.

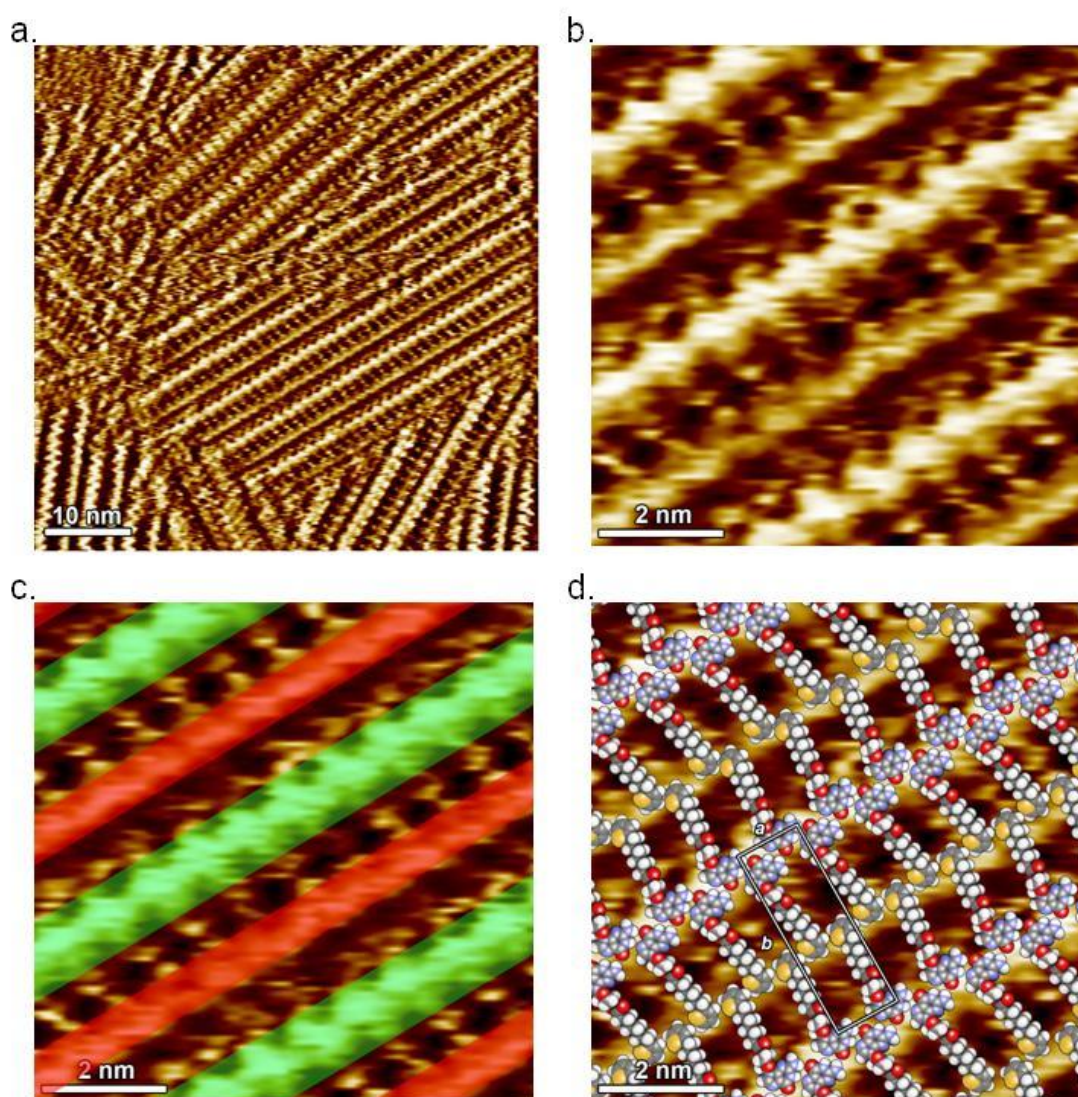


Figure 3.1.3.3: STM images of derivative 11 on HOPG 10x10 nm (a.) and 2x2 nm (b.). (c.) Red lines represents thiophene stacking moieties and green lines guanosine ribbons. c.

Chapter IV: Functionalized guanosines for organic electronic devices

Molecular modeling matching STM images (unit cell parameters: $a = (1.13 \pm 0.1)$ nm, $b = (3.33 \pm 0.1)$ nm, $\alpha = (90 \pm 2)^\circ$, $A = (3.76 \pm 0.66)$ nm², $N_m = 2$)

These preliminary studies demonstrated that we can obtain π - π stacking interaction on surface between thiophenes, but also that only one tail can lie on surface.

3.2 Terthiophene guanosine derivatives

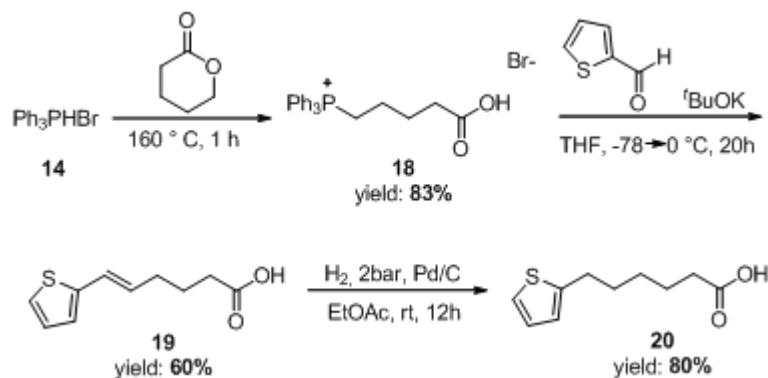
The main problem observed with compound **10** was that terthiophene moieties are not directly π -stacked in ribbon-like aggregates, due to interdigitation of decyl groups. We planned the synthesis of two terthiophene compounds to avoid this problem and reach the desired cross-talk between thienyl groups. The first derivative (**12**) has a linker with ribose and a terminal alkyl chain of the same length; we decided for C6 long spacer and tail to achieve good balance and solubility. In addition we prepared a second compound (**13**), which has no terminal tail and a C7 long spacer, to understand whether this terminal alkyl chain is necessary or not.

3.2.1 *Synthetic procedure*

The synthesis of guanosines **12** and **13** can be divided in four parts:

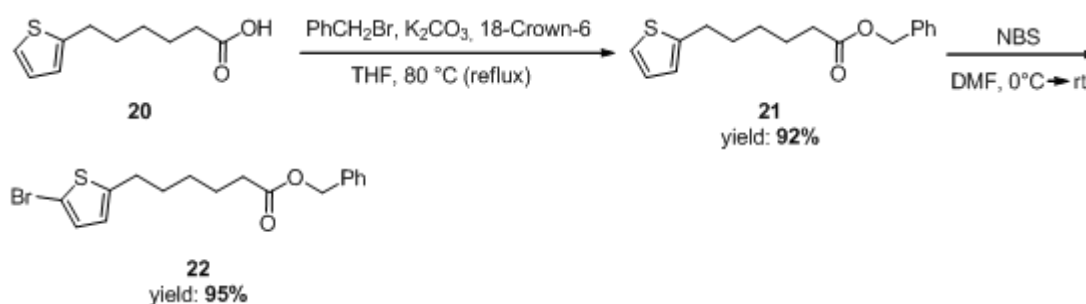
- Preparation of monothiophene linker
 - Synthesis of bithiophene “tail”
 - Stille coupling to obtain terthiophene acid
 - Reaction with guanosine to obtain the desired derivative
-
- Synthesis of **12**

Following the procedure used for acid **17**, we prepared thiophene acid **20** by a Wittig reaction of 5-(triphenylphosphonium bromide)-pentanoic acid **18** (prepared with δ -valerolactone and **14**) and 2-thiophene-carboxyaldehyde and a subsequent hydrogenation of **19** (Scheme 3.2.1.1).



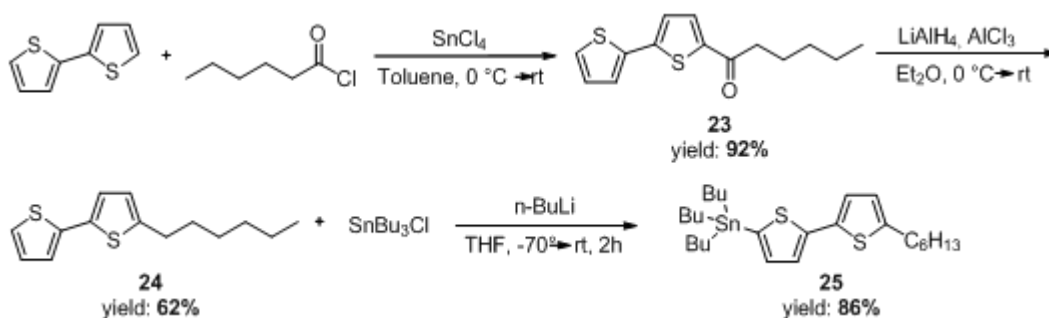
Scheme 3.2.1.1: Synthesis of **20**

Acid **20** was protected as benzyl ester (**21**)⁹ and brominated in the free 2 position with *N*-bromosuccinimide (NBS) (**22**)⁹ for the Stille coupling (**Scheme 3.2.1.2**).



Scheme 3.2.1.2: Synthesis of **22**

To obtain the organostannane **25** we first prepared 2-hexyl-bithiophene **24**¹⁰ by acylation of 2,2'-bithiophene with hexanoyl chloride (**23**) and reduction of the carbonyl function with lithium aluminium hydride (LiAlH₄). Reaction of **24** with tributylstannyl chloride (SnBu₃Cl) provided the organostannane **25** (**Scheme 3.2.1.3**).



Scheme 3.2.1.3: Synthesis of **25**.

Once obtained the two reaction partners **22** and **25**, we proceeded with Stille reaction. The Stille coupling reaction allows the formation of a C-C bond between an aryl halide and an organostannane catalyzed by a palladium complex (**Figure 3.1.2.1**). An initial step of

oxidative addition of the aryl halide (R^1-X) to the catalyst in its reduced form (Pd^0) is followed by a transmetalation with the organostannane (R^2-SnBu_3), to form a complex where Pd^{II} coordinates both R^1 and R^2 . A reductive elimination from this complex yields the coupled product R^1-R^2 and the reduced catalyst Pd^0 .

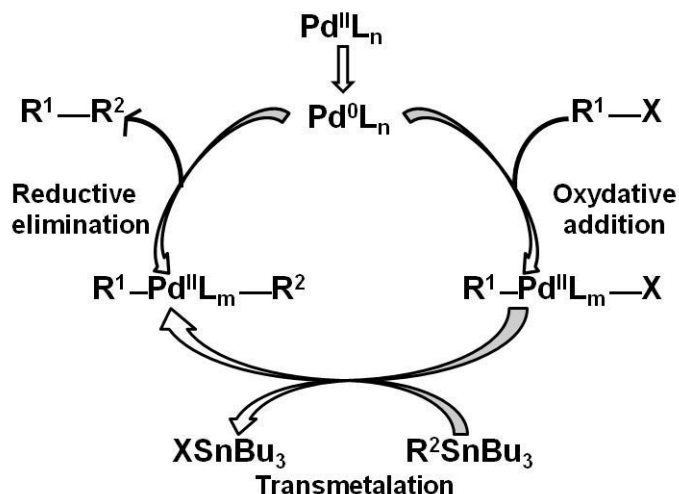
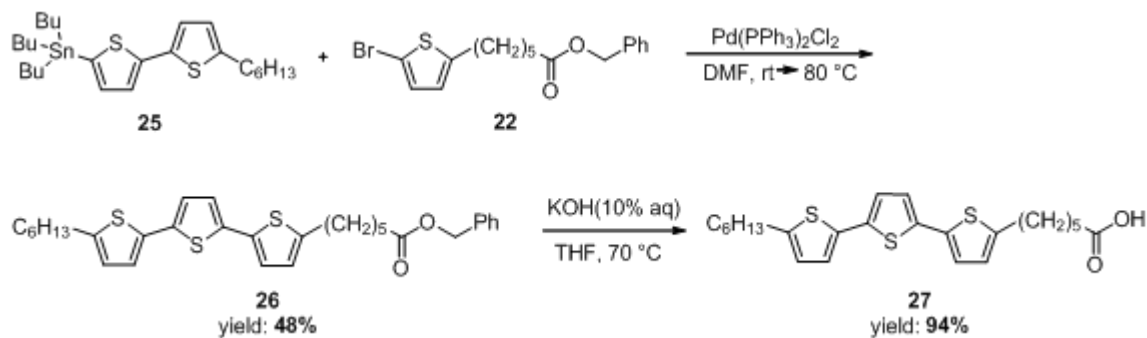


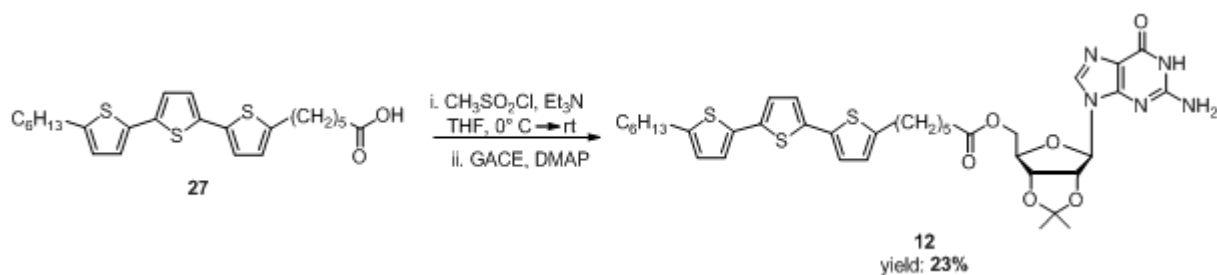
Figure 3.2.1.1: Stille catalytic cycle.

The Stille reaction between bromide **22** and organostannane **25** provided the ester **26** in 48% yield⁹. The basic hydrolysis of benzyl ester gave access to terthiophene acid **27**⁹ (Scheme 3.2.1.4).



Scheme 3.2.1.4: Synthesis of **27**.

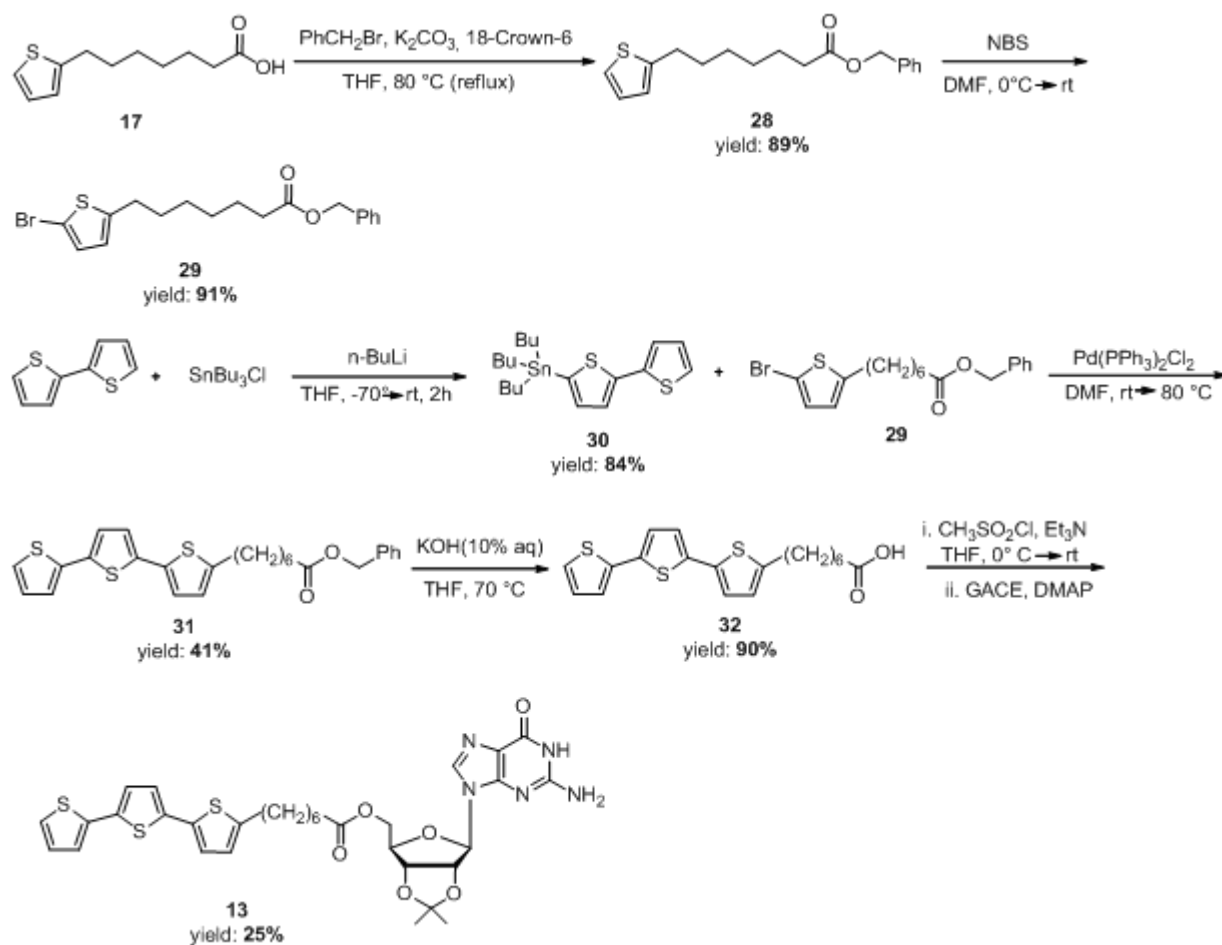
Analogously to derivative **11**, the guanosine **12** was synthesized through a mixed anhydride strategy.



Scheme 3.2.1.5: Synthesis of GACE **12**.

- Synthesis of **13**

7-(thiophen-2-yl)-heptanoic acid (**17**), whose synthesis was described before, was protected as benzyl ester (**28**) and brominated (**29**) following the procedure used for compound **22**. After preparing 5-tributylstannyl-2,2'-bithiophene **30**, it was coupled with bromide **29** with a Stille procedure, obtaining benzyl ester **31**. Deprotection with potassium hydroxide gave terthiophene acid **32**, which reacted with GACE to give compound **13**.



Scheme 3.2.1.6: Synthesis of GACE **13**.

3.2.2 Supramolecular studies in solution

Terthiophene guanosines **12** and **13** were characterized by using NMR spectroscopy in DMSO- d_6 as solvent (**Figure 3.2.2.1**). Once confirmed the structures, supramolecular aggregates were studied in $CDCl_3$: the high insolubility of **13**, due to the absence of a terminal alkyl chain, did not allow supramolecular studies in solution neither in $CDCl_3$ nor in tetrachloroethane. For this reason only **12** was fully studied.

As mentioned before, in $CDCl_3$ we can recognize the formation of aggregates by NMR, from the broadening and shift of signals: in this case not only a ribbon but also other species are present in solution, due to a not complete removal of cations, residual of synthetic work-up, through crystallization (**Figure 3.2.2.1**). During chromatographic purification in fact guanosine, especially the isopropylidene derivative (GACE), extracts cations naturally present in silica: these cations (Na^+ , K^+) are strongly complexed by guanosine tetramers and also crystallization cannot remove all of them.

Addition to this solution of 0.125 equivalents of potassium picrate (1/8 equiv.) converted the aggregates in solution in octameric species: we can recognize only one set of signals, a feature typical of a D_4 -symmetric octamer. N^1H shifts from 10.71 ppm in DMSO to 12.35 ppm for octamers in $CDCl_3$, while N^2H_2 splits in two peaks, one corresponding to N^2 ---H involved in hydrogen bonding at 9.40 ppm and the other corresponding to N^2H “free” (6.12 ppm), while the same chemical shift for both N^2H_2 is observed in DMSO (6.55 ppm) (**Figure 3.2.2.1**).

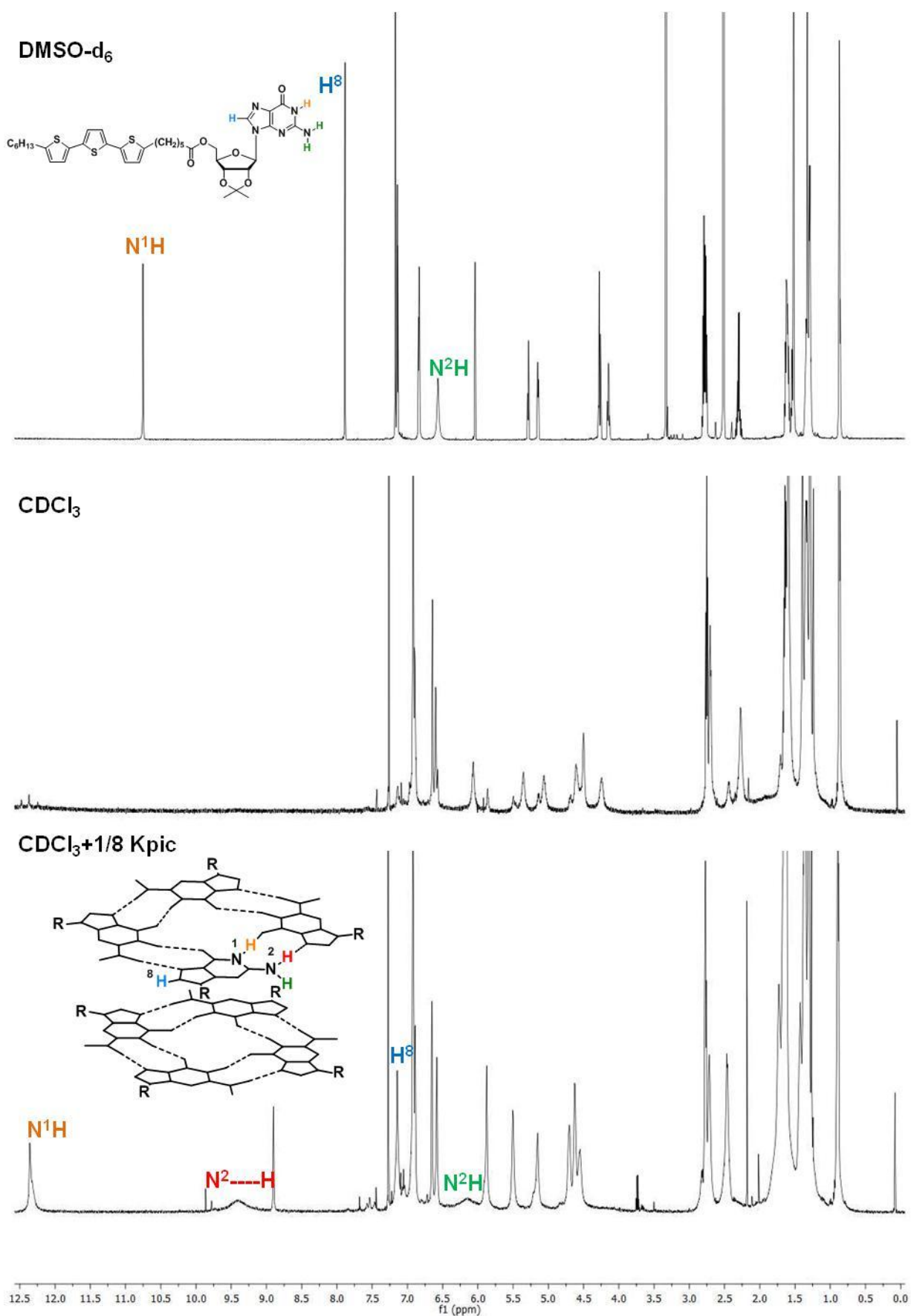


Figure 3.2.2.1: NMR spectra of **12** in DMSO-d₆ (a.), in CDCl₃ (b.) and with 1/8 of potassium picrate (c.)

CD spectroscopy was used not only to confirm the formation of a D_4 octamer, but for a switching study between octameric and ribbon structures, as shown for derivative **10** (Figure 3.2.2.2). After recording the CD spectrum of **12** in THF (3 mM solution, A, black line, which is hidden by other lines), 1/8 equivalents of potassium picrate were added and the intense signal of the D_4 symmetric octamer appeared (solution B, blue line). The addition of cryptand, that coordinates potassium ions, restored the signal of a G-ribbon (solution C, red line), while with triflic acid and the subsequent protonation of cryptand the octameric complex is regenerated by the release of K^+ , but the signal is less intense (solution D, pink line). Adding triethylamine, cryptand was able again to coordinate potassium ions and G-ribbon formed (solution E, green line).

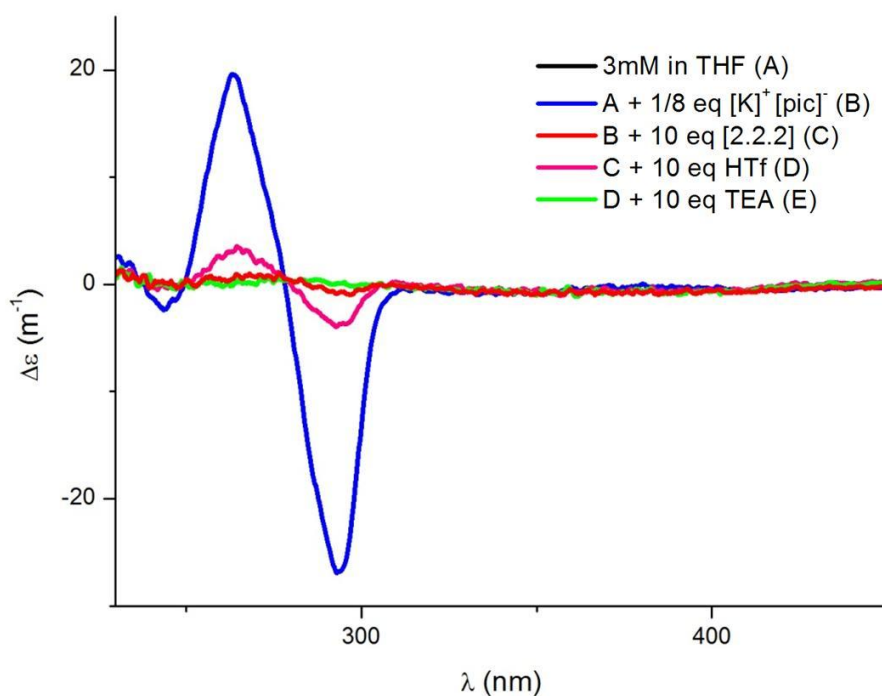


Figure 3.2.2.2: CD study of the switching between ribbon and octamer formed by **12** in THF.

3.2.3 Aggregation on surface

The aim of this work was the fabrication of devices with our guanosines: aggregation on surface is fundamental for organoelectronic applications. In collaboration with the group of Professor Samorì in Strasbourg, we studied the self-assembly of these compounds on silicon oxide (SiOx) supports with Atomic Force Spectroscopy (AFM).

AFM is a scanning probe microscopy like STM, but it exploits the interaction of a fine tip attached to the free end of a cantilever with the force field associated to the surface. When the tip is in physical contact with the surface (few angstroms, Contact Mode AFM), the force is repulsive and the deflection of the cantilever is proportional to this force³¹. Instead, when the tip is ten or hundred angstroms far from the surface, the force involved is attractive (Non Contact Mode AFM).

Although contact mode allows “atomic resolution” images, it is not suitable for organic soft materials, which can be damaged or modified during the scanning of the surface. A good compromise between high resolution and minimal changes of surface is the Tapping Mode AFM³². In this technique the cantilever is oscillating close to its resonance frequency while scans the surface. to detect the position of the cantilever an incident beam is reflected to a photodiode. An electronic feedback loop ensures that the oscillation amplitude, and so the tip-sample interaction, remains constant during scanning by vertical adjustments of the piezo-scanner, giving us a height image of the sample (**Figure 3.2.3.1, a.**).

Forces that act between the sample and the tip will not only cause a change in the oscillation amplitude, but also change in the resonant frequency and phase of the cantilever. The phase is a response to variations in composition, adhesion, friction, viscoelasticity, and other properties, including electric and magnetic; the phase changes are used for the topographic image of surface³³ (**Figure 3.2.3.1, b.**).

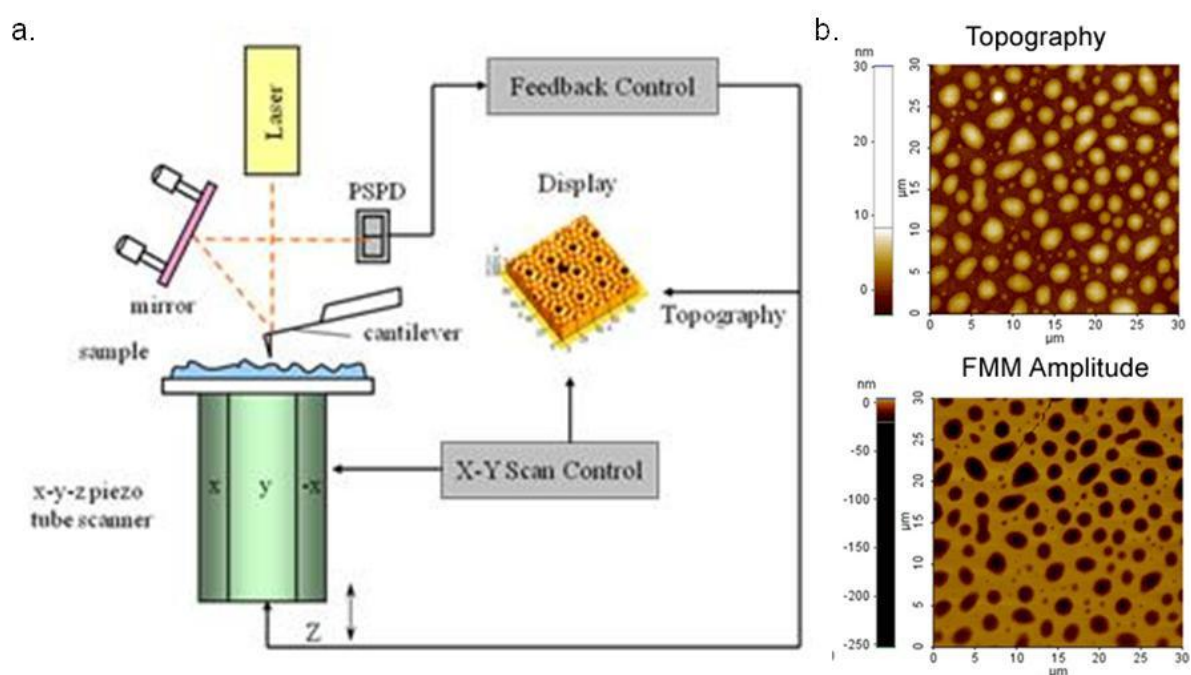


Figure 3.2.3.1: Schematic representation of atomic force microscope³⁴. b. AFM images of a lubricant on plastic board³⁵.

As mentioned before, the intermittent contact in tapping mode lessens the damage done to the soft surface and to the tip, so it is the method of choice for imaging functionalized surfaces: for this reason we used this technique for our self-assembled guanosine architectures.

Preparation of the substrate is a key step to obtain a good image: to reach an high resolution the surface must be as flat as possible and homogeneous for a better reproducibility. The formation of a self-assembled layer on the substrate was achieved by deposition of a proper solution of our compounds and a slow evaporation of the solvent. These solutions can be prepared in different ways: we tried different methods for each derivative, depending on its solubility.

- Derivative **12**

Derivative **12** is soluble in chlorinated solvents: taking into account the results obtained for compound **10**, we prepared a 1 mM solution of **12** in TCB, warming at 90 ° C. The solution was allowed to cool at room temperature, we took 20 µL of it with a micropipette and deposited drop by drop this solution on a silicon oxide substrate (SiO_x, approximately 1 cm²) until the surface was completely covered. We let the solvent evaporate during the night and then we took some images with AFM. From these first images (**Figure 3.2.3.2, a.**) we couldn't observe any ordered structure, but only big agglomerates and an inhomogeneous layer that covered the substrate.

The second strategy adopted was a deposition technique called Solvent Induced Precipitation (SIP)³⁶: a little amount of a concentrated solution of the functional molecule is injected in a non-solvent leading to sudden reduction in solubility and so to precipitation of nanoaggregates. As non-solvent we chose chloroform, a solvent where compound **12** is less soluble than in TCB, but that allows supramolecular assembly of guanosine. 100 µL of 1 mM solution of **12** in TCB were added to 1 mL of CHCl₃ (ratio TCB/CHCl₃ = 1/10); after one hour, we took 20 µL of this solution, we deposited it on the silicon substrate and waited for solvent evaporation.

AFM images revealed the formation of fibers, few µm long, all over the surface (**Figure 3.2.3.2, b.-d.**). These fibers, that form a “rose-like” motif, are likely formed by self-assembled guanosine ribbon aggregates.

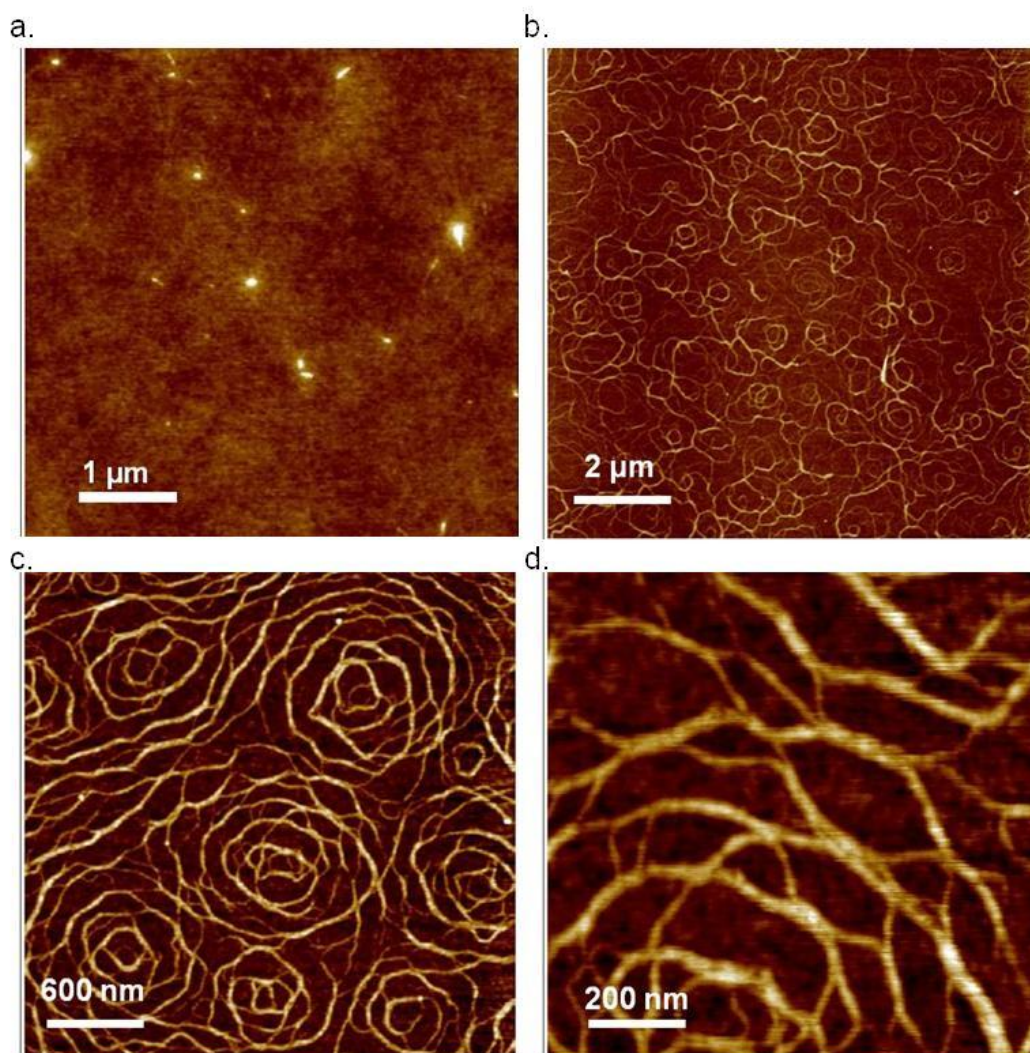


Figure 3.2.3.2: AFM images of **12** in TCB (a., 5x5 μm) and in TCB/CHCl₃ = 1/10 with different surface areas: 10x10 μm (a.), 3x3 μm (b.) and 1x1 μm (d.).

- Derivative **13**

As mentioned before, compound **13** is insoluble also in TCB and only hot DMSO seemed to solubilise it. Also in this case we used SIP technique for sample preparation, by adding 100 μL of 1mM solution of **13** in DMSO to 1 mL of TCB to favour the formation of aggregates. After depositing our solution on SiO_x and waiting for solvent evaporation, AFM images were acquired, showing some long fibers on surface. In **Figure 3.2.3.3** we can see the topographic image of them and also a phase image.

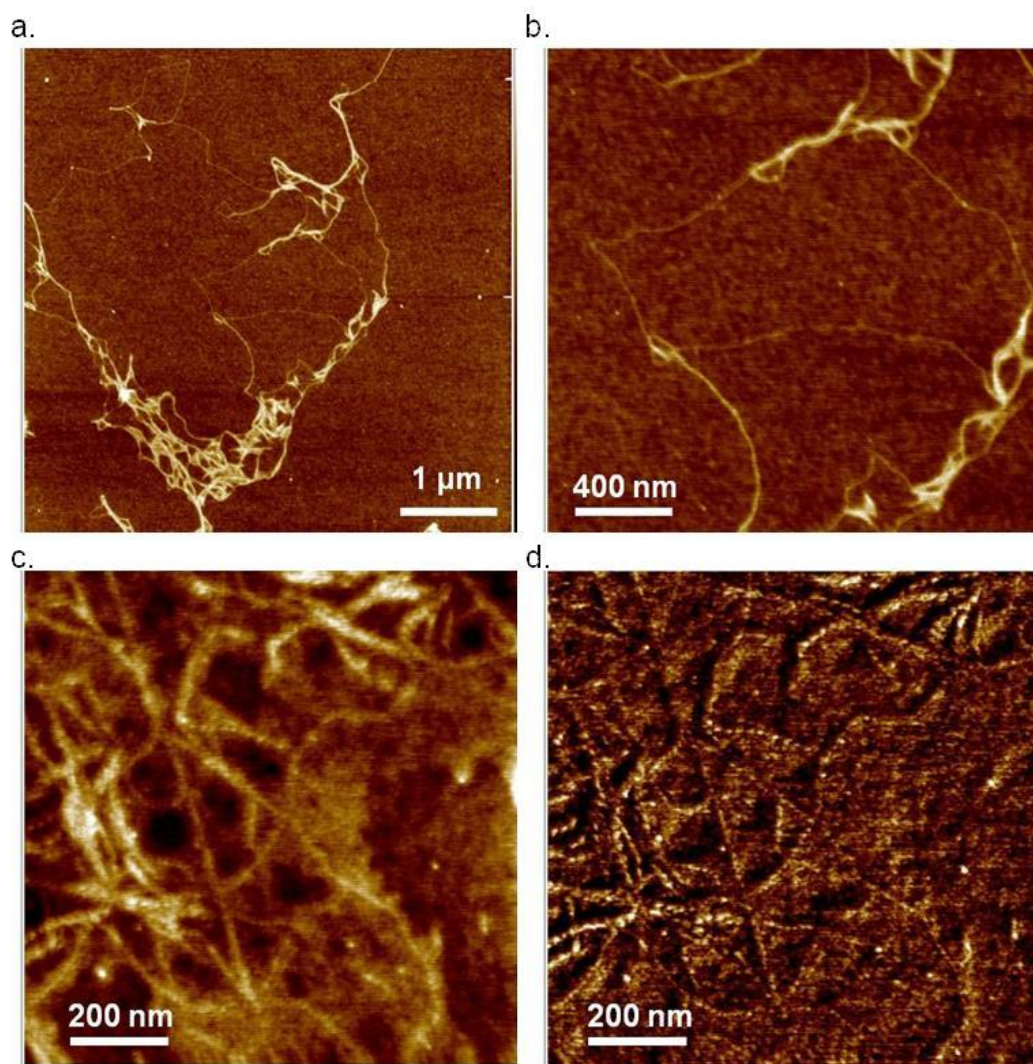


Figure 3.2.3.3: AFM images of **13** in DMSO/TCB = 1/10 with different surface area (5x5 μm , a.; 2x2 μm , b.; 1x1 μm , c.). d. phase image of the same area shown in c.

3.2.4 Electrical measurements

To verify the conductive proprieties of guanosines films, we performed some electrical measurements adopting a three terminal device configuration and using **12** and **13** as semiconductors.

These measurements were done in a glove box apparatus, with a controlled N_2 atmosphere in absence of oxygen and humidity. Solutions of **12** and **13** were prepared inside the glove box, using anhydrous solvents, following the same SIP procedures described above. For electrical characterization, we deposited our solutions (20 μL) on patterned silicon oxide substrates with sixteen gold interdigitated electrodes, which have different channel lengths (2.5 μm , 5 μm , 10 μm , 20 μm).

After solvent evaporation and thermal annealing at 80 $^\circ\text{C}$ overnight for a complete elimination of TCB, we connected the gold electrodes to a source meter, an instrument that

allows three terminal devices characterization. In our case, devices have a top-contact, bottom-gate configuration, with gold electrodes as source and drain, while the gate terminal is represented by the metallic support of the silicon substrate. Output characteristics ($I_d V_d$) and transfer characteristics ($I_d V_g$) were measured for electrodes with different channel length and for both terthiophene derivatives: the curves of a device with 20 nm channel length and **12** as semiconductor are reported as example. Even when V_g potential was very high (± 80 V), the device didn't behave like a FET: the current was very low and positive at positive V_g and low and negative at negative V_g (**Figure 3.2.4.1**, a.). Also transfer characteristic curve revealed a similar but opposite trend, very far from the one expected for a transistor (**Figure 3.2.4.1**, b.). If we increased respectively V_g or V_d potentials, devices burned. We tried different devices, made both with **12** and with **13**, but no one seemed to work.

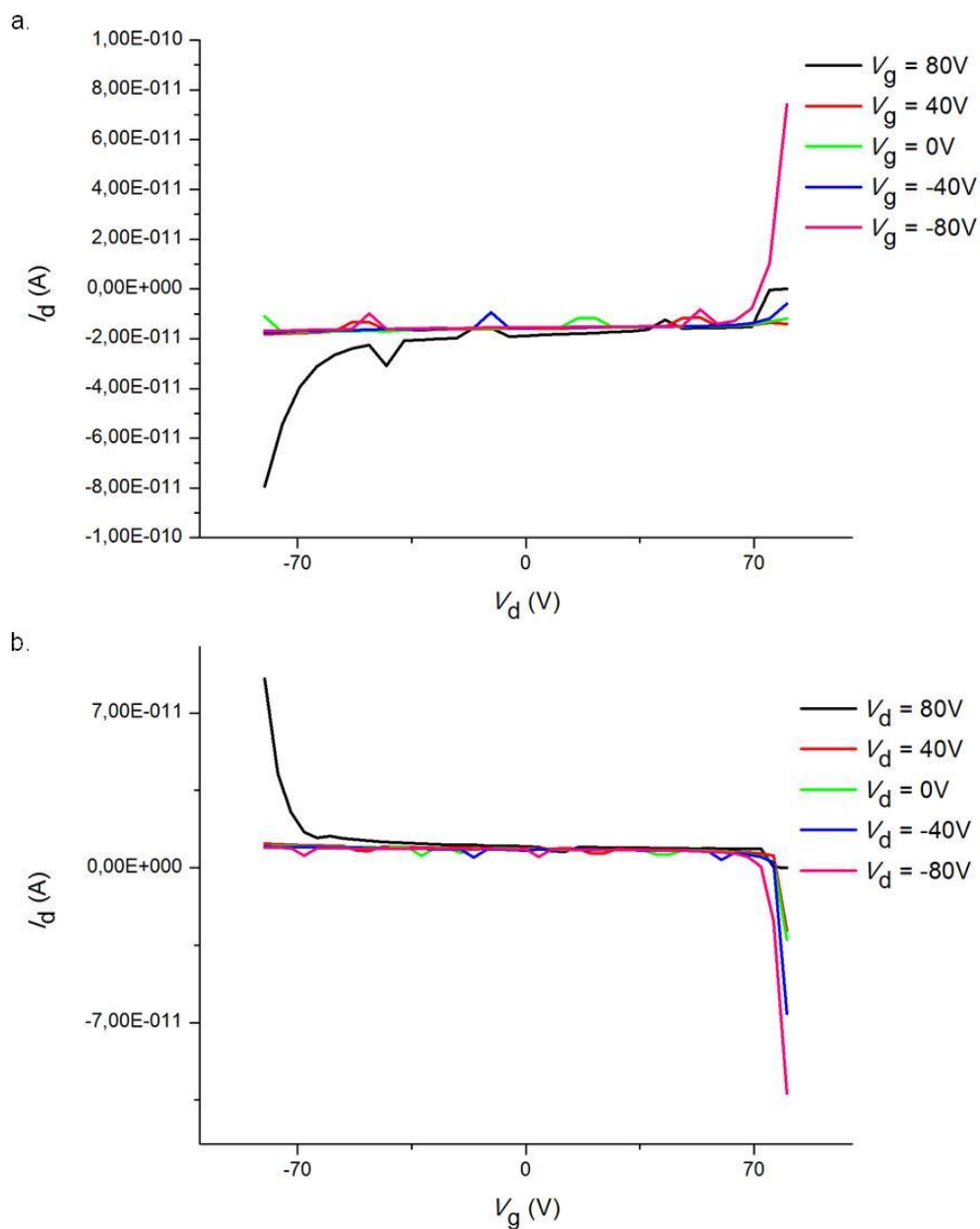


Figure 3.2.4.1: $I_d V_d$ (a.) and $I_d V_g$ (b.) curves of a transistor fabricated with **12** ($L = 20 \mu\text{m}$).

4. Conclusions

The possibility of using guanosine ribbon structures as organic semiconductor has been demonstrated for devices with a distance between electrodes less than 100 nm, taking advantage of the well oriented dipole moments owned by ribbon A aggregates. New terthiophene functionalized guanosines were studied to improve the conductivity of these materials, exploiting the π - π stacking of thiophene once organized in a ordered guanosine ribbon structure. Our first attempts made by depositing these ribbons between gold electrodes in a three terminal device (FET) were unsuccessful: although long fibers were detected with AFM imaging, indicating the formation of ordered structures, no current was registered in these experiments. STM images could clarify these results and give an useful feed-back to improve the molecular design.

Bibliography

- (1) Facchetti, A. *Materials Today* **2007**, *10*, 28.
- (2) Mei, J.; Diao, Y.; Appleton, A.; Fang, L.; Bao, Z. *Journal Of The American Chemical Society* **2013**, *135*, 6724.
- (3) Zaumseil, J.; Sirringhaus, H. *Chemical Reviews* **2007**, *107*, 1296.
- (4) Wang, C.; Dong, H.; Hu, W.; Liu, Y.; Zhu, D. *Chemical Reviews* **2012**, *112*, 2208.
- (5) Rang, Z.; Haraldsson, A.; Kim, D.; Ruden, P.; Nathan, M.; Chesterfield, R.; Frisbie, C. *Applied Physics Letters* **2001**, *79*, 2731.
- (6) Lin, Y.; Gundlach, D.; Nelson, S.; Jackson, T. *Ieee Electron Device Letters* **1997**, *18*, 606.
- (7) Tsumura, A.; Koezuka, H.; Ando, T. *Applied Physics Letters* **1986**, *49*, 1210.
- (8) Maruccio, G.; Visconti, P.; Arima, V.; D'amico, S.; Blasco, A.; D'amone, E.; Cingolani, R.; Rinaldi, R.; Masiero, S.; Giorgi, T.; Gottarelli, G. *Nano Letters* **2003**, *3*, 479.
- (9) Chen, J.; Murphy, A.; Esteve, J.; Ogletree, D.; Salmeron, M.; Frechet, J. *Langmuir* **2004**, *20*, 7703.
- (10) Nicolas, Y.; Blanchard, P.; Levillain, E.; Allain, M.; Mercier, N.; Roncali, J. *Organic Letters* **2004**, *6*, 273.
- (11) Brzozowski, Z.; Saczewski, F. *Journal Of Medicinal Chemistry* **2002**, *45*, 430.
- (12) Gottarelli, G.; Masiero, S.; Mezzina, E.; Pieraccini, S.; Rabe, J.; Samori, P.; Spada, G. *Chemistry-A European Journal* **2000**, *6*, 3242.
- (13) Giorgi, T.; Grepioni, F.; Manet, I.; Mariani, P.; Masiero, S.; Mezzina, E.; Pieraccini, S.; Saturni, L.; Spada, G.; Gottarelli, G. *Chemistry-A European Journal* **2002**, *8*, 2143.
- (14) Spada, G.; Lena, S.; Masiero, S.; Pieraccini, S.; Surin, M.; Samori, P. *Advanced Materials* **2008**, *20*, 2433.
- (15) Pieraccini, S.; Masiero, S.; Pandoli, O.; Samori, P.; Spada, G. *Organic Letters* **2006**, *8*, 3125.
- (16) Marlow, A.; Mezzina, E.; Spada, G.; Masiero, S.; Davis, J.; Gottarelli, G. *Journal Of Organic Chemistry* **1999**, *64*, 5116.
- (17) Mezzina, E.; Mariani, P.; Itri, R.; Masiero, S.; Pieraccini, S.; Spada, G.; Spinozzi, F.; Davis, J.; Gottarelli, G. *Chemistry-A European Journal* **2001**, *7*, 388.

Chapter IV: Functionalized guanosines for organic electronic devices

- (18) Pieraccini, S.; Bonacchi, S.; Lena, S.; Masiero, S.; Montalti, M.; Zaccheroni, N.; Spada, G. *Organic & Biomolecular Chemistry* **2010**, *8*, 774.
- (19) Harada, N.; Nakanishi, K. *Circular Dichroic Spectroscopy–Exciton Coupling In Organic Stereochemistry* Mill Valley, Ca, 1983.
- (20) Azumi, R.; Gotz, G.; Bauerle, P. *Synthetic Metals* **1999**, *101*, 569.
- (21) Kiuchi, F.; Nakamura, N.; Saitoh, M.; Komagome, K.; Hiramatsu, H.; Takimoto, N.; Akao, N.; Kondo, K.; Tsuda, Y. *Chemical & Pharmaceutical Bulletin* **1997**, *45*, 685.
- (22) Hercouet, A.; Lecorre, M. *Phosphorus Sulfur And Silicon And The Related Elements* **1987**, *29*, 111.
- (23) Hardouin, C.; Kelso, M.; Romero, F.; Rayl, T.; Leung, D.; Hwang, I.; Cravatt, B.; Boger, D. *Journal Of Medicinal Chemistry* **2007**, *50*, 3359.
- (24) Tersoff, J.; Hamann, D. *Physical Review B* **1985**, *31*, 805.
- (25) Ciesielski, A., 2010.
- (26) [Http://Www.Utwente.Nl/Tnw/Cpm/Research/Scanning/](http://Www.Utwente.Nl/Tnw/Cpm/Research/Scanning/).
- (27) Rabe, J.; Buchholz, S. *Science* **1991**, *253*, 424.
- (28) Burattini, S.; Colquhoun, H.; Greenland, B.; Hayes, W. *Faraday Discussions* **2009**, *143*, 251.
- (29) Giancarlo, L.; Flynn, G. *Annual Review Of Physical Chemistry* **1998**, *49*, 297.
- (30) [Http://Nanoprobes.Aist-Nt.Com/Apps/Hopg%20info.Htm](http://Nanoprobes.Aist-Nt.Com/Apps/Hopg%20info.Htm).
- (31) Binnig, G.; Rohrer, H. *Ibm Journal Of Research And Development* **1986**, *30*, 355.
- (32) Tamayo, J.; Garcia, R. *Langmuir* **1996**, *12*, 4430.
- (33) Frangis, N., Principles Of Atomic Rinciples Force Microscopy (Afm).
- (34) [Http://Www.Parkafm.Com/Afm_Guide/True_Non_Contact_Mode_1.Php](http://Www.Parkafm.Com/Afm_Guide/True_Non_Contact_Mode_1.Php).
- (35) [Http://Www.Parkafm.Com/Afm_Guide/Spm_Modes_1.Php?Id=1176](http://Www.Parkafm.Com/Afm_Guide/Spm_Modes_1.Php?Id=1176).
- (36) De Luca, G.; Pisula, W.; Credgington, D.; Treossi, E.; Fenwick, O.; Lazzarini, G.; Dabirian, R.; Orgiu, E.; Liscio, A.; Palermo, V.; Mullen, K.; Cacialli, F.; Samori, P. *Advanced Functional Materials* **2011**, *21*, 1279.

Chapter V: Experimental section

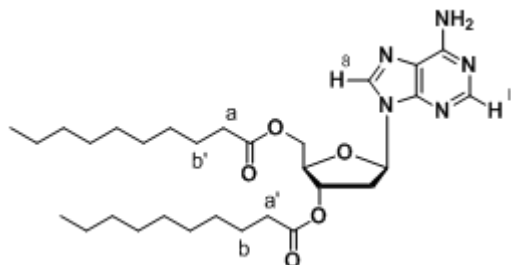
1. General

All reactions were carried out under magnetic or mechanical stirring. Reactions requiring anhydrous conditions were carried out in oven-dried glassware under dry argon atmosphere. For TLC analyses, Baker IB2-F silica gel plates were used. Column chromatography was performed on Aldrich silica gel 230-400 mesh. Reagents and solvents, including dry solvents, were purchased from Aldrich, Fluka or Alfa Aesar.

NMR spectra were recorded with Varian (Gemini 200, Inova 400, Mercury 600 MHz) instruments; decoupled ^{13}C NMR spectra were usually recorded. To assign carbons, HSQC and HMBC multidimensional spectra were recorded. All NMR spectra were referenced relative to residual solvent peaks. Electrospray (ES) ionization mass spectra were obtained with a Micromass ZMD 4000.

2. Synthesis of lipophilic nucleosides

3',5'-Di-*O*-decanoyl-2'-deoxyadenosine (4)



2'-Deoxyadenosine (673 mg, 2.5 mmol) was vacuum dried over P₂O₅ at 50 °C for 4 h and dissolved in dry MeCN (20 mL). Redistilled Et₃N (0.84 mL, 6 mmol), DMAP (20 mg) and decanoic anhydride (2.2 mL, 6.0 mmol) were then added and the mixture was stirred at room temp. for 4 h: the formation of a white precipitate was observed. MeOH (0.5 mL) was added and stirring was continued for 20 min. The crude reaction mixture was filtered and the precipitate was washed with MeCN, water and MeCN again. Crystallization from EtOH afforded the pure diester as a white solid (770 mg, 55%).

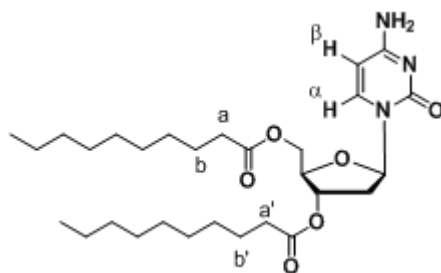
M.p. 51-52 °C.

ESI-MS: *m/z* (%): 582 (100) [1+Na]⁺.

¹H NMR (600 MHz, CDCl₃): δ (ppm) 8.36 (s, 1H, H^a), 7.99 (s, 1H, H^b), 6.43 (m, 1H, H^I), 5.69 (s, 2H, NH₂), 5.42 (m, 1H, H³), 4.39 (m, 2H, H⁴ & H⁵), 4.33 (m, 1H, H^{5'}), 2.89 (m, 1H, H²), 2.63 (m, 1H, H^{2'}), 2.33 (m, 4H, CH₂^a & CH₂^{a'}), 1.61 (m, 4H, CH₂^b & CH₂^{b'}), 1.27 (m, 24H, 12 CH₂), 0.87 (m, 6H, 2 CH₃).

¹³C NMR (600 MHz, CDCl₃): δ (ppm) 173.5, 155.5, 153.4, 149.9, 138.9, 120.2, 84.8, 83.1, 74.7, 63.8, 37.9, 34.3, 32.4, 29.8, 29.4, 24.9, 22.7, 14.3.

3',5'-Di-*O*-decanoyl-2'-deoxycytidine (5)



2'-Deoxycytidine (540 mg, 2.2 mmol) was vacuum dried over P₂O₅ at 50 °C for 2 h and suspended in dry MeCN (20 mL). Redistilled Et₃N (0.65 mL, 4.6 mmol), DMAP (20 mg) and decanoic anhydride (1.7 mL, 4.6 mmol) were then added and the mixture was stirred at room temp. for 4 h. The crude was then filtered and the precipitate was washed several times with MeCN and water. The filtrate was concentrated in vacuo and purified by column chromatography (Et₂O was passed until complete elution of decanoic acid, then gradient DCM to DCM:MeOH 97:3). The solid thus obtained was crystallized from EtOH to afford 340 mg (29%) of the title compound as a white solid.

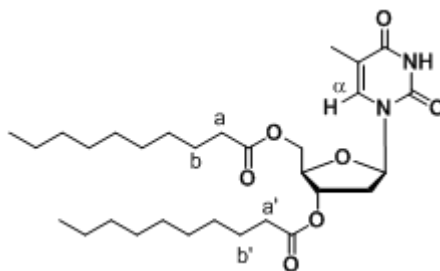
M.p. 106-107 °C.

ESI-MS: *m/z* (%): 558 (100) [1+Na]⁺.

¹H NMR (600 MHz, CD₃OD): δ (ppm) 7.76 (d, 1H, H^α), 6.24 (s, 1H, H¹), 5.95 (m, 1H, H^β), 5.27 (m, 1H, H³), 4.42 (m, 1H, H⁵), 4.33 (m, 2H, H⁴ & H^{5'}), 2.56 (m, 1H, H²), 2.41 (m, 4H, CH₂^a & CH₂^{a'}), 2.27 (m, 1H, H^{2'}), 1.65 (m, 4H, CH₂^b & CH₂^{b'}), 1.32 (m, 24H, 12 CH₂), 0.92 (m, 6H, 2 CH₃).

¹³C NMR (600 MHz, CDCl₃): δ (ppm) 174.8, 167.5, 158.1, 141.6, 95.8, 87.5, 83.6, 75.4, 64.6, 38.7, 34.5, 32.8, 29.8, 25.6, 23.3, 14.2.

3',5'-Di-O-decanoylthymidine (6)



Thymidine (200 mg, 0.82 mmol) was vacuum dried over P₂O₅ at 50 °C for 2 h and suspended in dry MeCN (12 mL). Redistilled Et₃N (0.5 mL, 3.6 mmol) DMAP (20 mg) and decanoyl chloride (0.40 mL, 1.93 mmol) were added and the mixture was stirred overnight at room temp. A further portion of decanoyl chloride (0.40 mL, 1.93 mmol) was added and stirring was continued for 24 h. The course of the reaction was monitored by ESI-MS and TLC (DCM/MeOH 95:5). Methanol (0.5 mL) was added and solvents were then evaporated in vacuo. The residue was partitioned between chloroform (20 mL) and 5% NaHCO₃ (20 mL). The aqueous phase was washed with chloroform (3x15 mL) and the combined organic fractions were dried over MgSO₄ and concentrated in vacuo. The residue was purified by column chromatography over silica (eluent chloroform), affording 284 mg (62%) of the title compound as a colorless oil.

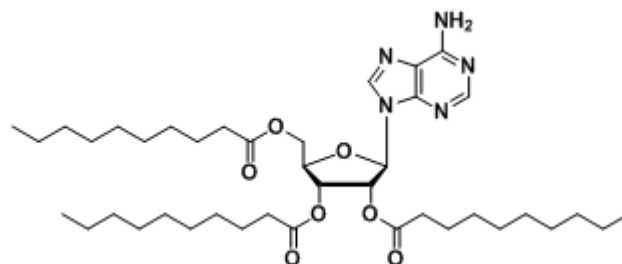
ESI-MS: *m/z* (%): 573 (100) [1+Na]⁺.

¹H NMR (600 MHz, CDCl₃): δ (ppm) 9.61 (s, 1H), 7.28 (m, 1H), 6.31 (m, 1H), 5.20 (m, 1H), 4.32 (m, 3H), 2.33 (m, 6H), 2.12 (m, 1H), 1.93 (m, 2H), 1.61 (m, 4H), 1.26 (m, 20H), 0.87 (m, 6H).

¹³C NMR (600 MHz, CDCl₃): δ (ppm) 173.3, 173.1, 163.9, 150.3, 134.7, 111.5, 84.8, 82.4, 73.9, 37.7, 34.1, 34.0, 33.9, 31.8, 29.3, 29.2, 29.1, 24.8, 24.7, 22.6, 14.0, 12.6.

Chapter V: Experimental section

2',3',5'-Tri-*O*-decanoyladenine (7)



Adenosine (267 mg, 1.0 mmol) was vacuum dried over P_2O_5 at 50 °C for 8 h and suspended in dry MeCN (15 mL). Redistilled Et_3N (0.7 mL, 5 mmol), DMAP (20 mg) and decanoic anhydride (1.2 mL, 3.3 mmol) were then added and the mixture was stirred overnight at room temp. The crude was filtered and the precipitate was washed several times with MeCN and water. The filtrate was concentrated in vacuo and purified by column chromatography (DCM was flushed until complete elution of decanoic acid, then gradient DCM to DCM:MeOH 97:3). The solid thus obtained was crystallized from EtOH to afford 280 mg (38%) of the title compound as a white solid.

M.p. 59-60 °C.

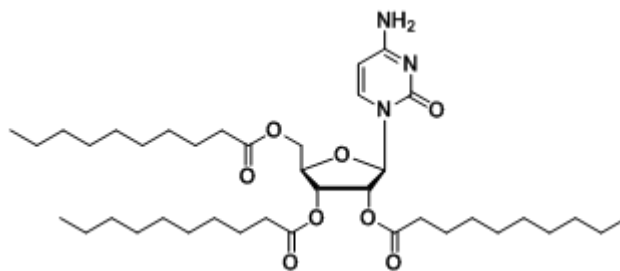
ESI-MS: m/z (%): 731 (100) $[1+H]^+$; 753 (100) $[1+Na]^+$.

1H (600 MHz, $CDCl_3$): δ (ppm) 8.36 (s, 1H,), 8.00 (s, 1H,), 6.18 (m, 1H, H^1), 6.05 (s, 2H, NH_2), 5.87 (m, 1H, H^2), 5.64 (m, 1H, H^3), 4.44 (m, 1H, H^4), 4.40 (m, 2H, H^5 & $H^{5'}$), 2.37 (m, 4H, CH_2^a & CH_2^a), 2.30 (m, 2H, $CH_2^{a''}$), 1.64 (m, 4H, CH_2^b & $CH_2^{b'}$), 1.56, (m 2H, $CH_2^{b''}$), 1.28 (m, 36H, 18 CH_2), 0.87 (m, 9H, 3 CH_3).

^{13}C NMR (600 MHz, $CDCl_3$): δ (ppm) 173.6, 155.1, 149.7, 119.9, 86.7, 80.6, 73.2, 70.7, 63.0, 33.9, 31.8, 29.1, 24.5, 22.4, 13.8.

Chapter V: Experimental section

2',3',5'-Tri-*O*-decanoylcytidine (8)



Cytidine (244 mg, 1.0 mmol) was vacuum dried over P₂O₅ at 50 °C for 8 h and suspended in dry MeCN (15 mL). Redistilled Et₃N (0.6 mL, 4.3 mmol) DMAP (20 mg) and decanoic anhydride (1.36 mL, 3.7 mmol) were added and the suspension was stirred at room temperature for 24 h. Methanol (0.5 mL) was added and, after 20 min., the mixture was filtered. The precipitate was washed several times with MeCN, then with water and with MeCN again. Crystallization from EtOH afforded the pure product as a white solid (698 mg, 97%).

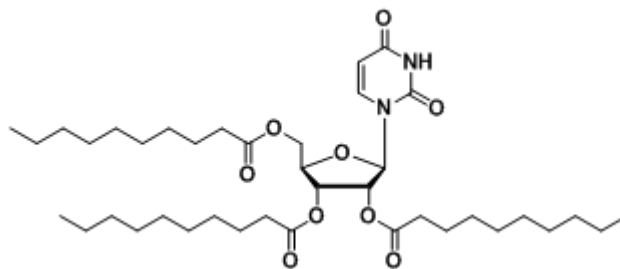
M.p. 108-109 °C.

ESI-MS: *m/z* (%): 706 (100) [1+H]⁺.

¹H NMR (600 MHz, CD₃OD): δ (ppm) 7.52 (d, 1H, H^α), 6.11 (s, 1H, H¹), 5.87 (m, 1H, H^β), 5.33 (m, 2H, H² & H³), 4.34 (m, 3H, H⁴, H⁵ & H^{5'}), 2.35 (m, 6H, CH₂^a, CH₂^{a'} & CH₂^{a''}), 1.62 (m, 6H, CH₂^b, CH₂^{b'} & CH₂^{b''}), 1.27 (m, 24H, 12 CH₂), 0.86 (m, 9H, 3 CH₃).

¹³C NMR (600 MHz, CD₃OD): δ (ppm) 172.9, 165.2, 155.1, 141.3, 95.5, 88.7, 80.0, 77.4, 73.5, 70.1, 63.1, 34.1, 32.3, 29.3, 24.9, 22.7, 14.3.

2',3',5'-Tri-*O*-decanoyluridine (9)



The same procedure as described above was followed, starting from uridine (200 mg, 0.82 mmol) but using 0.6 mL (4.3 mmol) of redistilled Et₃N and 0.84 mL (4.0 mmol) of decanoyl chloride (in two portions). After work-up and chromatography as above, of the title compound was obtained as a colorless oil which solidifies on standing (276 mg, 47%).

M.p. 34-35 °C.

ESI-MS: m/z (%): 729 (100) [1+H]⁺.

¹H NMR (600 MHz, DMSO-d₆): δ (ppm) 11.45 (s, 1H), 7.70 (m, 1H), 5.88 (m, 1H), 5.70 (m, 1H), 4.45 (m, 1H), 5.35 (m, 1H), 4.24 (m, 3H), 2.31 (m, 6H), 1.51 (m, 6H), 1.23 (m, 20H), 0.85 (m, 6H).

¹³C NMR (600 MHz, DMSO-d₆): δ (ppm) 172.5, 171.7, 162.9, 150.3, 141.3, 102.4, 87.8, 79.2, 78.9, 71.8, 69.7, 62.8, 33.1, 33.0, 31.2, 28.9, 28.8, 28.7, 28.6, 28.5, 28.4, 28.3, 24.3, 24.2, 22.1, 13.9.

3. Synthesis of thiophene functionalized guanosines

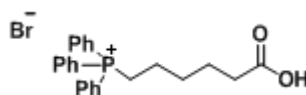
3.1 Synthesis of 3',5'-Di-O-[7-(thiophen-2-yl)-heptan-1-oyl]-2'-deoxyguanosine

Triphenylphosphonium bromide (11)¹



A solution of PPh₃ (40 mmol, 10.52 g) in HBr (48% aq., 28 mL) was stirred at 70 °C for 10 minutes; after cooling at room temperature, the solution was extracted with CHCl₃ (3x30 mL) and the combined organic phases were dried over MgSO₄. The solvent was evaporated and the crude product was washed several times with EtOAc to remove traces of PPh₃, obtaining a white powder (37.2 mmol, 12.76g, yield: 93%).

6-(triphenylphosphonium bromide)-hexanoic acid (12)²

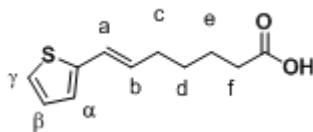


A mixture of ϵ -caprolactone (30 mmol, 2.85 mL) and triphenylphosphonium bromide (1 equiv., 30 mmol, 10.3 g) was stirred at 160 °C for one hour and thirty minutes: the solid dissolved when the temperature was reached and then crystallized again. The crude was allowed to cool at room temperature, water was removed at reduced pressure. Chloroform (10 mL) was added at the gluey precipitate and the suspension was sonicated to obtain white crystals, which were filtered (26.70 mmol, 12.98 g, yield: 89%).

ESI-MS: m/z (%): 377 (100) [1+H]⁺; 399 (100) [1+Na]⁺

¹H NMR (200 MHz, CDCl₃): δ (ppm) 7.79 (m, 15H, Ph), 4.14 (bs, 1H, OH), 3.64 (m, 2H), 2.78 (t, 2H, J = 6.9 Hz), 1.96 (m, 4H), 1.72 (m, 2H).

7-(thiophen-2-yl)-heptenoic acid (13)³



To a solution of 6-(triphenylphosphonium bromide) hexanoic acid (20 mmol, 8.84g) in dry THF (100 mL) under nitrogen was added thiophene-2-carboxyaldehyde (0.95 equiv., 19 mmol, 1.37 mL); after cooling the mixture at -78 °C, a suspension of potassium tert-butoxyde (2.2 equiv., 44 mmol, 4.93 g) in dry THF (25 mL) was added dropwise. The solution was allow to warm at 0 °C and stirred for 20 h in an ice bath. Then, after evaporating the solvent, the crude was diluted with 4N solution of NaOH (80 mL) and extracted with EtOAc (3x20 mL). The aqueous phase was neutralized with a 4N solution of HCl and re-extracted with EtOAc until the aqueous phase was clear. The organic layer was dried over MgSO₄, filtered and concentrated; the crude product was purified through chromatography on silica gel (solvent: petroleum ether/EtOAc = 7/3), obtaining a yellowish oil (2.26g, yield: 55%). From NMR spectra both E and Z isomer were observed (cis/trans = 60/40).

ESI-MS: *m/z* (%): 209 (100) [1-H]⁻.

¹H NMR (600 MHz, CDCl₃):

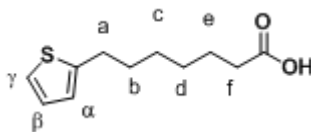
Cis: δ (ppm) 7.24 (d, 1H, J = 5.1, H^γ), 6.99 (dd, J₁ = 5.1 Hz, J₂ = 3.4 Hz, H^β), 6.96 (d, 1H, J = 3.4 Hz, H^α), 6.54 (d, 1H, J = 11.4 Hz, H^a), 5.55 (d, 1H, J = 6.9 Hz, H^b), 2.44 (qt, 2H, J₁ = 7.5 Hz, CH₂, H^c), 2.39 (t, 2H, J = 7.4 Hz, CH₂, H^f), 1.73 (m, 2H, CH₂, H^e), 1.57 (m, 2H, CH₂, H^d).

Trans: δ (ppm) 7.08 (d, 1H, J = 5.1, H^γ), 6.92 (dd, J₁ = 5.1 Hz, J₂ = 3.4 Hz, H^β), 6.86 (d, 1H, J = 3.4 Hz, H^α), 6.51 (d, 1H, J = 16.5 Hz, H^a), 6.03 (d, 1H, J = 7.2 Hz, H^b), 2.38 (t, 2H, J = 7.4 Hz, CH₂, H^f), 2.20 (qt, 2H, J₁ = 7.4 Hz, CH₂, H^c), 1.69 (m, 2H, CH₂, H^e), 1.52 (m, 2H, CH₂, H^d).

¹³C NMR (600 MHz, CDCl₃): δ (ppm) 179.25, 130.14, 127.19, 126.71, 124.33, 124.33, 123.52, 123.17, 33.74, 33.69, 32.39, 29.69, 28.82, 28.56, 24.37, 24.16.

Chapter V: Experimental section

7-(thiophen-2-yl)-heptanoic acid (14)³



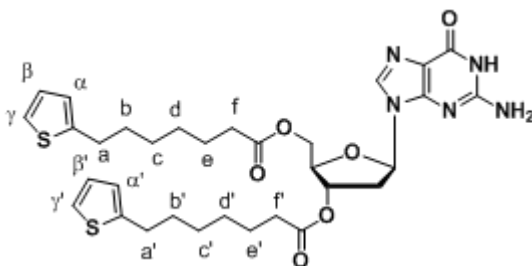
Both isomers (2.28g, 11mmol) was diluted with EtOAc (80 mL) and 50% Pd/C (0.2 eq, 2.2 mmol, 466 mg) was added; the solution was treated with H₂ (2 bar) in a Parr shaker apparatus for 5 hours at room temperature. The reaction mixture was filtered through Celite, concentrated and purified by chromatography on silica gel (solvent: petroleum ether/EtOAc = 7/3) to effort a yellowish oil (2.05 g, 9.46 mmol).

ESI-MS: *m/z* (%): 211 (100) [1-H]⁻.

¹H NMR (600 MHz, CDCl₃): δ (ppm) 10.20 (bs, 1H, OH), 7.10 (dd, 1H, J₁ = 5.1 Hz, J₂ = 1.1 Hz, H ^{γ}), 6.91 (dd, J₁ = 5.1 Hz, J₂ = 3.4, H ^{β}), 6.77 (dd, 1H, 3.4 Hz, 1.1 Hz, H ^{α}), 2.82 (t, 2H, J = 7.4 Hz, CH₂ ^{a}), 2.36 (t, 2H, J = 7.5 Hz, CH₂ ^{f}), 1.66 (m, 4H, 2 CH₂), 1.37 (m, 4H, 2 CH₂)

¹³C NMR (600 MHz, CDCl₃): δ (ppm) 178.42, 143.2, 124.93, 124.64, 124.39, 32.83, 31.76, 29.97, 28.95, 28.64, 24.71.

3',5'-Di-O-[7-(thiophen-2-yl)-heptanoyl]-2'-deoxyguanosine (15)



In dry atmosphere of N₂, to a solution of 7-(thien-2-yl)-1--heptanoic acid (1.1 equiv, 4.4 mmol, 933 mg) in dry THF (30 mL) Et₃N (2 equiv., 8 mmol, 1.11 mL) was added; the mixture was cooled at 0 °C in an ice bath and CH₃SO₂Cl (1.1 equiv., 4.4 mmol, 358 μ L) was added dropwise. After 30 minutes at 0 °C and 1 hour at room temperature, dG (dried under vacuum at 50 °C for 4 hour) (4 mmol, 1.14 g) and a catalytic amount of DMAP were added. The reaction was carried out for 15 hours and then, after solvent removal, the crude product was diluted with CH₂Cl₂ (30 mL) and wash with H₂O (3x10 mL). The organic phase was dried over MgSO₄ and the solvent evaporated; purification through chromatography on silica

Chapter V: Experimental section

gel (eluent: dichloromethane/methanol = 99/1→98/2) and crystallization in MeOH gave a white solid as product (1.4 mmol, 917 mg, yield: 35%).

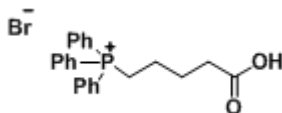
ESI-MS: m/z (%): 655 (100) [1+H]⁺; 678 (100) [1+Na]⁺

¹H NMR (600 MHz, DMSO-d₆): δ (ppm) 10.68, (s, 1H, NH), 7.98 (s, 1H, H⁸), 7.28 (m, 2H, H ^{γ} & H ^{γ'}), 6.88 (m, 2H, H ^{β} & H ^{β'}), 6.83 (m, 2H, H ^{α} & H ^{α'}), 6.49 (s, 2H, NH₂), 6.12 (dd, 1H, J₁ = 6.1 Hz, J₂ = 8.4 Hz, H¹), 5.31 (dt, 1H, J₁ = 6.1 Hz, J₂ = 2.2 Hz, H³), 4.21 (m, 2H, H⁵ & H^{5'}), 4.16 (m, 1H, H⁴), 2.91 (m, 1H, H²), 2.76 (m, 4H, CH₂^a), 2.43 (m, 1H, H^{2'}), 2.34 (m, 4H, CH₂^f & CH₂^{f'}), 1.54 (m, 4H, CH₂^b & CH₂^{b'}), 1.43 (m, 4H, CH₂^e & CH₂^{e'}), 1.32 (m, 4H, CH₂^d & CH₂^{d'}), 1.27 (m, 4H, CH₂^c & CH₂^{c'}).

¹³C NMR (600 MHz, DMSO-d₆): δ (ppm) 135.34, 127.07, 124.53, 123.54, 82.31, 81.82, 74.54, 63.72, 35.79, 33.6, 29.28, 28.34, 24.47.

3.2 Synthesis of 2',3'-O-Isopropylidene-5'-O-[6-(5"-hexyl-[2,2';5',2"]-terthiophen-5-yl)-hexanoyl]-guanosine

5-(triphenylphosphonium bromide) pentanoic acid² (16)

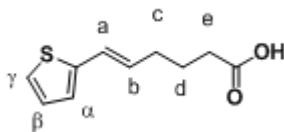


A mixture of δ -valerolactone (30 mmol, 2.81 mL) and triphenylphosphonium bromide (1 equiv., 30 mmol, 10.3 g) was stirred at 160 °C for one hour and thirty minutes: the solid dissolved when the temperature was reached and then crystallized again. The crude was allowed to cool at room temperature, water was removed at reduced pressure. Chloroform (10 mL) was added at the gluey precipitate and the suspension was sonicated to obtain white crystals, which were filtered (24.90 mmol, 11.01 g, yield: 83%).

ESI-MS: m/z (%): 363 (100) [1-Br+H]⁺; 385 (100) [1-Br+Na]⁺

¹H NMR (200 MHz, CDCl₃): δ (ppm) 7.81 (m, 15H, Ph), 4.19 (bs, 1H, OH), 3.73 (m, 2H), 2.81 (t, 2H, J = 6.9 Hz), 2.02 (m, 2H), 1.76 (m, 2H).

6-(thiophen-2-yl)-5-hexenoic acid³ ()



To a solution of 5-(triphenylphosphonium bromide) pentanoic acid (20 mmol, 8.84g) in dry THF (100 mL) under nitrogen was added thiophene-2-carboxyaldehyde (0.95 equiv., 19 mmol, 1.37 mL); after cooling the mixture at $-78\text{ }^{\circ}\text{C}$, a suspension of potassium tert-butoxyde (2.2 equiv., 44 mmol, 4.93 g) in dry THF (25 mL) was added dropwise. The solution was allow to warm at $0\text{ }^{\circ}\text{C}$ and stirred for 20 h in an ice bath. Then, after evaporating the solvent, the crude was diluted with 4N solution of NaOH (80 mL) and extracted with EtOAc (3x20 mL). The aqueous phase was neutralized with a 4N solution of HCl and re-extracted with EtOAc until the aqueous phase was clear. The organic layer was dried over MgSO_4 , filtered and concentrated; the crude product was purified through chromatography on silica gel (solvent: petroleum ether/EtOAc = 7/3), obtaining a yellowish oil (11.5 mmol, 2.26 g, yield: 60%). From NMR spectra both E and Z isomer were observed (cis/trans = 65/35)

ESI-MS: m/z (%): 195 (100) $[1-\text{H}]^-$.

^1H NMR (600 MHz, CDCl_3):

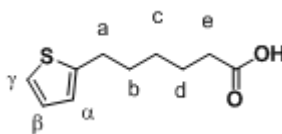
Cis: δ (ppm) 7.24 (d, 1H, $J = 5.1$, H^γ), 6.99 (dd, $J_1 = 5.1$ Hz, $J_2 = 3.5$ Hz, H^β), 6.97 (d, 1H, $J = 3.5$ Hz, H^α), 6.57 (d, 1H, $J = 11.2$ Hz, H^a), 5.54 (dt, 1H, $J_1 = 11.2$ Hz, $J_2 = 6.9$ Hz, H^b), 2.50 (qt, 2H, $J_1 = 7.1$ Hz, CH_2 , H^c), 2.44 (t, 2H, $J = 7.9$ Hz, CH_2 , H^e), 1.84 (m, 2H, CH_2 , H^d).

Trans: δ (ppm) 7.08 (d, 1H, $J = 5.1$, H^γ), 6.93 (dd, $J_1 = 5.1$ Hz, $J_2 = 3.5$ Hz, H^β), 6.87 (d, 1H, $J = 3.5$ Hz, H^α), 6.53 (d, 1H, $J = 15.5$ Hz, H^a), 6.01 (dt, 1H, $J_1 = 15.5$ Hz, $J_2 = 7.2$ Hz, H^b), 2.40 (t, 2H, $J = 7.9$ Hz, CH_2 , H^e), 2.24 (qt, 2H, $J_1 = 6.9$ Hz, CH_2 , H^c), 1.84 (m, 2H, CH_2 , H^d).

^{13}C NMR (600 MHz, CDCl_3): δ (ppm) 178.85, 140.32, 129.28, 129.20, 127.39, 127..22, 126.76, 125.52, 125.13, 124.55, 124.19, 123.36, 123.77, 33.39, 33.13, 31.99, 28.45, 24.39, 24.11

Chapter V: Experimental section

6-(thiophen-2-yl)-hexanoic acid³



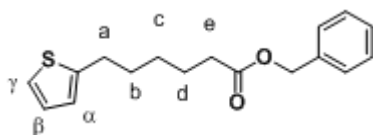
Both isomers (2.26 g, 11.4 mmol) was diluted with EtOAc (80 mL) and 50% Pd/C (0.2 equiv., 2.28 mmol, 483 mg) was added; the solution was treated with H₂ (2 bar) in a Parr shaker apparatus for 4 hours at room temperature. The reaction mixture was filtered through Celite, concentrated and purified by chromatography on silica gel (solvent: petroleum ether/EtOAc = 7/3) to effort a yellowish oil (9.14 mmol, 1.81g, yield : 80%).

ESI-MS: m/z (%): 197 (100) [1-H]⁻.

¹H NMR (600 MHz, CDCl₃): δ (ppm) 10.45 (bs, 1H, OH), 7.10 (dd, 1H, J = 5.1 Hz, 1.1 Hz, H ^{γ}), 6.91 (dd, J = 5.1 Hz, 3.4, H ^{β}), 6.77 (dd, 1H, 3.4 Hz, 1.1 Hz, H ^{α}), 2.94 (t, 2H, J = 7.4 Hz, CH₂^a), 2.36 (t, 2H, J = 7.6 Hz, CH₂^c), 1.7 (m, 4H, 2 CH₂), 1.43 (m, 2H, CH₂)

¹³C NMR (600 MHz, CDCl₃): δ (ppm) 179.12, 126.84, 124.23, 123.04, 107.72, 33.79, 31.51, 29.80, 28.59, 24.53.

6-(thiophen-2-yl)-hexanoic acid benzyl ester⁴



To a solution of 6-(thiophen-2-yl)-hexanoic acid (1.81 g, 9.12 mmol) in dry THF (10 mL) were added potassium carbonate (2 equiv., 18.24 mmol, 2.76 g), 18-crown-6 (0.02 equiv., 0.18, 47 mg) and benzyl bromide (1 equiv., 9.12 mmol, 1.08 mL); the mixture was refluxed at 80 °C under nitrogen atmosphere for 12 hour. After cooling at room temperature, the solution was concentrated in vacuum, diluted with hexane/EtOAc = 3/1 (30 mL) and filtered on a silica gel pad, washing with the same solution. The solvent was evaporated and the product was collected as a yellow oil (8.39 mmol, 2.42 g, yield: 92%).

ESI-MS: m/z (%): 311 (100) [1+Na]⁺

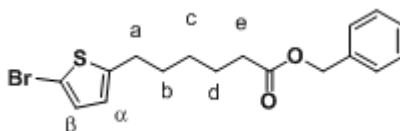
¹H NMR (200 MHz, CDCl₃): δ (ppm) 7.36 (m, 5H, bz), 7.12 (dd, 1H, J₁ = 5.1 Hz, J₂ = 1.1 Hz, H ^{γ}), 6.92 (dd, 1H, J₁ = 5.1 Hz, J₂ = 3.4 Hz, H ^{β}), 6.77 (dd, 1H, J₁ = 3.4 Hz, J₂ = 1.1 Hz,

Chapter V: Experimental section

H^a), 5.12 (s, H, CH_2 bz), 2.82 (t, 2H, $J = 7.2$ Hz, CH_2^a), 2.37 (t, 2H, $J = 7.3$ Hz, CH_2^e), 1.66 (m, 4H, CH_2^b & CH_2^d), 1.40 (m, 2H, CH_2^c).

^{13}C NMR (600 MHz, $CDCl_3$): δ (ppm) 173.56, 147.89, 139.11, 128.88, 128.65, 128.50, 128.27, 127.76, 126.74, 124.11, 122.92, 66.21, 33.83, 31.46, 29.78, 28.63, 24.77.

6-(5-bromo-thiophen-2-yl)-hexanoic acid benzyl ester⁴



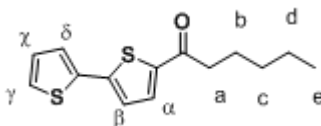
A solution of 6-(thiophen-2-yl)-hexanoic acid benzyl ester (8.39 mmol, 2.42 g) in dry DMF (20 mL) was protected from light and cooled at 0 °C; NBS (1 equiv., 8.39 mmol, 1.93 g) was added and the mixture was stirred overnight. The solvent was then removed and EtOAc was added (60 mL); the solution was washed with brine (40 mLx3) and water (30 mLx3). The organic layer was dried over $MgSO_4$, filtered and concentrated, obtaining a orange-yellow oil (7.97 mmol, 2.93 g, 95% yield).

ESI-MS: m/z (%): 391 (100) $[1+Na]^+$

1H NMR (600 MHz, $CDCl_3$): δ (ppm) 7.33 (m, 5H, bz), 6.83 (d, $J = 3.7$ Hz, H^β), 6.51 (d, $J = 3.7$ Hz, H^α), 5.11 (s, H, CH_2 bz), 2.73 (t, 2H, $J = 7.2$ Hz, CH_2^a), 2.38 (t, 2H, $J = 7.2$ Hz, CH_2^e), 1.65 (m, 4H, CH_2^b & CH_2^d), 1.40 (m, 2H, CH_2^c).

^{13}C NMR (200 MHz, $CDCl_3$): δ (ppm) 173.46, 147.21, 136.18, 129.51, 128.64, 128.28, 124.57, 108.79, 66.23, 34.23, 31.10, 30.17, 28.46, 24.68.

1-(2,2'-bithiophen-5-yl)heptan-1-one⁵



A solution of bithiophene (20 mmol, 3.32 g) in dry toluene (25 mL) was cooled at 0 °C with an ice bath while N_2 was fluxing; hexanoil chloride (1.05 equiv., 21 mmol, 2.89 mL) and $SnCl_4$ (1.05 equiv., 21 mmol, 2.46 mL) were added dropwise. The reaction was carried out for 1h at 0 °C and for an additional hour at room temperature, then was quenched with ice. After

Chapter V: Experimental section

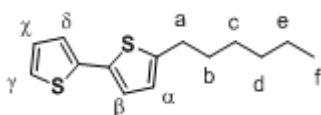
diluting with DCM (30 mL), the mixture was washed with H₂O (30 mL) and a saturated solution of NaHCO₃ (20 mL); the aqueous layer was re-extracted with DCM (30 mL). The collected organic phases were dried over MgSO₄, filtered and concentrated to obtain a yellow-green solid. (4.86 g, 18.40 mmol, 92% yield).

ESI-MS: m/z (%): 265 (100) [1+H]⁺

¹H NMR (200 MHz, CDCl₃): δ (ppm) 7.60 (d, 1H, J = 3.9 Hz, H^a), 7.30 (m, 2H, H ^{δ} & H ^{χ}), 7.18 (d, 1H, J = 3.9 Hz, H ^{β}), 7.06 (t, 1 H, J = 4.5 Hz, H ^{γ}), 2.88 (t, 2H, J = 7.2 Hz, CH₂^a), 1.76 (m, 2H, CH₂^b), 1.37 (m, 4H, CH₂^c & CH₂^d), 0.91 (t, 3H, J = 6.8 Hz, CH₃).

¹³C (200 MHz, CDCl₃): δ (ppm) 198.10, 172.07, 151.06, 132.52, 128.44, 128.28, 126.43, 125.60, 124.19, 39.15, 31.62, 24.72, 22.56, 14.00.

5-hexyl-2,2'-bithiophene⁵



After cooling at 0 °C 80 mL of Et₂O in N₂ atmosphere, LiAlH₄ (7.5 equiv., 138 mmol, 5.17 g) and AlCl₃ (1.8 equiv., 33.12 mmol, 4.42 g) were added very slowly to avoid a temperature rise. To this stirring mixture a solution of 1-([2,2'-bithiophen]-5-yl)heptan-1-one (18.40 mmol, 4.86 g) in dry toluene (20 mL, kept warm to solubilize the product) was added dropwise in 30 minutes. The solution was allowed to warm at room temperature; after 3 h the reaction was quenched with EtOAc very slowly and neutralized with HCl 6N. When gas evolution was ended, the mixture was extracted with Et₂O (3x30 mL), the organic layer was dried over MgSO₄, filtered and concentrated. The crude product was purified by chromatography on silica gel (solvent: petroleum ether) to obtain a green-yellow oil (11.6 mmol, 2.85 g, 62% yield).

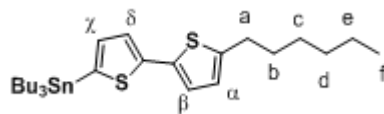
ESI-MS: m/z (%): 251 (100) [1+H]⁺

¹H NMR (200 MHz, CDCl₃): δ (ppm) 7.16 (m, 1H), 7.09 (m, 1H), 6.98 (m, 2H), 6.67 (m, 1H), 2.79 (t, 2H, J = 7.2 Hz, CH₂^a), 1.67 (m, 2H, CH₂^b), 1.33 (m, 4H, CH₂^c & CH₂^d), 0.79 (t, 3H, J = 5.8 Hz, CH₃).

¹³C NMR (200 MHz, CDCl₃): δ (ppm) 145.5, 137.9, 134.7, 127.4, 124.6, 123.6, 123.3, 122.9, 31.5, 30.1, 28.7, 22.5, 14.0.

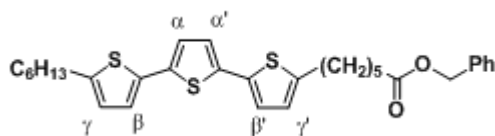
Chapter V: Experimental section

5-tributylstannyl-5'-hexyl-2,2'-bithiophene⁴



A solution of 5-hexyl-2,2'-bithiophene (11.6 mmol, 2.85 g) in 50 mL of dry THF with N,N,N,N-tetramethyl-1,2-ethylenediamine (TMEDA, 1 equiv., 11.6 mmol, 1.75 mL) was cooled at -78 °C with a bath of acetone and dry ice; a 1.6 M solution of n-BuLi in hexane (1 equiv., 11.6 mmol, 7.25 mL) was added dropwise and the solution was stirred for 1 hour at -78 °C. Then tributyltin chloride (1 equiv., 11.6 mmol, 3.14 mL), dissolved in 5 mL of dry THF, was added slowly at the mixture, which was allowed to warm at room temperature. After 2 hours the solvent was evaporated, the resulting liquid was diluted with 50 mL of EtOAc and washed with brine (3x25 mL) and H₂O (3x30 mL). The combined organic layers were concentrated obtaining a yellow oil (9.98 mmol, 5.33 g, yield: 86%) and used directly for the next reaction.

6-(5''-Hexyl-[2,2';5',2'']-terthiophen-5-yl) hexanoic acid benzyl ester⁴



A solution of 6-(5-bromo-thien-2-yl)-hexanoic acid benzyl ester (7.97 mmol, 2.93 g) and 5-tributylstannyl-5'-hexyl-2,2'-bithiophene (1 equiv., 7.97 mmol, 4.33 g) in dry DMF (20 mL) was degassed in N₂ flux for 40 minutes; subsequently Pd(Ph₃)₂Cl₂ (0.04 equiv., 0.32 mmol, 223 mg) was added and the mixture was degassed for additional 20 minutes. Then the reaction was carried out overnight at 80 °C and, after cooling at room temperature, 60 mL of EtOAc was added. The solution was washed three times with brine (3x20 mL) and with H₂O (3x30 mL); the organic phase was dried over MgSO₄, the solvent evaporated and the crude product was purified by flash chromatography through silica gel (eluent: petroleum ether/dichloromethane = 95/5 → 8/2 → 1/1). The product, after crystallization in hexane, is a yellow solid (3.83 mmol, 2.05 g, yield: 48%).

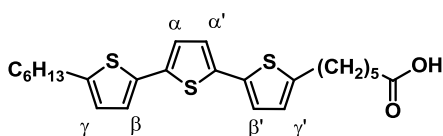
ESI-MS: *m/z* (%): 559 (100) [1+Na]⁺

Chapter V: Experimental section

^1H NMR (300 MHz, CDCl_3): δ (ppm) 7.35 (m, 5H), 6.96 (s, 2H, H^α), 6.95 (dd, 2H, $J_1 = 3.5$ Hz, $J_2 = 1.6$ Hz, H^β), 6.67 (d, 2H, $J = 3.5$ Hz, H^γ), 5.12 (s, 2H, CH_2 bz), 2.79 (dt, 4H, $J = 7.5$ Hz), 2.38 (t, 2H, $J = 7.5$ Hz), 1.69 (m, 6H), 1.44 (m, 2H), 1.38 (m, 2H), 1.31 (m, 4H), 0.89 (t, 3H, $J = 7.2$ Hz).

^{13}C NMR (200 MHz, CDCl_3) δ (ppm): 198.10, 173.56, 145.43, 137.89, 136.20, 129.11, 128.88, 128.64, 128.50, 128.40, 128.27, 127.76, 127.07, 126.75, 124.11, 122.92, 69.82, 66.21, 65.51, 57.00, 34.29, 33.62, 31.45, 30.43, 29.77, 28.62, 24.76, 9.98.

6-(5''-Hexyl-[2,2';5',2'']-terthiophen-5-yl) hexanoyl acid⁴



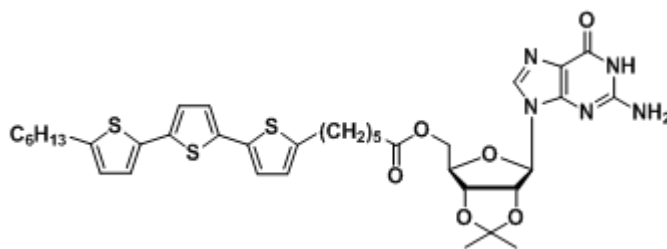
To a solution of ester (3.83 mmol, 2.05 g) in THF (500 mL) were added 100 mL of KOH solution (5% w/w) and the resulting mixture was stirred at 70 °C overnight. The reaction was quenched with 1M HCl until pH 2 was achieved. THF was evaporated, the yellow suspension was filtered and wash with H₂O to neutrality (pH = 7) and with methanol. The product is a yellow solid (3.60 mmol, 1.62 g, yield: 94%).

ESI-MS: m/z (%): 469 (100) $[1+\text{Na}]^+$

^1H NMR (300 MHz, CDCl_3): δ (ppm) 6.97 (s, 2H, H^α & $\text{H}^{\alpha'}$), 6.96 (dd, 2H, $J_1 = 3.5$ Hz, $J_2 = 1.6$ Hz, H^β & $\text{H}^{\beta'}$), 6.67 (d, 2H, $J = 3.5$ Hz, H^γ & $\text{H}^{\gamma'}$), 2.79 (dt, 4H, $J = 7.5$ Hz), 2.38 (t, 2H, $J = 7.5$ Hz), 1.69 (m, 6H), 1.44 (m, 2H), 1.38 (m, 2H), 1.31 (m, 4H), 0.89 (t, 3H, $J = 7.2$ Hz).

^{13}C NMR (200 MHz, CDCl_3): δ (ppm) 198.26, 151.07, 145.52, 144.81, 136.32, 134.92, 134.69, 125.02, 124.84, 123.61, 123.53, 123.27, 33.57, 31.63, 31.22, 30.26, 29.99, 28.83, 28.48, 24.47, 22.64, 14.13.

2',3'-O-Isopropylidene-5'-O-[4-(5''-hexyl-[2,2';5',2'']terthiophen-5-yl)-hexanoyl]-guanosine



In dry atmosphere of N₂, to a solution of 5''-Hexyl-[2,2';5',2'']-terthiophen-5-yl) hexanoyl acid (1.1 equiv., 4.4 mmol, 2.09 g) in dry THF (30 mL) Et₃N (2 equiv., 8 mmol, 1.11 mL) was added; the mixture was cooled at 0 °C in an ice bath and CH₃SO₂Cl (1.1 equiv., 4.4 mmol, 358 μL) was added dropwise. After 30 minutes at 0 °C and 1 hour at room temperature, GACE (dried under vacuum at 50 °C for 4 hour) (4 mmol, 1.29 g) and a catalytic amount of DMAP were added. The reaction was carried out for 15 hours and then, after solvent removal, the crude product was diluted with CH₂Cl₂ (30 mL) and wash with H₂O (3x10 mL). The organic phase was dried over MgSO₄ and the solvent evaporated; purification through chromatography on silica gel (eluent: dichloromethane/methanol = 99/1→97/3) and crystallization in AcCN gave a white solid as product (0.92 mmol, 690 mg, yield: 23%).

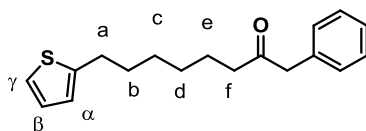
ESI-MS: *m/z* (%): 751 (100) [1+H]⁺

¹H NMR (600 MHz, DMSO-*d*₆): δ (ppm) 10.69, (s, 1H, NH), 7.84 (s, 1H, H⁸), 7.13 (s, 2H, H^α & H^{α'}), 7.10 (t, 2H, J = 4.2 Hz, H^β & H^{β'}), 6.79 (t, 2H, J = 4.2 Hz, H^γ & H^{γ'}), 6.53 (s, 2H, NH₂), 6.01 (d, 1H, J = 2.0 Hz, H¹) 5.26 (dd, 1H, J₁ = 6.3 Hz, J₂ = 2.0 Hz, H²), 5.12 (dd, 1H, J₁ = 6.3 Hz, J₂ = 3.4 Hz, H³), 4.25 (m, 2H, H⁴ & H⁵), 4.12 (m, 1H, H^{5'}), 2.76 (m, 4H, CH₂^a), 2.28 (m, 2H), 1.61 (m, 4H), 1.51 (m, 4H), 1.30 (m, 9H), 0.87 (t, 3H, J = 6.9 Hz, CH₃).

¹³C NMR (600 MHz, DMSO-*d*₆): δ (ppm) 151.0, 136.6, 125.8, 124.4, 123.9, 117.3, 88.6, 84.4, 83.9, 81.3, 40.21, 64.2, 33.4, 31.2, 31.1, 29.5, 29.4, 28.3, 28.1, 27.3, 25.6, 24.4, 22.3, 14.2.

3.3 Synthesis of 2',3'-O-Isopropylidene-5'-O-[7-([2,2';5',2'']-terthiophen-5-yl)-heptanoyl]-guanosine

7-(thiophen-2-yl)-heptanoic acid benzyl ester⁴



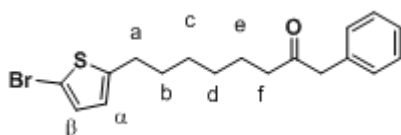
Following the procedure used for compound, 7-(thiophen-2-yl)-heptanoic acid benzyl ester was prepared using 7-(thiophen-2-yl)-6-heptanoic acid (9.46 mmol, 2.05 g,) in THF (10 mL) with K_2CO_3 (2 equiv., 18.92 mmol, 2.61 g), 18-crown-6 (0.02 equiv., 0.19, 50 mg) and benzyl bromide (1 equiv., 9.12 mmol, 1.12 mL). After filtration and evaporation of the solvent, . The solvent was evaporated, the product was collected as a yellow oil (8.41 mmol, 2.54 g, yield: 89%).

ESI-MS: m/z (%): 325 (100) $[1+Na]^+$

1H NMR (600 MHz, $CDCl_3$): δ (ppm) 7.37 (m, 5H, bz), 7.11 (dd, 1H, $J_1 = 5.1$ Hz, $J_2 = 1.1$ Hz, H^γ), 6.91 (dd, 1H, $J_1 = 5.1$ Hz, $J_2 = 3.4$ Hz, H^β), 6.77 (dd, 1H, $J_1 = 3.4$ Hz, $J_2 = 1.1$ Hz, H^α), 5.12 (s, H, CH_2 bz), 2.81 (t, 2H, $J = 7.2$ Hz, CH_2^a), 2.36 (t, 2H, $J = 7.3$ Hz, CH_2^f), 1.64 (m, 4H, CH_2^b & CH_2^e), 1.37 (m, 4H, CH_2^c & CH_2^d).

^{13}C NMR (600 MHz, $CDCl_3$): δ (ppm) 173.65, 145.65, 136.24, 129.12, 128.89, 128.64, 128.50, 128.27, 126.74, 124.05, 122.86, 66.18, 34.36, 31.63, 29.88, 28.90, 28.76, 24.94.

7-(5-bromo-thien-2-yl)-heptanoic acid benzyl ester⁴



Following the procedure used for compound, 7-(5-bromo-thiophen-2-yl)-heptanoic acid benzyl ester was prepared from 7-(thiophen-2-yl)-heptanoic acid benzyl ester (8.41 mmol, 2.54 g) in dry DMF (20 mL) with NBS (1 equiv., 8.41 mmol, 2.03 g). The product, after solvent evaporation is a orange-yellow oil (7.65 mmol, 2.91 g, 91% yield).

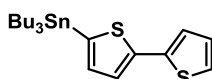
ESI-MS: m/z (%): 404 (100) $[1+Na]^+$

Chapter V: Experimental section

^1H NMR (600 MHz, CDCl_3): δ (ppm) 7.36 (m, 5H, bz), 6.89 (d, 1H, $J = 3.7$, H^β), 6.54 (d, 1H, $J = 3.7$, H^α), 5.11 (s, H, CH_2 bz), 2.77 (t, 2H, $J = 7.2$ Hz, CH_2^a), 2.38 (t, 2H, $J = 7.3$ Hz, CH_2^f), 1.66 (m, 4H, CH_2^b & CH_2^e), 1.39 (m, 4H, CH_2^c & CH_2^d).

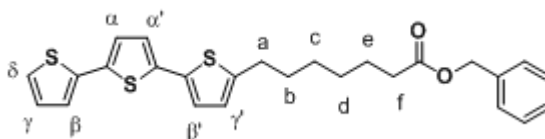
^{13}C NMR (600 MHz, CDCl_3): δ (ppm) 173.59, 145.32, 134.46, 129.65, 128.52, 128.47, 128.18, 124.05, 121.94, 68.32, 33.98, 30.93, 29.36, 28.71, 27.95, 25.80.

5-tributylstannyl-2,2'-bithiophene⁴



Following the procedure used for compound, 5-tributylstannyl-2,2'-bithiophene was prepared in THF (20 mL) using 2,2'-bithiophene (10 mmol, 1.66 g), TMEDA (1 equiv., 10 mmol, 1.51 mL), 1.6 M solution of *n*-BuLi in hexane (1 equiv., 10 mmol, 6.25 mL) and a solution of tributyltin chloride (1 equiv., 10 mmol, 2.71 mL) in 5 mL of dry THF. The product, after solvent evaporation, was obtained as yellow-orange liquid (3.82 g, 8.4 mmol, yield: 84%) and used directly for the next reaction.

7-([2,2';5',2'']-terthiophen-5-yl)-heptanoyl acid benzyl ester⁴



Following the procedure used for compound, 7-([2,2';5',2'']-terthiophen-5-yl)-heptanoyl acid benzyl ester was prepared in dry DMF (20 mL) with 7-(5-bromo-thien-2-yl)-heptanoic acid benzyl ester (7.65 mmol, 2.91 g), 5-tributylstannyl-2,2'-bithiophene (1 equiv., 7.65 mmol, 3.48 g) and $\text{Pd}(\text{Ph}_3)_2\text{Cl}_2$ (0.04 equiv., 0.31 mmol, 215 mg). The product was purified by flash chromatography through silica gel (eluent: petroleum ether/dichloromethane = 95/5 \rightarrow 8/2 \rightarrow 1/1). The product, after crystallization in hexane, is a yellow solid (3.16 mmol, 1.46 g, yield: 41%).

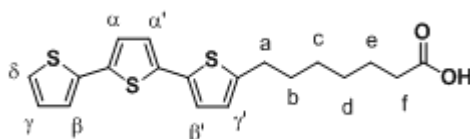
ESI-MS: m/z (%): 489 (100) $[1+\text{Na}]^+$

^1H NMR (600 MHz, DMSO-d_6): δ (ppm) 11.97 (s, 1H, OH), 7.52 (dd, 1H, $J_1 = 5.1$ Hz, $J_2 = 1.3$ Hz, H^δ), 7.36 (m, 5H, Ph), 7.32 (dd, 1H, $J_1 = 3.6$ Hz, $J_2 = 1.3$ Hz, H^β), 7.24 (d, 1H, $J = 3.6$

Chapter V: Experimental section

Hz, H^α), 7.16 (d, 1H, J = 3.6 Hz, H^α), 7.13 (d, 1H, J = 3.6 Hz, H^β), 7.10 (dd, 1H, J1 = 5.1 Hz, J2 = 3.6 Hz, H^γ), 6.80 (d, 1H, J = 3.6 Hz, H^γ), 5.08 (s, 2H, CH₂ bz), 2.76 (t, 2H, J = 7.6 Hz, H^a), 2.350 (t, 2H, J = 7.6 Hz, H^f), 1.60 (m, 2H, H^b), 1.54 (m, 2H, H^c), 1.31 (m, 4H, H^c & H^d).
¹³C NMR (200 MHz, DMSO-d₆): δ (ppm) 198.10, 173.63, 151.06, 145.64, 136.23, 129.11, 128.87, 128.63, 128.49, 128.26, 126.72, 124.04, 122.85, , 66.17, 34.36, 33.61, 31.63, 29.88, 28.90, 28.76, 24.94.

7-([2,2';5',2'']-terthiophen-5-yl)-heptanoyl acid



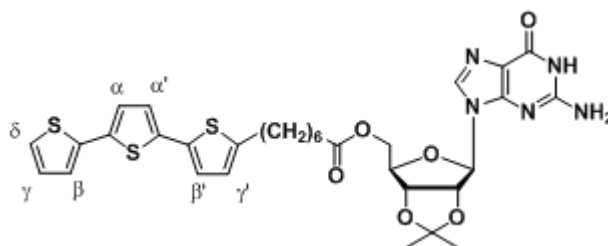
Following the procedure used for compound , 7-([2,2';5',2'']-terthiophen-5-yl)-heptanoyl acid was prepared in THF (500 mL) with 7-([2,2';5',2'']-terthiophen-5-yl)-heptanoyl acid benzyl ester (3.16 mmol, 1.46 g) and 100 mL of KOH solution (5% ^{w/w}). The product was collected as a yellow solid (2.84 mmol, 1.06 g, yield: 90%).

ESI-MS: *m/z* (%): 398 (100) [1+Na]⁺

¹H NMR (600 MHz, DMSO-d₆): δ (ppm) 11.97 (s, 1H, OH), 7.52 (dd, 1H, J1 = 5.1 Hz, J2 = 1.3 Hz, H^δ), 7.32 (dd, 1H, J1 = 3.6 Hz, J2 = 1.3 Hz, H^β), 7.24 (d, 1H, J = 3.6 Hz, H^{α'}), 7.17 (d, 1H, J = 3.6 Hz, H^α), 7.14 (d, 1H, J = 3.6 Hz, H^{β'}), 7.10 (dd, 1H, J1 = 5.1 Hz, J2 = 3.6 Hz, H^γ), 6.81 (d, 1H, J = 3.6 Hz, H^{γ'}), 2.78 (t, 2H, J = 7.6 Hz, H^a), 2.20 (t, 2H, J = 7.6 Hz, H^f), 1.61 (m, 2H, H^b), 1.50 (m, 2H, H^c), 1.32 (m, 4H, H^c & H^d).

¹³C NMR (200 MHz, DMSO-d₆) δ (ppm): 172.93 ,161.20, 146.95, 129.13, 126.37, 125.55, 124.88, 124.66, 34.35, 31.61, 29.99, 28.91, 25.11.

2',3'-O-Isopropylidene-5'-O-[7-([2,2';5',2'']-terthiophen-5-yl)-heptanoyl]-guanosine



In dry atmosphere of N₂, to a solution of 7-([2,2';5',2'']-terthiophen-5-yl)-heptanoyl acid (1.1 eq, 4.4 mmol, 2.09 g) in dry THF (30 mL) Et₃N (2 equiv., 8 mmol, 1.11 mL) was added; the mixture was cooled at 0 °C in an ice bath and CH₃SO₂Cl (1.1 equiv., 4.4 mmol, 358 μL) was added dropwise. After 30 minutes at 0 °C and 1 hour at room temperature, GACE (dried under vacuum at 50 °C for 4 hour) (4 mmol, 1.29 g) and a catalytic amount of DMAP were added. The reaction was carried out for 15 hours and then, after solvent removal, the crude product was diluted with CH₂Cl₂ (30 mL) and wash with H₂O (3x10 mL). The organic phase was dried over MgSO₄ and the solvent evaporated; purification through chromatography on silica gel (eluent: dichloromethane/methanol = 99/1→97/3) and crystallization in AcCN gave a white solid as product (1.4 mmol, mg).

ESI-MS: *m/z* (%): 703 (100) [1+Na]⁺

¹H NMR (600 MHz, DMSO-*d*₆): δ (ppm) 10.69 (s, 1H, NH), 7.83 (s, 1H, H^δ), 7.52 (dd, 1H, J₁ = 5.1 Hz, J₂ = 1.3 Hz, H^δ), 7.32 (dd, 1H, J₁ = 3.6 Hz, J₂ = 1.3 Hz, H^β), 7.22 (d, 1H, J = 3.6 Hz, H^{α'}), 7.16 (d, 1H, J = 3.6 Hz, H^α), 7.13 (d, 1H, J = 3.6 Hz, H^{β'}), 7.10 (dd, 1H, J₁ = 5.1 Hz, J₂ = 3.6 Hz, H^γ), 6.81 (d, 1H, J = 3.6 Hz, H^{γ'}), 6.53 (s, 2H, NH₂), 6.01 (d, 1H, J = 2.0 Hz, H¹), 5.26 (dd, 1H, J₁ = 5.8 Hz, J₂ = 2.0 Hz, H²), 5.12 (dd, 1H, J₁ = 5.8 Hz, J₂ = 3.3 Hz, H³), 4.25 (m, 2H, H⁴ & H⁵), 4.12 (m, 1H, H^{5'}), 2.76 (t, 2H, J = 7.6 Hz, H^a), 2.27 (m, 2H, H^f), 1.59 (m, 2H, H^b), 1.51 (s, 3H, CH₃), 1.48 (m, 2H, H^e), 1.31 (s, 3H, CH₃), 1.32 (m, 4H, H^c & H^d).

¹³C NMR (600 MHz, DMSO-*d*₆): δ (ppm) 156.89, 145.50, 128.88, 124.59, 124.38, 113.767, 84.63, 81.51, 33.62, 31.27, 29.66, 28.44, 27.44, 25.75, 24.66.

Bibliography

(1) Hercouet, A.; Lecorre, M. *Phosphorus Sulfur And Silicon And The Related Elements* **1987**, *29*, 111.

(2) Kiuchi, F.; Nakamura, N.; Saitoh, M.; Komagome, K.; Hiramatsu, H.; Takimoto, N.; Akao, N.; Kondo, K.; Tsuda, Y. *Chemical & Pharmaceutical Bulletin* **1997**, *45*, 685.

(3) Hardouin, C.; Kelso, M.; Romero, F.; Rayl, T.; Leung, D.; Hwang, I.; Cravatt, B.; Boger, D. *Journal Of Medicinal Chemistry* **2007**, *50*, 3359.

(4) Chen, J.; Murphy, A.; Esteve, J.; Ogletree, D.; Salmeron, M.; Frechet, J. *Langmuir* **2004**, *20*, 7703.

(5) Nicolas, Y.; Blanchard, P.; Levillain, E.; Allain, M.; Mercier, N.; Roncali, J. *Organic Letters* **2004**, *6*, 273.